Dissertation zur Erlangung des Doktorgrades
der Fakultät für Chemie und Pharmazie
der Ludwig-Maximilians-Universität München

Structural and functional analysis of the eukaryotic DNA repair proteins Mre11 and Nbs1

Christian Bernd Schiller

aus

Kassel

2011

Erklärung

Diese Dissertation wurde im Sinne von § 13 Abs. 3 bzw. 4 der Promotionsordnung vom 29. Januar 1998 (in der Fassung der sechsten Änderungssatzung vom 16. August 2010)
von Herrn Prof. Dr. Karl-Peter Hopfner betreut.

Ehrenwörtliche Versicherung

Diese Dissertation wurde selbständig, ohne unerlaubte Hilfe erarbeitet.

München, am 07.06.2011

.....

(Christian Bernd Schiller)

Dissertation eingereicht am 07.06.2011
1. Gutachter: Herr Prof. Dr. Karl-Peter Hopfner
2. Gutachter: Herr Prof. Dr. Dietmar Martin
Mündliche Prüfung am 21.07.2011

During the work of this thesis, the following publication was published:

Lammens K., Bemeleit D. J., Möckel C., Clausing E., Schele A., Hartung S., Schiller C. B., Lucas M., Angermüller C., Soding J., Strässer K. and K. P. Hopfner (2011). "The Mre11:Rad50 Structure Shows an ATP-Dependent Molecular Clamp in DNA Double-Strand Break Repair." Cell **145**(1): 54-66.

Parts of the present thesis will be submitted for publication:
Schiller C.B., Lammens K., Guerini I., Coordes B., Schlauderer F., Möckel C., Schele A., Sträßer K., Jackson S. P., Hopfner K.-P.:
"Insights into DNA double-strand break repair and ataxia-telangiectasia like disease from the structure of an Mre11-Nbs1 complex", manuscript in preparation.

Parts of this thesis have been presented at international conferences and workshops:

Talk and poster at the Biannual International Meeting of the German Society of DNA Repair Research (DGDR) - Repair meets Replication, September 7-10, 2010 in Jena, Germany

Poster presentation at the Gordon Research Conference on Mutagenesis - Consequences of Mutation and Repair for Human Disease, August 1-6, 2010 in Waterville, Maine, USA.

Poster presentation at the 2nd EU-IP DNA Repair Workshop for Young Scientists,
June 23-27, 2008 in Porto, Portugal.

Poster presentation at the 1st EU-IP DNA Repair Workshop for Young Scientists,
May 13-16, 2007, 2007 in Gent, Belgium.

TABLE OF CONTENTS

1. SUMMARY 1

2. INTRODUCTION 2

2.1 Biological roles of DNA double-strand breaks 2

2.1.1 DNA double strand breaks in cellular metabolism processes 2

2.1.2 Environmentally caused DNA double strand breaks 3

2.2 DNA double-strand repair pathways - A short overview 5

2.3 The Mre11-Rad50-Nbs1 complex - biochemistry and structural architecture 7

2.3.1 Biochemical *in vitro* activities of Mre11-Rad50-Nbs1 8

2.3.2 Structural architecture of the Mre11-Rad50-Nbs1 complex 9

2.4 The Mre11-Rad50-Nbs1 complex in double-strand break repair 13

2.4.1 The Mre11-Rad50-Nbs1 complex in homologous recombination 13

2.4.2 The Mre11-Rad50-Nbs1 complex in meiotic recombination 15

2.4.3 The Mre11-Rad50-Nbs1 complex in telomere maintenance 16

2.4.4 The Mre11-Rad50-Nbs1 complex in non-homologous end joining pathways 17

2.5 The Mre11-Rad50-Nbs1 complex in DNA damage signaling 18

2.6 Diseases linked with mutations in Mre11-Rad50-Nbs1 20

2.7 Objectives 22

3. MATERIALS AND METHODS 23

3.1 Materials 23

3.1.1 Antibodies 23

3.1.2 Oligonucleotides 24

3.1.3 Plasmids 27

3.1.4 Strains 29

3.2 Media and antibiotics 30

3.3 Methods 31

3.3.1 Molecular biology methods 31

3.3.1.1 Molecular cloning 31

3.3.1.2 Site Directed Mutagenesis by Overlap Extension PCR 32

3.3.1.3 Transformation in E. coli 33

3.3.2 Protein biochemistry methods 33

3.3.2.1 Protein expression in E. coli 33

3.3.2.2 Recombinant selenomethionine expression in E. coli ... *33*

3.3.2.3 Purification of GST-labelled proteins ... *34*

3.3.2.4 Purification of His-tag labeled proteins ... *35*

3.3.2.5 Discontinous Polyacrylamide Gel Electrophoresis (SDS-PAGE) ... *36*

3.3.2.6 Western blot analysis ... *37*

3.3.2.7 Analytical size exclusion chromatography ... *38*

3.3.2.8 Limited Proteolysis ... *38*

3.3.2.9 Nuclease activity assay ... *38*

3.3.2.10 EMSA (electrophoretic mobility shift assay) ... *39*

3.3.3 Structural biology methods ... 39

3.3.3.1 Crystallization ... *39*

3.3.3.2 Data collection, structure solution and model building ... *40*

3.3.3.3 Small angle x-ray scattering ... *41*

3.3.4 Yeast specific methods ... 42

3.3.4.1 Yeast transformation ... *42*

3.3.4.2 Plate survival assays ... *42*

3.3.4.3 Co-immunoprecipitation ... *42*

3.3.4.4 Indirect immunofluorescence ... *43*

3.3.5 Bioinformatical methods ... 44

3.3.5.1 Structure based sequence alignments ... *44*

4. RESULTS ... 46

4.1 Cloning and expression of Mre11 and Nbs1 from *S. pombe* ... 46

4.2 Crystallization, structure solution and refinement ... 49

4.2.1 $Nbs1^{mir}$-$Mre11^{cd}$ complex ... 49

4.2.2 Apo-$Mre11^{cd}$ ... 52

4.3 Analysis of the apo-$Mre11^{cd}$ structure ... 52

4.4 Analysis of the $Nbs1^{mir}$-$Mre11^{cd}$ complex structure ... 55

4.4.1 The structure of $Nbs1^{mir}$-$Mre11^{cd}$ - An overview ... 55

4.4.2 Analysis of protein interaction sites in the structure of $Nbs1^{mir}$-$Mre11^{cd}$ ... 56

4.5 Conformational impact of $Nbs1^{mir}$ binding on the $Mre11^{cd}$ dimer configuration ... 61

4.6 Comparison of $Nbs1^{mir}$-$Mre11^{cd}$ structures with different metal coordinating states 63

4.7 SAXS analysis of $Mre11^{cd}$ and comparison with $Nbs1^{mir}$-$Mre11^{cd}$ ... 64

4.8 Structural and biochemical characterization of the Mre11-Nbs1 interface and disease causing Mre11 mutations 65

4.8.1 Analysis of A-TLD and NBS-like disease mutations 65

4.8.2 Structural and biochemical link between Nbs1 interaction and the nuclease active site of Mre11 67

4.9 Biochemical analysis of Mre11 and Nbs1 from *S. pombe* 69

4.10 Structure guided *in vivo* analysis of Mre11 from *S. cerevisiae* 71

4.10.1 Mutational analysis of functional motifs in *S. cerevisiae* Mre11 by plate survival assays 72

4.10.2 Indirect immunofluorescence reveals nuclear localization defects of different latching loop targeting mutations 77

4.10.3 Analysis of *S. cerevisiae* Mre11-Rad50-Xrs2 complex integrity and Mre11 dimer interaction for different Mre11 latching loop targeting mutations 78

5. DISCUSSION 81

5.1 Preparation and crystallization of *S. pombe* apo-Mre11^{cd} and Nbs1^{mir}-Mre11^{cd} 81

5.2 The eukaryotic Mre11 dimer resembles the principal domain architecture of prokaryotic Mre11 but exhibits additional structural characteristics 83

5.3 Nbs1 binds to the Mre11 dimer via multiple contacts and controls its dimeric configuration 84

5.4 The extended structure of the Mre11-Nbs1 interface may explain the hypomorphic character of A-TLD causing mutations 86

5.5 The latching loops of *S. cerevisiae* Mre11 are crucial for the general functionality of the Mre11-Rad50-Xrs2 complex 87

5.6 A model for Mre11 dimer and Nbs1 mediated DSB signaling 90

6. REFERENCES I

7. ABBREVATIONS XII

8. CURRICULUM VITAE XV

9. ACKNOWLEDGEMENTS XVI

1. SUMMARY

The integrity of the genome is constantly threatened by environmental influences and cellular metabolism processes. DNA double strand breaks (DSBs) are among the most hazardous of all DNA lesions and arise from failures in genome metabolism processes and from exogenous sources. In addition they are important programmed intermediates in DNA metabolism. Cells have evolved efficient pathways to repair DSBs and here the Mre11-Rad50-Nbs1 (MRN) complex is a central key factor. Mre11 and Rad50 are conserved in all domains of life, whereas Nbs1 is a eukaryote-specific protein and plays regulatory roles within the complex. MRN senses and binds DSBs, recruits other repair factors and also stabilizes DSBs by its tethering activity. Furthermore it processes DSB ends for repair and is involved in DNA damage signaling by co-activating the checkpoint kinase ATM.

Null mutations of Mre11-Rad50-Nbs1 coding genes are lethal in higher eukaryotes, whereas hypomorphic mutations induce different heredity diseases. Ataxia-telangiectasia like disorder (A-TLD) and Nijmegen breakage syndrome (NBS) are linked to mutations in Mre11 and Nbs1 respectively. However, also mutations in Mre11 and Rad50 may lead to an NBS-like disorder. All diseases share genomic instability and delayed checkpoint activation.

The aim of this work was to characterize the structural and functional interplay between eukaryotic Mre11 and Nbs1 and to analyze how it influences the role of the complex in repair and checkpoint activation. For this purpose proteins form the fission yeast *Schizosaccharomyces pombe* were studied and the Mre11 nuclease dimer alone and in complex with the interacting region of Nbs1 determined as crystal structures. The Mre11-Nbs1 structure reveals binding of two Nbs1 molecules as extended peptides to one Mre11 dimer at the outside of the nuclease domains. One Nbs1 molecule mediates also a second interaction with Mre11 by asymmetrically binding across the Mre11 dimer and thereby determining its dimeric conformation. The interfaces of Mre11 and Nbs1 were analyzed and verified by mutational analysis *in vitro* using recombinant *S. pombe* proteins and *in vivo* in *Saccharomyces cerevisiae*. The structures also allowed studying of the molecular basis for several A-TLD and NBS-like disease mutations. As a result, all analyzed A-TLD mutations exhibited a weakened but not abolished Nbs1 interaction, which might explain the hypomorphic phenotype of A-TLD. Finally a model is proposed, in which a conformational switch in the Mre11 dimer and modulated Nbs1 interactions permit subsequent DSB repair and signaling.

2. INTRODUCTION

2.1 Biological roles of DNA double-strand breaks

The maintenance of genomic stability is a fundamental problem for all living organisms, since the integrity of every genome is constantly threatened by different sources of DNA damage. DNA double strand breaks (DSBs) are among the most hazardous DNA lesions. They can lead to chromosomal rearrangements and induction of cancerogentic diseases, if not repaired properly. However, DSBs are also important intermediates in different DNA metabolism processes where they are temporary inserted into the genome. The following chapter is giving a short overview about the different sources of DSBs and their impact on the genomic stability.

2.1.1 DNA double strand breaks in cellular metabolism processes

The majority of accidentally occurring DSBs in proliferating cells arise from aberrations in DNA replication: Replication at blocking lesions or single-strand nicks can lead to a replication fork collapse, which results in the generation of DSBs. (Costanzo et al. 2001; Kuzminov 2001). But also (by)products of normal cellular metabolism processes like e.g. reactive oxygen species (ROS) contribute significantly to the introduction of these blocking lesions into the DNA (Cadet et al. 1997; Borde and Cobb 2009). Since most often a sister chromatid is available as a repair template in S-phase, DSBs arising from collapsed replication forks are mainly repaired by the homologous recombination (HR) machinery (Errico and Costanzo 2010).

Importantly, DSBs are not solely harmful, but also play beneficial roles in the cell. During various biological processes, DSBs are introduced transitionally into the genome in programmed ways: One example is the switching of mating types in the budding yeast *S. cerevisiae*: This process is initiated by a site specific cleavage of the HO endonuclease at the MAT gene locus, which generates a DSB. Subsequently, the mating type gene is switched by unidirectional gene conversation via recombination with the HML or HMR gene cassette, which carry silenced copies of the mating types a and α respectively (Haber 1998; Coic et al. 2006).

The programmed introduction of DSBs is also a crucial event during the generation of immunoglobulins (Ig) and T cell receptors (TCR) by the vertebrate immune system. The required diversity of these molecules is achieved by a process called V(D)J recombination. Combination of Variable (V), Diversity (D) and Joining (J) encoding gene segments through a specific DNA rearrangement mechanism leads to a broad diversity of proteins and allows the recognition of many different antigens (Tonegawa 1983; Dudley et al. 2005). The process begins with the introduction of DSBs by the RAG1/RAG2 proteins, which recognize recombination signal sequences (RSS) at the borders of the V, D and J gene elements. This results in two hairpin-sealed coding ends and two blunt signal ends. The following processing steps are carried out by proteins of the non-homologous end joining (NHEJ) machinery, which mediate the error prone repair of the breaks (Raghavan et al. 2005).
The specificity and efficiency of immunoglobulins is further increased after activation of the humoral immune response by antigens via two different processes: Class switch recombination (CSR) leads to the exchange of the Ig constant region of antibodies and allows the generation of different antibody classes, whereas somatic hypermutation introduces additional mutations into the Ig variable region. The activation-induced cytidine deaminase (AID) in both processes initiates the introduction of DSBs which are joined and subsequently repaired by NHEJ (Soulas-Sprauel et al. 2007; Dinkelmann et al. 2009; Zha et al. 2011). Important roles of the Mre11-Rad50-Nbs1 complex in different NHEJ dependent repair processes are discussed below (2.4.4).

In most sexually reproducing organisms programmed DSBs are also generated during the process of meiosis. After the alignment of homologous chromosomes in meiotic prophase I, DSBs are introduced at specific hot spot sites on the chromosomes by the type II topoisomerase-like enzyme Spo11. The covalently bound Spo11 is then removed from the DNA by the Mre11-Rad50-Nbs1 complex and resection of the 5`-strand takes place. Finally, the DSBs are repaired by meiotic recombination between homologous chromosomes resulting in gene conversion or chromosomal crossing over (Borde 2007; Inagaki et al. 2010).

2.1.2 Environmentally caused DNA double strand breaks

The genome is not only exposed to endogenous mutagens like oxidative byproducts of cellular respiration, but also environmental agents like ionizing radiation, UV-light or

genotoxic chemicals can cause various DNA damages. These include directly or indirectly introduced DSBs (Hoeijmakers 2001).

Ionising radiation (IR) occurs naturally *e.g.* by radioactive decay of instable atomic nuclei or by cosmic radiation. Besides, IR is used in medical procedures like X-ray inspections or radiation therapy in cancer treatment (Ciccia and Elledge 2010). IR produces a broad spectrum of different DNA damages, which are introduced via the production of reactive oxygen species (Mahaney et al. 2009). Most often IR leads to DNA base damages or introduction of DNA single-strand breaks (SSBs), which are repaired by base excision repair (BER) or single strand repair pathways (Almeida and Sobol 2007; Dianov and Parsons 2007). IR-caused DSBs occur when two SSBs are introduced in close proximity on opposite DNA strands (Sutherland et al. 2000). Therefore, IR caused DSBs often possess single strand overhangs. In addition IR produces DNA breaks with 3' termini carrying phosphate or phosphoglycolate groups, which need to be removed before ligation of the breaks (Henner et al. 1983).

UV light on the other hand can indirectly provoke DSB formation by introducing 6-4 photoproducts and cyclobutane pyrimidine dimers into the DNA. These bulky lesions may induce replication-fork collapse and thereby DSBs if not repaired properly by the nucleotide excision repair (NER) machinery (Limoli et al. 2002). Similar effects are induced by different genotoxic chemicals, which also create replication blocking lesions like *e.g.* different alkylating agents, the intrastrand crosslinking anti-cancer-drug cisplatin or the interstrand crosslinking agent mitomycin (Bosco et al. 2004; Al-Minawi et al. 2009).

In addition, chemicals, which poison the topoisomerase enzymes, can promote DSB formation by stabilizing the cleavage complex in which the topoisomerase is covalently attached to the cleaved DNA (Degrassi et al. 2004). The Topoisomerase I (TopI) inhibitor camptothecin (CPT) triggers the accumulation of TopI-bound SSBs, which may be converted to DSBs when a replication fork collides with the cleavage complex (Jacob et al. 2005). Topoisomerase II (TopII) enzymes introduce DSBs in the DNA during their catalytic cycle. Top II inhibitors like etoposide increase the concentration of cleavage complexes, which can be converted to permanent DSBs by collision with polymerases or helicases (Bromberg et al. 2003).

2.2 DNA double-strand repair pathways - A short overview

To protect the genome and thus ensure the integrity of its coded information, cells have evolved different sophisticated mechanisms to repair DSBs: The two major pathways here are homologous recombination (HR) and non-homologous end joining (NHEJ) (Harper and Elledge 2007).

HR enables the cell to repair DSBs in a relatively error free manner by using a sister- or homologous chromatid as a template (Figure 2.1). The repair of DSBs by HR comprises several sequential steps. First, 3´ ssDNA tails adjacent to the break have to be generated by the combined action of several nucleases and helicases. The Mre11-Rad50-Nbs1 (MRN) complex plays here crucial roles in the first steps of HR by sensing and tethering the break but also in mediating the initiation of resection (2.4.1) (Huertas 2010). The resected 3´ ssDNA tail is first coated by RPA, which is replaced by Rad51 (RecA in bacteria). Rad51 assembles on the ssDNA to build a helical nucleoprotein filament, which in concert with proteins of the Rad52 epistasis group and other HR proteins screens for a homologous sequence (New et al. 1998; Symington 2002). The nucleoprotein filament invades into the homologous donor sequence and after removal of Rad51 hybridizes with it via normal base pairing, thereby building a displacement loop (D-loop) structure (Sung and Klein 2006). After strand extension by a DNA polymerase, using the donor strand as a template, the D-loop intermediate can be repaired by two different HR mechanisms: (1) the double-strand break repair (DSBR) pathway or (2) synthesis-dependent single strand annealing (SDSA). In DSBR the second 3´ ssDNA tail, which was not involved in D-loop formation, is captured by annealing to the extended D-loop and thereby an intermediate structure with two Holliday junctions is formed (Bzymek et al. 2010). Depending on how the Holiday junctions are resolved, DSBR results in crossover or non-crossover recombination products (Heyer 2004). In the alternative SDSA pathway the invading 3´ ssDNA tail is displaced after its extension and reanneals to the single-stranded DNA tail, that was not involved in D-loop formation. Repair of DSBs by the SDSA results always in non-crosslinking recombination products (San Filippo et al. 2008).

Sometimes DSBs are closely flanked by repeat sequences. In this case recombination repair via single-strand annealing (SSA) may occur. Like in DSBR or SDSA also SSA is initiated by end resection, which generates 3´ ssDNA tails, although it does not require a homologous chromosome for recombination. Instead, the resected ends anneal via their repeat sequences,

followed by nucleolytical removal of nonhomologous flap structures and ligation. SSA results in the deletion of the sequence regions between the repeat elements and is therefore considered to be potentially mutagenic (Ivanov et al. 1996; Mansour et al. 2008).

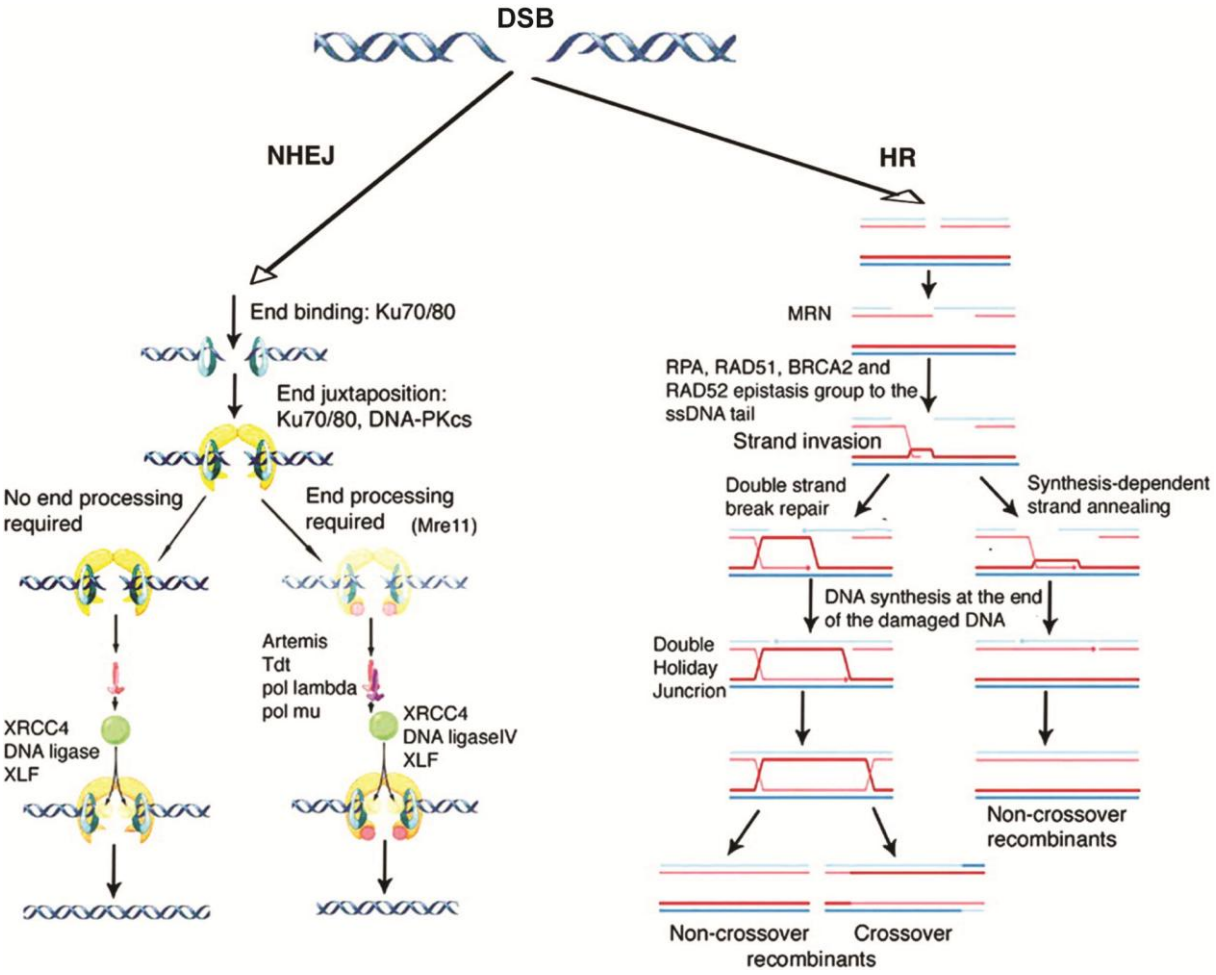

Figure 2.1: Overview of the major DSB repair pathways. Figure adapted from (Pandita and Richardson 2009). DSBs can be repaired by either non-homologous end joining (NHEJ) or homologous recombination (HR). For details see text.

The more error-prone NHEJ pathway is utilized especially in G1 phase when no sister chromatid is available for recombinational repair (Figure 2.1). Depending on the organism, however it also occurs in S- and G2 phase cells. NHEJ promotes direct ligation of the two ends. The main NHEJ pathway, also called classical NHEJ (c-NHEJ) pathway, is initiated through binding of the Ku70/80 heterodimer to the DSB (Weterings and van Gent 2004). Next, the Ku heterodimer recruits the catalytic subunit of the DNA-dependent protein kinase (DNA-PK). The newly formed Ku/DNA-PK complex then places both DSBs into

juxtaposition. DNA-PK gets autophosphorylated upon binding to Ku and the DNA. This is required for the further recruitment of other NHEJ proteins to the DSB (Meek et al. 2007). If the DSB ends do not require further processing, they are directly ligated by a complex consisting of DNA ligase IV, XRCC4 and XLF/Cernunnos (Ahnesorg et al. 2006). Often, the DNA ends are not compatible for direct ligation, for example if the ends possess ssDNA overhangs or damaged bases. In this case different other NHEJ factors like the Artemis nuclease, the Pol TdT (terminal deoxynucleotidyl transferase), pol lambda, pol mu and also the Mre11-Rad50-Nbs1 complex process the end to allow ligation by the ligase IV/XRCC4 complex (Figure 2.1) (Lieber 2010).

Sometimes NHEJ employs also alternative pathways (a-NHEJ), in which additional factors distinct from the c-NHEJ machinery facilitate the repair. One of these a-NHEJ pathways is called microhomology-mediated endjoining (MMEJ) in which several bases are nucleolytically removed from the DSB. This allows hybridization of single-stranded DNA ends at short stretches of sequence homology. Therefore, MMEJ is considered to be highly mutagenic (Haber 2008; Fattah et al. 2010). Mre11 was reported to be the major nuclease in the resection procedure of MMEJ, which generates DSBs with compatible microhomology sequences (Rahal et al. 2010).

2.3 The Mre11-Rad50-Nbs1 complex - biochemistry and structural architecture

The Mre11-Rad50-Nbs1/Xrs2 (MRN(X) complex plays various central roles in most, if not all DNA double-strand break repair pathways. It senses and binds to DSBs and functions as a recruiting platform for many other DNA repair proteins. Furthermore, it is a scaffold protein, which stabilizes DSBs via its tethering activity. MRN is also involved in nucleolytic processing of DNA ends and functions in DNA damage signaling by co-activating the checkpoint kinase ATM. MRN comprises the Mre11 endo/exonuclease dimer, two Rad50 ATP-binding cassette proteins and contains in eukaryotic organisms also the third subunit Nbs1 (Xrs2 in *S. cerevisiae*) as a regulatory factor (Assenmacher and Hopfner 2004; Williams et al. 2010). The core complex consisting of the catalytic subunits Mre11 and Rad50 is conserved from bacteria and archaea to eukaryotes and is even found in some viruses like the bacteriophage T4 (Sharples and Leach 1995; Hopfner et al. 2000; Herdendorf et al. 2011). Mre11, which stands for Meiotic recombination 11, was first identified in a genetic screen for proteins functioning in meiosis in *S. cerevisiae* (Ajimura et al. 1993). Rad50 was discovered

already earlier in genetic yeast studies were its deletion mutant strain was reported to be sensitive to ionizing radiation and to produce inviable spores in meiosis (Game and Mortimer 1974). The human homologue of Nbs1, which is also called Nibrin, was functionally identified in 1998, even though the genetic disease Nijmegen breakage syndrome, which is linked to mutations in the *Nbs1* gene, was known since much longer times (Weemaes et al. 1981; Varon et al. 1998).

2.3.1 Biochemical *in vitro* activities of Mre11-Rad50-Nbs1

Biochemical *in vitro* studies with bacterial, archaeal, yeast and human Mre11 and Rad50 proteins revealed that Mre11 possesses Mn^{2+} dependent nuclease activities: The dsDNA 5-3´ exonuclease activity of Mre11 is dependent on ATP binding by Rad50 in bacteria and archaea, while being rather unaffected by ATP binding in eukaryotes. The ssDNA endonuclease activity appears to be ATP independent (Furuse et al. 1998; Paull and Gellert 1998; Trujillo et al. 1998; Connelly et al. 1999; Hopfner et al. 2001). Mre11 exhibits also the ability to open and process hairpin DNAs in an ATP dependent manner (Paull and Gellert 1998; Connelly et al. 1999; Trujillo and Sung 2001). Additionally, its nuclease activity can remove covalently bound proteins from DNA ends (Connelly et al. 2003). The importance of Mre11`s nuclease activity for its *in vivo* functions is discussed below (2.4).

The exact function of the ATPase activity of Rad50 was longtime puzzling. As already mentioned, it stimulates the nucleolytic cleavage activity of Mre11 on hairpin structures. Further, it was shown to be important for tethering DNA ends, and a Rad50 signature motif mutant, which is impaired in ATP binding, lacks the ability to stimulate the checkpoint kinase ATM *in vitro* (Lee and Paull 2005; Dupre et al. 2006). In addition, biochemical studies with recombinant human MRN proteins indicated also a stimulatory role of Rad50 ATP binding for melting and unwinding of DNA secondary structures (Paull and Gellert 1999). Recent data from the Hopfner group revealed that ATP binding by Rad50 induces conformational changes within the Mre11-Rad50 complex which promotes binding of DNA ends (Lammens et al. 2011).

Nbs1 possesses no own catalytic activity but plays regulatory roles within the eukaryotic MRN complex. Human Nbs1 and the homologous Xrs2 protein from *S. cerevisiae* were shown to stimulate DNA binding as well as nucleolytic hairpin processing by Mre11-Rad50 (Paull and Gellert 1999; Lee et al. 2003). Moreover, Nbs1 is a co-activator of the checkpoint

kinase ATM in concert with Mre11-Rad50, which was also observed by *in vitro* reconstitution assays with the recombinant human proteins (Falck et al. 2005; Lee and Paull 2005; You et al. 2005).

2.3.2 Structural architecture of the Mre11-Rad50-Nbs1 complex

The Mre11-Rad50 (MR) core complex is a heterotetramer consisting of two Mre11 and two Rad50 molecules. In eukaryotes it associates furthermore with one or two molecules of Nbs1 (or the homologous Xrs2 protein in *S. cerevisiae*) to build the MRN(X) complex (Figure 2.2 A) (Paull and Gellert 1999; van der Linden et al. 2009). Atomic force microscopy data (Figure 2.2 B) showed that MRN consists of a globular head region, which harbors the catalytic functions of the complex and contains the Mre11 dimer, the ABC-ATPase domains of Rad50 and the Nbs1 molecules. A large helical region, which links the N- and C-terminal ATPase domains of Rad50, folds into a long coiled coil tail, which protrudes from the catalytic head region (de Jager et al. 2001; Hopfner et al. 2002; Moreno-Herrero et al. 2005).

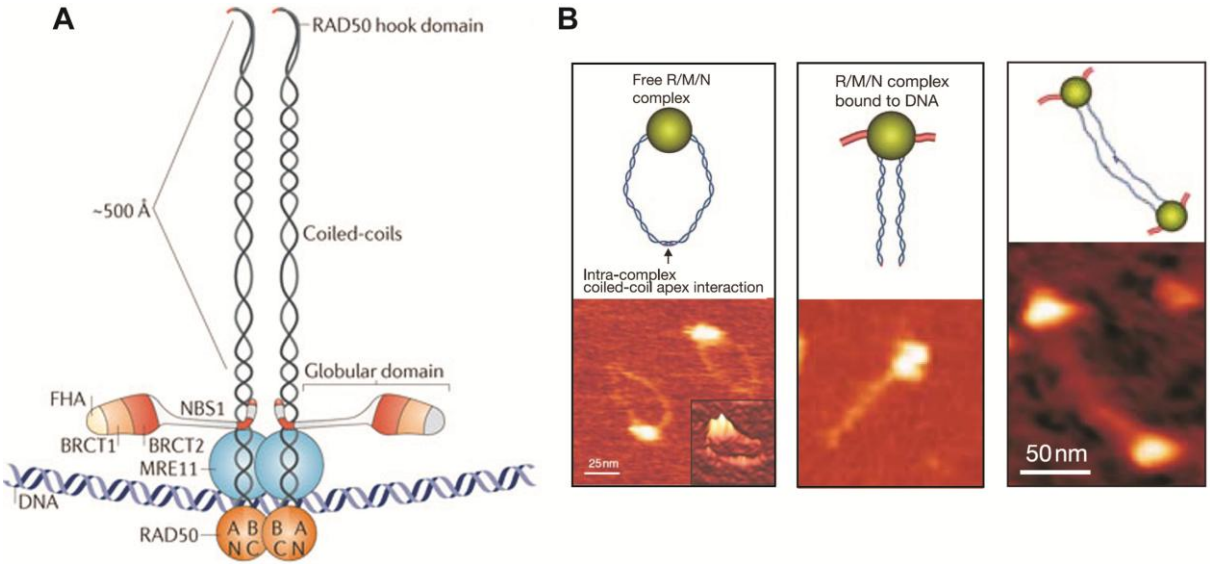

Figure 2.2: Structural organization of the MRN complex and DNA induced mesoscale conformational changes: (A) Model of the eukaryotic MRN complex. MRN consists of a globular head which contains the Mre11 dimer, two Rad50 ABC ATPases and two Nbs1 molecules. A long flexible coiled-coil region protrudes from each Rad50 molecule. A Zinc-hook dimerization domain at the other end of the coiled-coil allows interaction between different MRN complexes. The Figure was adapted from (Stracker and Petrini 2011).
(B) Atomic force microscopy (AFM) images of the human MRN complex in the presence and absence of DNA. For each structural arrangement of MRN a schematic model is shown. Left figure: Image of the human MRN

complex in the absence of DNA, resolving clearly the globular head and the coiled-coil region. Middle figure: Upon binding of the head region to DNA (here 90bp dsDNA), the coiled-coils are oriented in a parallel conformation. Left figure: MRN intercomplex interaction, mediated by the apical zinc-hook domain. All figures from (B) are adapted from (Moreno-Herrero et al. 2005).

The Rad50 coiled-coil tail harbors an apical zinc-hook dimerization motif that allows the interaction with other MRN complexes (Figure 2.2 A) (Hopfner et al. 2002).

The conserved N-terminus of Mre11 consists of a phosphodiesterase domain and a C-terminally adjacent DNA capping domain (Figure 2.3). Yeast two hybrid studies with human Mre11 and Nbs1 indicated that the phosphodiesterase domain harbors the interaction site for Nbs1 (Desai-Mehta et al. 2001). However, the exact locations of Nbs1 interaction regions within Mre11 were unknown and could be identified during the work for this thesis. The interaction region(s) in Mre11 for Rad50 were first roughly mapped with deletion mutants in *S. cerevisiae* and were recently confirmed by combined structural and biochemical studies (Chamankhah and Xiao 1999; Lammens et al. 2011; Lim et al. 2011; Williams et al. 2011). Eukaryotic Mre11 possesses two distinct DNA interaction motifs which flank the main binding site for Rad50 (Figure 2.3). Whereas the DNA interaction motif adjacent to the capping domain was reported to be important and sufficient for mitotic repair in *S. cerevisiae*, the C-terminal motif is crucial for DSB formation and spore viability in meiosis (Furuse et al. 1998; Usui et al. 1998).

Rad50 contains a bipartite ATP-binding cassette - ATPase (ABC-ATPase), which is build up by an N-terminal and a C-terminal domain, separated in the primary structure by a long coiled-coil region (Figure 2.3). The N-terminal domain harbors the Walker A motif and the C-terminal domain the Walker B and signature motifs. A highly conserved Cys-X-X-Cys sequence maps to the center of the coiled-coil region. It folds into the MRN intercomplex mediating zinc-hook motif. Rad50`s major binding sites for Mre11 map to the N- and C-terminal ends of the coiled-coil region (Hopfner et al. 2000; Hopfner et al. 2002; Lammens et al. 2011).

The eukaryotic Nbs1 /Xrs2 protein is the least conserved compound of the MRN(X) complex (Figure 2.3). Its N-terminal region consists of a Forkhead domain and two BRCT domains, which mediate binding of the MRN to different phosphoproteins in DNA repair (Palmbos et al. 2005; Hari et al. 2010). The C-terminal region appears to be mainly unstructured as seen by limited proteolysis analysis for the *S. pombe* protein homologue (Williams et al. 2009). It

contains interaction motifs for Mre11 and the checkpoint kinase ATM (Desai-Mehta et al. 2001; Ueno et al. 2003; Falck et al. 2005; You et al. 2005).

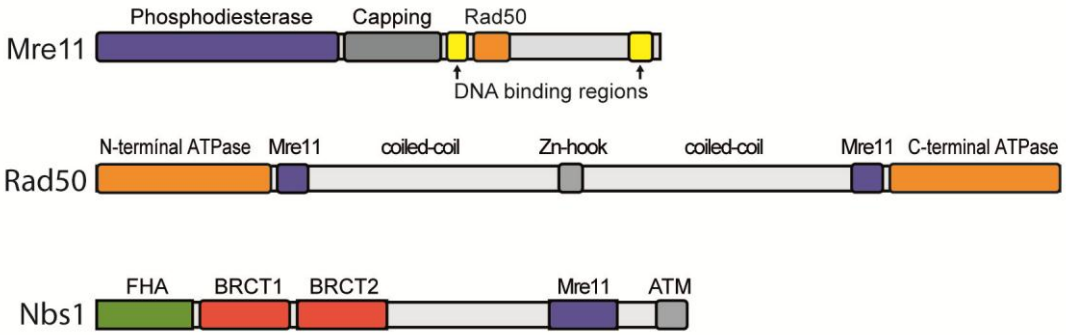

Figure 2.3: Domain architecture of Mre11-Rads50-Nbs1: Mre11 consists of a conserved N-terminal phosphodiesterase and an adjacent DNA capping domain. The C-terminal region contains a hydrophobic interaction motif for Rad50, which is flanked by two DNA binding regions. Rad50 is build up of a bipartite ABC-ATPase cassette, which is separated by a long coiled-coil region. An MRN intercomplex interaction mediating Zn-hook maps to the central coiled-coil region. Nbs1 contains an N-terminal phosphoprotein binding module, which comprises a Forkhead and two BRCT domains. The C-terminus possesses interaction sites for both Mre11 and ATM. Domain maps are adapted from (Assenmacher and Hopfner 2004; Stracker and Petrini 2011).

Mre11 is a dimeric molecule in solution and the Mre11-Mre11 interaction is mediated via the phosphodiesterase domains (Hopfner et al. 2001). Importantly, Mre11 dimerization is crucial for the functionality of the MR(N) complex. It was *e.g.* observed in the archaeal Mre11-DNA crystal structure from *Pyrococcus furiosus* that both molecules of the Mre11 dimer bind cooperatively to one DNA molecule (Figure 2.4 C). The same authors showed also biochemically, that mutations leading to Mre11 dimer disruption in the yeast *Schizosacchaormyces pombe* render cells sensitive to different genotoxic agents (Williams et al. 2008).

Recently, crystal structures of Mre11-Rad50 complexes from bacteria and archaea were published by the Hopfner group and others. These structures reveal that the complex exhibits an open form with a central Mre11 nuclease dimer and peripherial Rad50 molecules in the absence of ATP or DNA (Figure 2.4 A). Binding of ATP leads to the dimerization of Rad50 molecules (Figure 2.4 B) and also increases - at least in the case of *Thermotoga maritima* Mre11-Rad50 - the DNA affinity of the complex (Lammens et al. 2011; Lim et al. 2011; Williams et al. 2011).

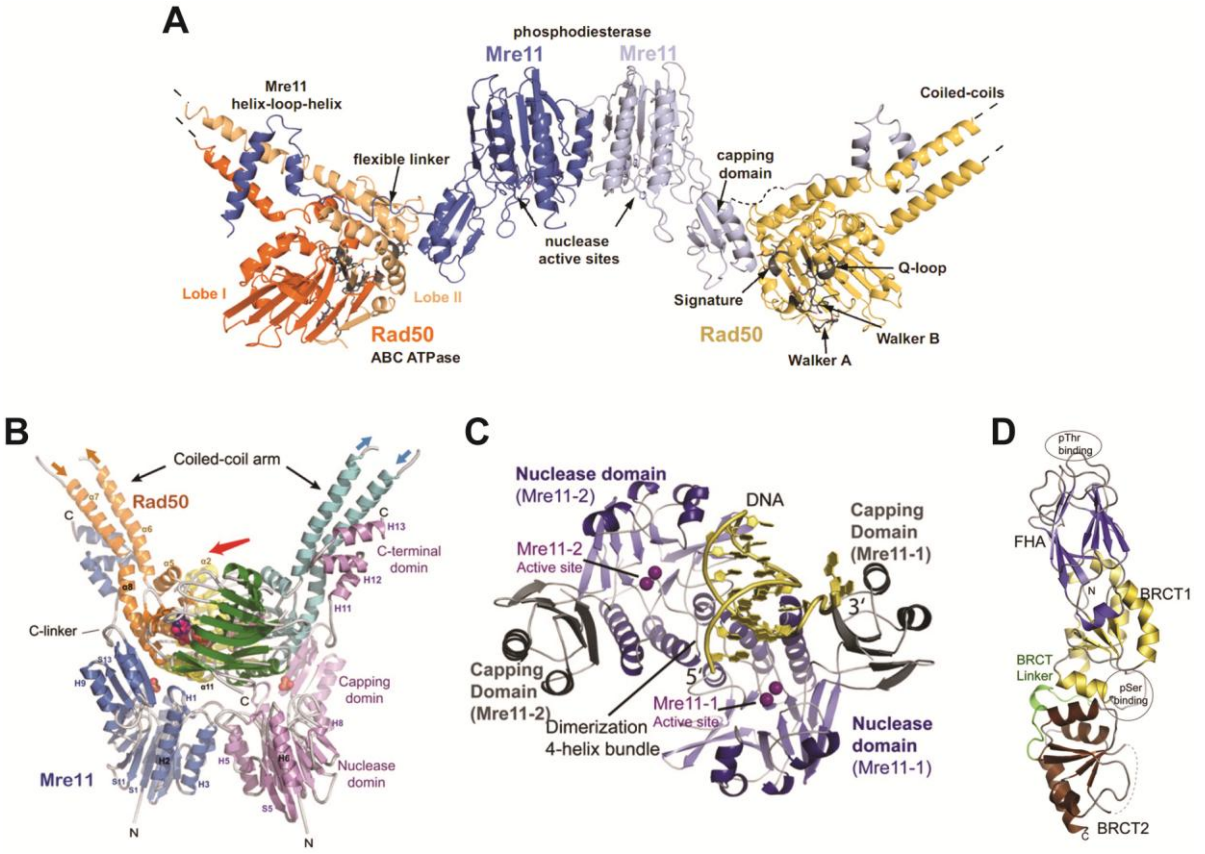

Figure 2.4: Published crystal structures of Mre11-Rad50 and Nbs1. (A) Structure of the Mre11-Rad50 complex from the thermophilic bacterium *Thermotoga maritima* at 3.4 Å resolution (Lammens et al. 2011). **(B)** Structure of Mre11-Rad50 from the archaeal organism *Methanococcus jannaschii* bound to ATPγS at 3.1 Å resolution (Lim et al. 2011). **(C) S**tructure of the Mre11 nuclease dimer from the archaeal organism *Pyrococcus furiosus* in complex with a hairpin DNA at 2.2 Å resolution (Williams et al. 2008). **(D)** Structure of the N-terminus of Nbs1 from *Schizosaccharomyces pombe* at 2.8 Å resolution. The structure contains the Forkhead domain and the two BRCT domains, which are all involved in binding of phosphoproteins (Williams et al. 2009).

For Nbs1/Xrs2, only the N-terminal region is structurally characterized by crystal structures of the Forkhead-domain and two BRCT domains from the fission yeast *Schizosaccharomyces pombe* and an NMR-structure of the second BRCT domain from *Xenopus laevis* (Figure 2.4 D). The structures from *S. pombe* Nbs1 show a very compact arrangement of the Forkhead and BRCT domains and were proposed to be linked to Mre11-Rad50 via the flexible C-terminus of Nbs1 (Xu et al. 2008; Lloyd et al. 2009; Williams et al. 2009). However, the interaction between Nbs1 and Mre11-Rad50 is not understood on a molecular level yet. Therefore, an atomic structure of eukaryotic Nbs1 in complex with Mre11 or Rad50 would be

highly valuable to help understanding the regulatory functions of Nbs1 within the MRN complex.

2.4 The Mre11-Rad50-Nbs1 complex in double-strand break repair

2.4.1 The Mre11-Rad50-Nbs1 complex in homologous recombination

The Mre11-Rad50-Nbs1/Xrs2 MRN(X) complex is one of the first complexes which localize to DSBs and plays various key roles in repair by sensing DSB ends, stabilizing breaks, initiation of DNA resection and damage signaling. Several studies suggest antagonistic roles for MRN(X) and the Ku complex, which is the second cellular DSB sensor, in the early phase of repair events. Both complexes sense and bind to DSBs but whereas the MRN(X) complex is the core initiation factor for HR, the Ku complex promotes NHEJ. However, MRN(X) is also involved in different NHEJ repair pathways (2.4.4). It has been shown that the Ku complex suppresses homologous recombination by inhibiting MRN(X) complex dependent DNA end resection in G1 phase, but much less in S and G2 phase. How exactly the choice of pathway is regulated in a cell-cycle dependent manner is only poorly understood yet, but it is clear that DNA 5´-strand resection by MRN(X) and other nucleases shifts the balance towards the HR pathway (Clerici et al. 2008; Zierhut and Diffley 2008; Shim et al. 2010).

Initiation of HR by resection depends strongly on the MRN(X) complex and the Sae2 protein (in *S. cerevisiae*) or its homologues Ctp1 (in *S. pombe*) and CtIP (in metazoans), which are poorly conserved in sequence (Figure 2.5 A). In addition, the phosphorylation of Sae2 or CtIP by cyclin-dependent protein kinases is crucial for this step (Limbo et al. 2007; Huertas et al. 2008; Huertas and Jackson 2009). The dependence of initial DNA 5´ end resection on the nuclease activity of Mre11 differs between organisms. Whereas the nuclease deficient Mre11 H125N mutant exhibits only a mild phenotype in *S. cerevisae*, the equivalent mutations in *S. pombe* (H134S) or mouse (H129N) cause severe radiosensitivity and embryonic lethality, respectively. One hypothesis which might explain these divergent phenotypes is that the presence of Ku is more dominating in *S. pombe* and mice, thereby raising the barrier to initiate resection. (Lewis et al. 2004; Limbo et al. 2007; Buis et al. 2008; Williams et al. 2008; Mimitou and Symington 2011).

The exact functional role of Sae2/Ctp1/CtIP in the resection procedure remains controversial. The *S. cerevisiae* Sae2 protein was shown to possess an *in vitro* nuclease activity on its own, which together with Mre11 might function in resection (Lengsfeld et al. 2007). However, no nuclease activity was reported for *S. pombe* Ctp1 and human CtIP. For both organisms, the proteins were suggested to act as co-factors of MRN and to stimulate the resection activity of Mre11 (Limbo et al. 2007; Sartori et al. 2007). Resection by MRN(X) and Sae2/Ctp1/CtIP is not processive but rather leads to the generation of a short 3´ ssDNA tail before other nuclease/helicase complexes take over for processive long range resection of several kilobases. In *S. cerevisae*, where the mechanistic details of resection are probably best understood, the MRX complex stimulates the recruitment of the Sgs1/Top3/Rmi1 (STR)/Dna2 complex and Exo1 to the break, which are responsible for the majority of long range resection (Shim et al. 2010). In addition, the Pso2 nuclease might play a backup role in this process, since it promotes a residual resistance to IR in the absence of nuclease active Mre11 and Exo1 in *S. cerevisiae* (Lam et al. 2008).

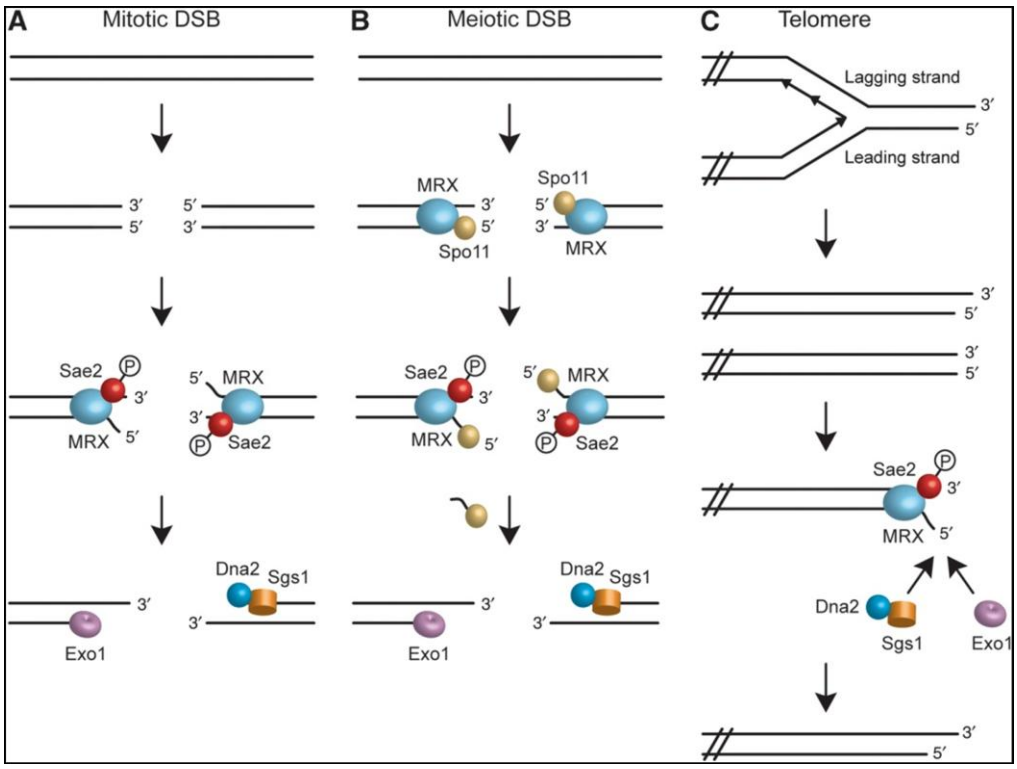

Figure 2.5: Roles of the MRN(X) complex in the resection of mitotic or meiotic DSBs and in telomere processing. (A) Mitotic DSBs: MRX and Sae2 sense and bind to free DSBs. Sae2 is phosphorylated by Cdk1 which promotes resection initiation by MRX and Sae2, leading to the generation of short 3´ ssDNA tails. These are then substrates for processive end resection carried out by Dna2/Sgs1 or Exo1. **(B)** Meiotic DSBs: MRX and other proteins stimulate the generation of DSBs by Spo11. MRX and Sae2 then nucleolytically remove the

covalently bound Spo11 from the DSBs. Cdk1 dependent phosphorylation of Sae2 is important for this processing step. **(C)** Telomere replication: The G strand is replicated by the lagging strand machinery which results in a short 3` ssDNA overhang after removal of the RNA primer. The leading strand machinery instead is expected to generate blunt ends by replication of the C strand. To generate the 3´ ssDNA strand overhangs of telomeres these blunt ends are resected by MRX and Sae2, similar to the situation in recombination resection. Also here resection by MRX and Sae2 depends on Cdk1 phosphorylation of Sae2 and processive resection is facilitated by Dna2/Sgs1 or Exo1. Figure from (Longhese et al. 2010).

Besides mediating DNA end resection, the MRN(X) complex is also important as a scaffold factor in HR, which tethers the two DNA ends of a DSB and holds them in close proximity. This function is dependent on the Rad50 zinc-hook domain, which mediates MRN(X) intercomplex interactions (Hopfner et al. 2002). Atomic force microscopy studies monitored this zinc-hook dependent MRN(X) intercomplex formation in the presence of DNA on a molecular level (de Jager et al. 2001; Hopfner et al. 2002; Moreno-Herrero et al. 2005).

2.4.2 The Mre11-Rad50-Nbs1 complex in meiotic recombination

The MRN(X) complex had long been implicated to be important for the DNA end resection in recombination repair since mutations in the genes encoding the complex cause a complete block of 5´ strand removal in meiosis (Ivanov et al. 1992; Keeney and Kleckner 1995; Usui et al. 1998). The roles of MRN(X) in meiosis are probably best understood for *S. cerevisiae*. Here, the complex is important for several sequential steps of the process (Figure 2.5 B): (1) First, MRX is recruited to meiotic DSB sites before the formation of DSBs, via its C-terminal region (Furuse et al. 1998; Usui et al. 1998). It then facilitates the generation of DSBs by Spo11, which is probably also mediated by the Mre11 C-terminus and is independent of Mre11`s nuclease activity as well as stable complex formation with Rad50 and Xrs2. This was shown by studies with the mre11-58 mutation, which is deficient for all of these functions, but still functional in meiotic DSB formation (Usui et al. 1998). (2) The MRX complex is crucial for the endonucleolytic removal of the covalently bound Spo11 from the 5´ strands of the DSB ends. The nuclease activity of Mre11 is likely responsible for this processing step since separation of function mutants (Mre11S), which have a defect in Spo11 removal, are nuclease deficient *in vitro* (Furuse et al. 1998; Usui et al. 1998; Moreau et al. 1999). Furthermore, nucleolytic removal of Spo11 depends on the Sae2/Com1 protein (McKee and Kleckner 1997; Prinz et al. 1997). Remarkably, a specific class of Rad50 separation of function mutants, named Rad50S, resembles the same phenotype as Δsae2 in meiosis (Alani et al. 1990; Keeney

et al. 1997). The Rad50S mutations cluster to the outer surface of the ABC-ATPase dimer in the homologous archaeal *P. furiosus* crystal structure, suggesting that they might affect a Sae2 interaction site, which is important for Spo11 removal. However, a direct *in vitro* interaction of MRX and Sae2 could not be observed (Hopfner et al. 2000; Lengsfeld et al. 2007). After removal of Spo11, the MRX complex also stimulates recruitment of other nucleases, which function in the processive generation of ssDNA tails for meiotic D-loop formation. Here especially the Exo1 nuclease plays an important role, whereas the activity of the SGS1/DNA2 complex appears to be rather dispensable (Zakharyevich et al. 2010; Keelagher et al. 2011).

2.4.3 The Mre11-Rad50-Nbs1 complex in telomere maintenance

Beside its many functions in DSB repair and signaling, the MRN(X) complex plays also crucial roles in telomere maintenance. Telomeres are specialized nucleoprotein structures that protect the ends of eukaryotic chromosomes from degradation, fusion, recombination and recognition by the DNA-damage repair machinery (Faure et al. 2010). They consist of several G-rich sequence repeats and a terminal 3´ ssDNA tail, which is capped by specific protecting factors like the CST (Cdc13-Stn1-Ten1) complex in *S. cerevisiae*. The length of telomeres is maintained by the telomerase complex, which uses its RNA template to add G-rich telomeric repeats to the terminal 3´ ssDNA tail (Hug and Lingner 2006). Recruitment of the telomerase to 3´ ssDNA ends strongly depends on the MRX complex and Tel1 as studies in *S. cerevisiae* showed. MRX recruits Tel1 to short telomeres, where its kinase activity stimulates telomerase dependent telomere lengthening (Goudsouzian et al. 2006; Hector et al. 2007; Hirano et al. 2009). In addition, the MRN(X) complex is also important for the generation of 3´ ssDNA overhangs after telomere leading strand replication (Figure 2.5 C). Replication at telomeres is thought to result in blunt ends on the leading strand. In *S. cerevisiae*, the generation of 3´ ssDNA overhangs on the leading strand blunt end is carried out by the MRX complex and Sae2, which initiate the resection of the 5´ strand. The thereby created short 3´ ssDNA overhang is then extended by Sgs1/Dna2 or Exo1 and finally capped by the CST complex (Bonetti et al. 2009; Mimitou and Symington 2009; Longhese et al. 2010).

2.4.4 The Mre11-Rad50-Nbs1 complex in non-homologous end joining pathways

Studies with mammalian cells showed that the MRN complex is involved in both the classical NHEJ (c-NHEJ) as well as alternative NHEJ pathways (a-NHEJ). Even though it is no core factor of mammalian c-NHEJ, it is crucial for V(D)J recombination, which is strongly dependent on c-NHEJ (Deriano et al. 2009; Helmink et al. 2009). In addition, depletion or inhibition of Mre11 reduces the end-joining efficiency of I-SceI endonuclease-induced DSBs up to 40% in both wild-type and Xrcc4$^{-/-}$ cells, indicating a role of MRN in mitotic repair by both c-NHEJ and a-NHEJ (Rass et al. 2009; Xie et al. 2009). However, the repair of I-SceI endonuclease-induced DSBs requires the nuclease activity of Mre11 only in deleterious a-NHEJ but not in c-NHEJ (Zhuang et al. 2009). The exact role of the MRN complex in c-NHEJ is only poorly understood and needs further studying, but it was proposed that one of the major roles for MRN in c-NHEJ is activation of the ATM checkpoint kinase, which is required for efficient c-NHEJ dependent repair (Rass et al. 2009).

In recent years more and more evidence has accumulated for alternative end-joining pathways, which can promote end-joining repair even in the absence of different c-NHEJ core factors. One important pathway is the so called micro-homology pathway (MMEJ) in which DSB ends are joined for ligation via short stretches of microhomology. The MRN complex is an essential component of MMEJ and the nuclease activity of Mre11 catalyzes short range resection at DSBs which generates ends with compatible microhomology sequences (Figure 2.6 A and B) (Rahal et al. 2010).

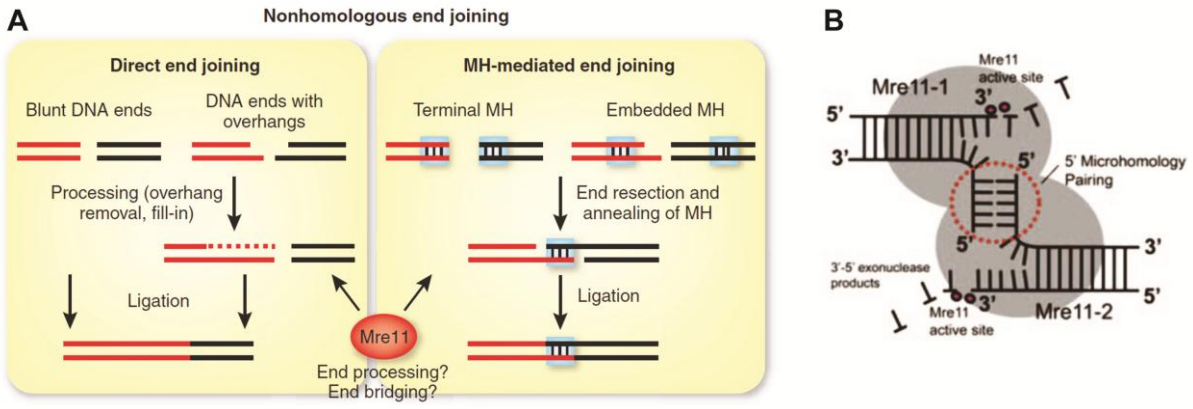

Figure 2.6: Functions of the MRN complex in non-homologous end joining pathways (A) Potential functions of Mre11 in C-NHEJ and A-NHEJ pathways. Repair of DSBs by NHEJ can be executed via direct (left side) and microhomology (MH)-mediated end joining (right side). Whereas blunt DNA ends can be ligated directly, DNA ends with overhangs may require fill-in or end resection before ligation. In micro-homology

mediated end-joining (MMEJ), the two ends are joined for ligation via short stretches of microhomologous sequences. The nuclease function of Mre11 is important for the resection procedure which generates these compatible ends. Figure from (Zha et al. 2009) **(B)** Schematic model for Mre11 dimer-mediated MMEJ: The Mre11 homodimer may bind two DNA ends. The 3' ends are degraded by Mre11 3'-5' exonuclease activity in the Mre11 active site whereas microhomology pairing of 5` tails takes place outside Mre11´s active site. Figure from (Rahal et al. 2010).

In *S. cerevisiae* where NHEJ plays only a minor role for mitotic DSBR, all components of MRX are essential core factors of the end-joining machinery and are *e.g.* required for the efficient rejoining of linear plasmid DNA molecules with cohesive ends (Boulton and Jackson 1998; Critchlow and Jackson 1998). Since a nuclease deficient H125N Mre11 mutant has no end-joining defect in *S. cerevisiae*, the complex is here assumed to rather play a role as a structural scaffolding protein for other NHEJ factors (Moreau et al. 1999; Chen et al. 2001).

2.5 The Mre11-Rad50-Nbs1 complex in DNA damage signaling

The MRN(X) is not only a mediator of DSBR but also a DNA damage signal transducer and promotes activation of cell-cycle arrest (and apoptosis in metazoan organisms) in response to DSBs by recruiting and activating the checkpoint kinase ATM (Tel1 in yeast). The MRN complex acts both upstream and downstream of ATM and there are two populations of the complex at DSB sites. One population associates independent of ATM at a very early time point to sites of DNA damage and acts upstream as a DNA damage sensor, which helps to recruit and activate ATM. Localization of the second population to DSBs is instead dependent on the phosporylation activity of ATM (Lavin 2008). Evidence for an upstream function of MRN has been reported from various different studies: Cells from NBS and A-TLD patients, which possess hypomorphic mutations in either the Nbs1 or Mre11 gene show decreased ATM activation after irradiation (Uziel et al. 2003). ATM is also activated by MRN *in vitro*, where it was observed to stimulate the dissociation of inactive ATM dimers into active monomers (Lee and Paull 2005). Nbs1 and its *S. cerevisiae* homologue Xrs2 contain a binding site for ATM at the C-terminal end of the protein close to the binding site for Mre11. Human cells with a deletion of the C-terminal ATM binding site in Nbs1 exhibit decreased phosphorylation of some ATM substrates and intra-S and G2/M checkpoint defects, although ATM activation is normal. Similarly a C-terminal Xrs2 deletion mutant is deficient in Tel1

dependent phosphorylation of the downstream kinase Rad53 in *S. cerevisiae* (Nakada et al. 2003; Falck et al. 2005).

In addition to monomerization, also ATM autophosphorylation at different sites is a hallmark of its activation *in vivo*. Activated ATM phosphorylates a variety of substrates which promotes both DNA damage checkpoint signaling as well as accumulation of repair proteins at DSB sites. Importantly, also the MRN complex is a downstream factor of ATM in DSB repair. Human Nbs1 is phosphorylated at residues 273 and 343, and once modified, facilitates phosphorylation of other ATM targets like *e.g.* SMC1, which is an important event for activation of the intra S-phase checkpoint. (Falck et al. 2002; Yazdi et al. 2002).

Phosphorylation of the histone variant H2AX by ATM (γH2AX) further facilitates the accumulation of MRN at DSBs and repair foci formation (Figure 2.7A). γH2AX is bound by the adaptor protein MDC1, which is additionally phosphorylated by the CK2 kinase. MDC1 then binds to MRN via the N-terminal Forkhead and BRCT domains of Nbs1 (Chapman and Jackson 2008; Melander et al. 2008; Spycher et al. 2008). MRN in turn recruits and activates more ATM molecules, which leads to an amplification of ATM promoted checkpoint signaling via the downstream kinase Chk2 and effector molecules like p53 and p21 (Figure 2.7B). In addition, MDC1 recruits the ubiquitin ligase RNF8, which in cooperation with UBC13 ubiquitinates H2AX, thereby leading to the accumulation of further repair proteins and repair foci formation (Deribe et al. 2010).

DSB induced checkpoint signaling by the ATM homologue Tel1 in *S. pombe* and *S. cerevisae* plays rather a minor role in addition to the activity of the Mec1 checkpoint kinase (ATR homologue in yeast), which is activated by ssDNA/RPA during resection of DSBs. However, Tel1 checkpoint signaling becomes important in the absence Mec1. In addition, MRX dependent Tel1 activity is crucial for telomere maintenance and a deletion of the Tel1 binding region in Xrs2 as well as functional mutations in all MRX proteins result in shortened telomeres (Haber 1998; Shima et al. 2005; Tsukamoto et al. 2005).

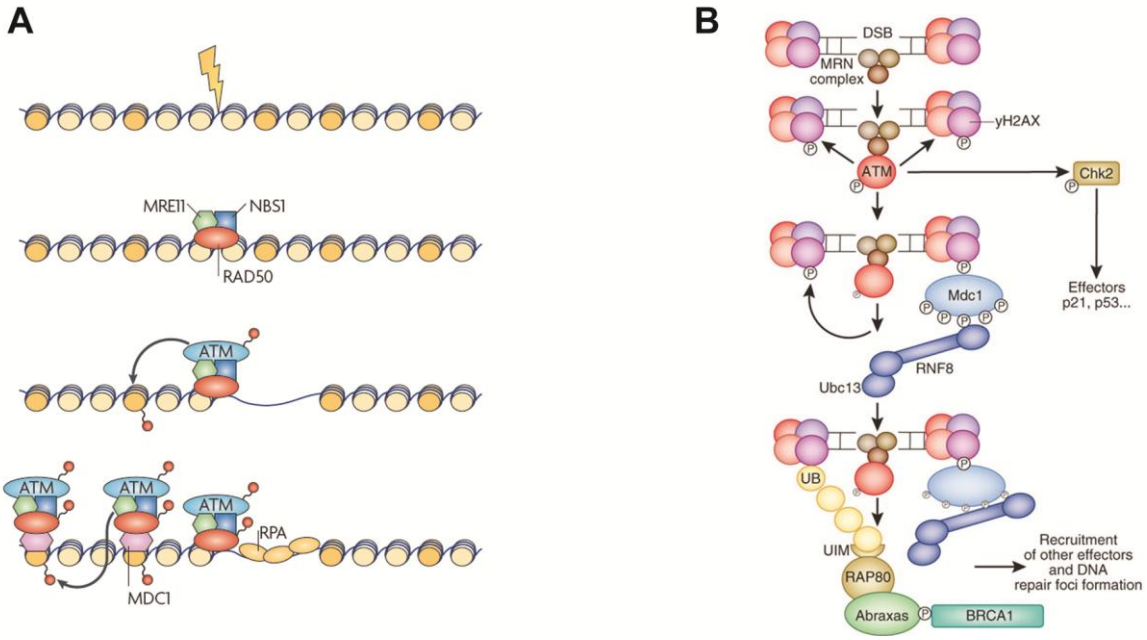

Figure 2.7: Mre11 is a co-activator of the cell-cycle checkpoint kinase ATM and promotes ATM dependent foci formation at the site of DSBs (A) A model for MRN dependent recruitment and activation of ATM at DSBs. After recruitment and co-activation by MRN the ATM kinase phosphorylates the histone variant H2AX in DSB-flanking nucleosomes. The MDC1 adaptor protein binds to γ-H2AX and promotes accumulation of more MRN and ATM molecules. By this, the repair machinery is spread at the site of break and the damage signaling by ATM is amplified. Figure from (Misteli and Soutoglou 2009) **(B)** Schematic model for ATM mediated checkpoint activation and repair foci formation. Activated ATM phosphorylates the downstream checkpoint kinase Chk2 which gets thereby activated and promotes cell-cycle arrest via effector proteins like p53 and p21. Moreover MDC1, when bound to γ-H2AX, recruits the RNF8-Ubc13 complex which ubiquinitates histones via Lys63 linkage. Ubiquitinated histones facilitate acummulation of Rap80, Abraxas and BRCA1, which help to promote foci formation of the repair machinery. Figure from (Deribe et al. 2010).

2.6 Diseases linked with mutations in Mre11-Rad50-Nbs1

The functional association between MRN and ATM is shown by the closely related disease syndromes linked with mutations in their genes: Ataxia telangiectasia (A-T) is caused by disruption of ATM, while A-T like disease (A-TLD), Nijmegen breakage syndrome (NBS) and NBS-like disease are caused by hypomorphic mutations in Mre11, Nbs1 and Rad50 respectively (Carney et al. 1998; Varon et al. 1998; Stewart et al. 1999; Frappart and McKinnon 2006; Waltes et al. 2009). These diseases share radiation sensitivity and chromosome instability of patient derived cells. In addition they are characterized by distinct neuropathologic phenotypes and patients have an inherited cancer predisposition. Although in

the case of A-TLD, cancer development was reported so far only for one specific subtype, which in addition also causes mental retardation (Uchisaka et al. 2009). The characteristic hallmark of AT and A-TLD is neurodegeneration, whereas NBS and NBS-like disease are characterized by microcephaly, mental retardation, a bird like face and growth defects. Based on *in vivo* studies with mouse models, this nonconformity of the neuropathology was proposed to result from different impacts of the mutations on DNA DSB signaling. Both A-TLD and NBS cells are partly defective in DSB repair and in the activation of the checkpoint kinase ATM. However, the residual ATM activation is lower in A-TLD cells compared to NBS cells. Therefore, A-TLD cells fail to efficiently induce ATM dependent apoptosis. As a consequence more malfunctional cells may be incorporated into the nervous system where they ultimately die and cause the observed neurodegeneration phenotype. NBS cells in contrast can activate ATM more efficiently and possess a higher apoptosis rate. Therefore, fewer brain cells survive initially, which may explain why NBS results in the development of microcephaly. (Shull et al. 2009).

Recently, a heterozygous Mre11 mutation was reported, which causes an NBS-like disease instead of A-TLD. Consistently, cells derived from NBS-like disease patients display a higher rate of ATM activation compared to A-TLD cells, indicating that also here differences in the apoptosis rate are the reason for the distinct neuropathological phenotypes (Matsumoto et al. 2011). While the somewhat related disease phenotypes demonstrate the tight functional interconnection of the three MRN components in both DNA repair and DSB signaling, the molecular basis for similarities and differences of A-T, A-TLD and NBS is poorly understood and lacks a structural framework for the interaction of Nbs1 with Mre11.

2.7 Objectives

DNA double-strand breaks (DSBs) are one of the most serious threats for the stability of the genome. They can occur accidently by failures in genome metabolism and by exogenous sources. In addition, they are also important intermediates in many DNA metabolism processes. The Mre11-Rad50-Nbs1 complex is a central component of the cellular response, which mediates the repair of DSBs. The complex senses, binds and stabilizes broken DSB ends. It also initiates DSB repair by recruiting other repair factors and by nucleolytic processing of the DNA ends. Importantly, it is also involved in cell-cycle checkpoint signaling by activating the kinase ATM. Mre11 and Rad50 exist in all domains of live, whereas Nbs1 is found only in eukaryotic organisms. Nbs1 is thought to play different regulatory roles in the complex. Most importantly, it is crucial for the signaling of sensed DNA damages to the cell cycle checkpoints. This function is mediated by direct binding of Nbs1 to the checkpoint kinase ATM and additionally depends on the concerted action of all three MRN proteins. Nbs1 also mediates important interactions of the MRN complex with other repair factors via its N-terminal phosphoprotein binding modules. Moreover, Nbs1 was reported to influence the DNA binding affinity and specificity of Mre11-Rad50 and to stimulate the nucleolytic processing activity of Mre11 on DNA hairpin structures.

Many biochemical roles of the MRN complex have been revealed in the last years and structures of the prokaryotic Mre11 and Rad50 proteins have been contributed importantly to the understanding of principle functions of the catalytic Mre11-Rad50 core complex. However, the structure of the eukaryotic MRN complex was only poorly characterized and there were no high resolution structures of any eukaryotic MRN protein available, when the work for this thesis was started. Therefore, it was not understood on a structural level how Nbs1 interacts with Mre11 and Rad50 and how it can thereby mediate its regulatory influences on the Mre11-Rad50 core complex. Thus, it was of high interest to gain insights into the eukaryotic MRN complex by atomic high resolution structures. The aim of this thesis was therefore to purify and crystallize a stable complex of Mre11-Nbs1 and to determine its atomic structure. The crystal structure should then be validated by biochemical studies. Here, one focus should also be on the structural characterization of disease causing Mre11 mutations. Furthermore, it was aimed to study motifs, which from the analysis of the structure were suggested to be functionally important, *in vivo* using *S. cerevisiae* as a model system.

3. MATERIALS AND METHODS

3.1 Materials

All chemicals used in this work were of the highest available grade obtained from Carl Roth, Merck, or Sigma-Aldrich, unless otherwise stated. Crystallisation screens and tools were from Hampton Research, NeXtal (QIAGEN), and Jena Bioscience. RP-HPLC purified oligonucleotides for EMSAs and crystallization were purchased from Thermo Scientific. Enzymes for molecular biology were obtained from Fermentas, Finnzymes, or New England Biolabs.

3.1.1 Antibodies

Table 3.1: List of used antibodies:

Primary Antibodies

Antibody	Source	Dilution	Company
α-c-Myc (monoclonal - 9E10)	Mouse	1:3000 for western blot 1:500 for immunofluorescence	Sigma-Aldrich, Taufkirchen
α-HA (monoclonal 12CA5)	Mouse	1:1000 for western blot	Abcam, Cambridge UK
α-Rad50 (*S. cerevisiae*)	Rabbit	1:1000 for western blot	Gift from J. Petrini, New York, USA
α-Xrs2 *(S. cerevisiae)*	Rabbit	1:1000 for western blot	Gift from J. Petrini, New York, USA
α-Actin (monoclonal ab8224)	Mouse	1:3000 for western blot	Abcam, Cambridge UK

Secondary Antibodies	Source	Dilution	Company
α-Mouse IgG - HRP	Sheep	1:3000 for western blot	GE Healthcare,
α -Mouse IgG (H+L) Alexa Fluor 488	Goat	1:2000 for western blot	Invitrogen, Darmstadt
α -Rabbit IgG (H + L)-HRP	Goat	1:2000 for western blot	Biorad, München

3.1.2 Oligonucleotides

Table 3.2: Oligonucleotide list - biochemical assays

Name	Label	Sequence
poly (T) 60mer ssDNA	5`-6-FAM	TTTTTTTTTTTTTTTTTTTTTTTTTTTTTTTTTTTTTTTTTTTTTTTTTTTTTTTTTTTT
13mer blunt end hairpin dsDNA	5`-6-FAM	CATCGTGACTTCGTTTTCGAAGTCACGATG

Table 3.3: Oligonucleotide list - *S. pombe* constructs:

SpNbs1 fwd	TTTTTTTGGATCCATGTGGATAATTGAGGCTGAGGGTG
SpNbs1 rev	AATTGCGGCCGCTTAAAAGTGAAACTTGAGATCATTAAATTCATCG
SpNbs1 E474 fwd	TTTTTTTGGATCCGAATCTGAAGATGATAAAGCATTTGAGG
SpNbs1 K531 SalI rev	TTTTTGTCGACTTTTTGTGAAGCTTTCTTTTG
SpNbs1 K531 NotI rev	TTTTTTTGCGGCCGCTCATTATTTTTGTGAAGCTTTCTTTTGAAATTTTTTA A
SpNbs1 E474 TEV f	AAAAAGTCGACGAAAATCTTTACTTCCAAGGTGAATCTGAAGATGATAA AGCATTTGAGG
SpNbs1 K428 fwd	AAAAAGGATCCAAGACCAAGGTTGAGTATGTTTCC
SpNbs1 F524E fwd	CGTAAAAATTTTAAAAAAGAGCAAAAGAAAGCTTCACA
SpNbs1 F524E rev	TGTGAAGCTTTCTTTTGCTCTTTTTTAAAATTTTTACG
SpNbs1 K522E K526E fwd	CAAAATATTATTCGGGCCGTAAAAATTTTGAAAAATTTCAAGAGAAAGCT TCACAAAAAGCACCTTTACA
SpNbs1 K522E K526E rev	TGTAAAGGTGCTTTTTGTGAAGCTTTCTCTTGAAATTTTTCAAAATTTTTA CGGCCCGAATAATATTTTG
Sp Mre11 fwd	TTTTTTGGATCCATGCCAAATGACCCCTCAGATATG
Sp Mre11 rev	TTTTTTTGCGGCCGCTCATTAATCATCTAAAATTTCGTCATCCTCGTTATC
Sp Mre11 E15 fwd	TTTAATGGATCCGAAAATACTATTAGAATCTTAATATCTTCTG
Sp Mre11 D7 fwd Prescission	TTTTTGGATCCCTGGAGGTTCTGTTTCAAGGGCCCGATATGAATAATGAA CTTCACAATGAAAATACTATTAG
SpMre11 E15 fwd Linker8	AAAAAGTCGACGGTTCTGCTGGTTCTGCTGGTTCTGAAAATACTATTAGA ATCTTAATATCTTCTG
SpMre11 K413 rev NotI	TTTTTTTGCGGCCGCCTATTACTTTTTAAGATAAAATTGGACAACATCTG
SpMre11 K413 rev SalI	TTTTTGTCGACCTTTTTAAGATAAAATTGGACAACATCTG

SpMre11 N421 rev NotI	TTTTTTTGCGGCCGCTTAGTTTCTTTTAGACCTAGTGTATTTTTTTTTAAG
SpMre11 R85A fwd	CACTTCGCTCACTCGCATTAAACTGTTTAG
SpMre11 R85A rev	CTAAACAGTTTAATGCGAGTGAGCGAAGTG
SpMre11 N122S fwd	CCGAACATCAGCGTGGCTATAC
SpMre11 N122S rev	GTATAGCCACGCTGATGTTCGG
SpMre11 W215C fwd	CGGGATGAATGCTTCAACTTATTG
SpMre11 W215C rev	CAATAAGTTGAAGCATTCATCCCG
SpMre11 W248R fwd	GACTTCGTGTTAAGGGGACACGAAC
SpMre11 W248R rev	GTTCGTGTCCCCTTAACACGAAGTC
SpMre11 H134S fwd	CAATTCATGGTAATTCCGATGACCCTTCTG
SpMre11 H134S rev	CAGAAGGGTCATCGGAATTACCATGAATTG
GST for	TTTTTTTCATATGTCCCCTATACTAGGTTATTGG
GST rev	AAAAAGGATCCCAGGGGCCC

Table 3.4: Oligonucleotide list - *S. cerevisisae* constructs:

HindIII_PAW8_13Myc_4417_f	TTTTTTAAGCTTATGCATTTCTTTCCAGACTTG
NotI_ScMre11_cds53_r	TTTTTTTGCGGCCGCTCTAGAACTAGTGG
P527 BamHI f (ScMre11end)	TTTTTGGATCCGTTTTCTTTTCTTAGCAAG
ScMre11 L72F fwd	GTCACTCTACCAAGTATTTAAGACTTTGAGATTATG
ScMre11 L72F rev	CATAATCTCAAAGTCTTAAATACTTGGTAGAGTGAC
ScMre11 L72R fwd	GTCACTCTACCAAGTAAGAAAGACTTTGAGATTATG
ScMre11 L72R rev	CATAATCTCAAAGTCTTTCTTACTTGGTAGAGTGAC
ScMre11 R76A fwd	GTACTGAAGACTTTGGCTTTATGTTGCATGGG
ScMre11 R76A rev	CCCATGCAACATAAAGCCAAAGTCTTCAGTAC
ScMre11 R76K fwd	CTGAAGACTTTGAAATTATGTTGCATGG
ScMre11 R76K rev	CCATGCAACATAATTTCAAAGTCTTCAG
ScMre11 R76Qfwd	GTACTGAAGACTTTGCAATTATGTTGCATGG
ScMre11 R76Q rev	CCATGCAACATAATTGCAAAGTCTTCAGTAC
ScMre11 R76M fwd	CTGAAGACTTTGATGTTATGTTGCATGGG
ScMre11 R76M rev	CCCATGCAACATAACATCAAAGTCTTCAG

ScMre11 R76F fwd	GTACTGAAGACTTTGTTTTTATGTTGCATGGGTG
ScMre11 R76F rev	CACCCATGCAACATAAAAACAAAGTCTTCAGTAC
ScMre11 S91A fwd	CGAGTTAGAATTATTGGCTGATCCCTCACAAGTT
ScMre11 S91A rev	AACTTGTGAGGGATCAGCCAATAATTCTAACTCG
ScMre11 S91E fwd	TGCGAGTTAGAATTATTGGAAGATCCCTCACAAGTTTTTC
ScMre11 S91E rev	GAAAAACTTGTGAGGGATCTTCCAATAATTCTAACTCGCA
ScMre11 D109N fwd	CCAACGTTAACTATGAGAATCCCAACTTTAATATTTC
ScMre11 D109N rev	GAAATATTAAAGTTGGGATTCTCATAGTTAACGTTGG
ScMre11 D109L fwd	CCAACGTTAACTATGAGTTACCCAACTTTAATATTTC
ScMre11 D109L rev	GAAATATTAAAGTTGGGTAACTCATAGTTAACGTTGG
ScMre11 D109M fwd	CAACGTTAACTATGAGATGCCCAACTTTAATATTTC
ScMre11 D109M rev	GAAATATTAAAGTTGGGCATCTCATAGTTAACGTTG
ScMre11 D109F fwd	CCAACGTTAACTATGAGTTTCCCAACTTTAATATTTC
ScMre11 D109F rev	GAAATATTAAAGTTGGGAAACTCATAGTTAACGTTGG
ScMre11 N113S fwd	GGACCCCAACTTTTCTATTTCTATTCCCG
ScMre11 N113S rev	CGGGAATAGAAATAGAAAAGTTGGGGTCC
ScMre11 D127A fwd	GTAATCATGATGCTGCGTCGGGGGAC
ScMre11 D1127A rev	GTCCCCCGACGCAGCATCATGATTAC
ScMre11 D127R fwd	GGTAATCATGATAGAGCGTCGGGGGAC
ScMre11 D127R rev	GTCCCCCGACGCTCTATCATGATTACC
ScMre11 D127R D131R fwd	GGCATATCAGGTAATCATGATAGAGCGTCGGGGAGATCACTGTTG TGTCCTATGGA
ScMre11 D127R D131R rev	TCCATAGGACACAACAGTGATCTCCCCGACGCTCTATCATGATTAC CTGATATGCC
ScMre11 I139F fwd	GTGTCCTATGGATTTTCTTCATGCGACTGG
ScMre11 I139F rev	CCAGTCGCATGAAGAAAATCCATAGGACAC
ScMre11 T143I fwd	GATATACTTCATGCGATTGGTCTAATAAATCA
ScMre11 T143I rev	TGATTTATTAGACCAATCGCATGAAGTATATC
ScMre11 P199A fwd	GTCACTTTTGAAGTAGCTACTATGCGAGAAGG
ScMre11 P199A rev	CCTTCTCGCATAGTAGCTACTTCAAAAGTGAC
ScMre11 F229E fwd	CATTTTTACCTGAACAGGAGTTGCCAGATTTCCTGG

ScMre11 F229E rev	CCAGGAAATCTGGCAACTCCTGTTCAGGTAAAAATG
ScMre11 Δ127-133 Insert Pf_RTQRG fwd	CATGATAGAACTCAAAGAGGTTTGTGTCCTATGGATATACTTCATGC
ScMre11 Δ127-133 Insert Pf_RTQRG rev	ACACAAACCTCTTTGAGTTCTATCATGATTACCTGATATGCCGAATAC
ScMre11 Δ127-134 Insert_ Pf_RTQRGP fwd	ATGATAGAACTCAAAGAGGTCCTTGTCCTATGGATATACTTCATGCGAC
ScMre11 Δ127-134 Insert_ Pf_RTQRGP rev	GGACAAGGACCTCTTTGAGTTCTATCATGATTACCTGATATGCCGAATAC
3HA pYM-N12 BamHI f	TTTTTGGATCCAATACCCATACGATGTTCCTGACTATG
3HA pYM-N12 EcoRI r	TTTTTGAATTCACTAAGCGTAATCTGGAACGTCATATGG
NLS BamHI fwd	TATAAGGATCCAATCTCCAAAAAAGAAGAGAAAGGTCGAAATCCCCGGGTTAATTAACGGTG

3.1.3 Plasmids

Table 3.5: Plasmid list *E. coli*:

Construct name	Encoded sequences	Restriction site	Tag	Plasmid name
Sp Mre11 1-649 His10TEV	Sp Mre11 aa 1-649 Wt	BamHI NotI	N-10x His + TEV site	pKP29His10 TEV
pET29 SpMre11 1-478 (from Nora Assenmacher, AG Hopfner)	Sp Mre11 aa 1-478 Wt	NdeI NotI	No Tag	pKP29
pGEX-6P-II SpMre11 1-421	Sp Mre11 aa 1-421	BamHI NotI	N-GST	pGEX-6P-II
pGEX-6P-II SpMre11 1-421 R85A	Sp Mre11 aa 1-421 R85A	BamHI NotI	N-GST	pGEX-6P-II
pGEX-6P-II SpMre11 1-421 H134S	Sp Mre11 aa 1-421 H134S	BamHI NotI	N-GST	pGEX-6P-II
pET21-GST SpMre11 15-421	Sp Mre11 aa 15-421	BamHI NotI	N-GST	pET21-GST
pET21-GST SpMre11 15-421 H134S	Sp Mre11 aa 15-421 H134S	BamHI NotI	N-GST	pET21-GST
pGEX-6P-II SpMre11 1-413	Sp Mre11 aa 1-413	BamHI NotI	N-GST	pGEX-6P-II
pGEX-6P-II SpMre11 1-413 N122S	Sp Mre11 aa 1-413 N122S	BamHI NotI	N-GST	pGEX-6P-II
pGEX-6P-II SpMre11 1-413 W215C	Sp Mre11 aa 1-413 W215C	BamHI NotI	N-GST	pGEX-6P-II
pGEX-6P-II SpMre11 1-413 W248R	Sp Mre11 aa 1-413 W248R	BamHI NotI	N-GST	pGEX-6P-II
pGEX-6P-II SpMre11 1-413 H134S	Sp Mre11 aa 1-413 H134S	BamHI NotI	N-GST	pGEX-6P-II
pGEX-6P-II SpMre11 15-413	Sp Mre11 aa 15-413	BamHI NotI	N-GST	pGEX-6P-II

Construct name	Encoded sequences	Restriction site	Tag	Plasmid name
pGEX-6P-II SpNbs1 1-613	Sp Nbs1 aa 1-613	BamHI NotI	N-GST	pGEX-6P-II
pGEX-6P-II SpNbs1 428-613	Sp Nbs1 aa 428-613	BamHI NotI	N-GST	pGEX-6P-II
pGEX-6P-II SpNbs1 428-613 F524E	Sp Nbs1 aa 428-613 F524E	BamHI NotI	N-GST	pGEX-6P-II
pGEX-6P-II SpNbs1 428-613 K522E K526E	Sp Nbs1 aa 428-613 K522E K526E	BamHI NotI	N-GST	pGEX-6P-II
pGEX-6P-II SpNbs1 474-613	SpNbs1 474-613	BamHI NotI	N-GST	pGEX-6P-II
pGEX-6P-II SpNbs1 474-531	SpNbs1 474-531	BamHI NotI	N-GST	pGEX-6P-II
pGEX-6P-II SpNbs1 474-531-L8-SpMre11 15-413	Sp Nbs1 aa 474-531 Linker (GSAGSAGS)	BamHI, SalI, NotI	N-GST	pGEX-6P-II
pET21-GST SpMre11 7-413 -L7TEV-SpNbs1 474-531	Sp Mre11 aa 7-413 TEV-site Sp Nbs1 aa 474-531	BamHI, SalI, NotI	N-GST	pET21-GST

Table 3.6: Plasmid list *S. cerevisiae:*

Construct name	Encoded sequences	Restriction site	Tag	Plasmid name
pRS416 ScMre11 Wt (D´Amours and Jackson, 2001)	Sc Mre11 Wt	NotI, HindIII	C-13myc	pRS416
pRS416 ScMre11 Wt-NLS	ScMre11 Wt-NLS	NotI, HindIII	C-13myc	pRS416
pRS416 ScMre11 L72F	ScMre11 L72F	NotI, HindIII	C-13myc	pRS416
pRS416 ScMre11 L72R	ScMre11 L72R	NotI, HindIII	C-13myc	pRS416
pRS416 ScMre11 R76A	ScMre11 R76A	NotI, HindIII	C-13myc	pRS416
pRS416 ScMre11 R76A-NLS	ScMre11 R76A-NLS	NotI, HindIII	C-13myc	pRS416
pRS416 ScMre11 R76K	ScMre11 R76K	NotI, HindIII	C-13myc	pRS416
pRS416 ScMre11 R76K-NLS	ScMre11 R76K-NLS	NotI, HindIII	C-13myc	pRS416
pRS416 ScMre11 R76M	ScMre11 R76M	NotI, HindIII	C-13myc	pRS416
pRS416 ScMre11 R76M D109N	ScMre11 R76M D109N	NotI, HindIII	C-13myc	pRS416
pRS416 ScMre11 R76Q D109N	ScMre11 R76Q D109N	NotI, HindIII	C-13myc	pRS416
pRS416 ScMre11 R76F D109M	ScMre11 R76F D109M	NotI, HindIII	C-13myc	pRS416
pRS416 ScMre11 R76M D109L	ScMre11 R76M D109L	NotI, HindIII	C-13myc	pRS416
pRS416 ScMre11 R76M D109M	ScMre11 R76M D109M	NotI, HindIII	C-13myc	pRS416
pRS416 ScMre11 R76M D109F	ScMre11 R76M D109F	NotI, HindIII	C-13myc	pRS416

Construct name	Encoded sequences	Restriction site	Tag	Plasmid name
pRS416 ScMre11 S91A	ScMre11 S91A	NotI, HindIII	C-13myc	pRS416
pRS416 ScMre11 S91A-NLS	ScMre11 S91A-NLS	NotI, HindIII	C-13myc	pRS416
pRS416 ScMre11 S91E	ScMre11 S91E	NotI, HindIII	C-13myc	pRS416
pRS416 ScMre11 S91E-NLS	ScMre11 S91E-NLS	NotI, HindIII	C-13myc	pRS416
pRS416 ScMre11 D109N	ScMre11 D109N	NotI, HindIII	C-13myc	pRS416
pRS416 ScMre11 N113S	ScMre11 N113S	NotI, HindIII	C-13myc	pRS416
pRS416 ScMre11 N113S-NLS	ScMre11 N113S-NLS	NotI, HindIII	C-13myc	pRS416
pRS416 ScMre11 D127A	ScMre11 D127A	NotI, HindIII	C-13myc	pRS416
pRS416 ScMre11 D127R	ScMre11 D127R	NotI, HindIII	C-13myc	pRS416
pRS416 ScMre11 D127R D131R	ScMre11 D127R D131R	NotI, HindIII	C-13myc	pRS416
pRS416 ScMre11 Δ127-133 Insert Pf_RTQRG	ScMre11 Δ127-133 Insert Pf_RTQRG	NotI, HindIII	C-13myc	pRS416
pRS416 ScMre11 Δ127-134 Insert_ Pf_RTQRGP	ScMre11 Δ127-134 Insert_ Pf_RTQRGP	NotI, HindIII	C-13myc	pRS416
pRS416 ScMre11 I139F	ScMre11 I139F	NotI, HindIII	C-13myc	pRS416
pRS416 ScMre11 T143I	ScMre11 T143I	NotI, HindIII	C-13myc	pRS416
pRS416 ScMre11 P199A	ScMre11 P199A	NotI, HindIII	C-13myc	pRS416
pRS416 ScMre11 F229E	ScMre11 F229E	NotI, HindIII	C-13myc	pRS416
pRS315 ScMre11 Wt	ScMre11 Wt	NotI, HindIII	3xHA Tag	pRS315
pRS315 ScMre11 R76A	ScMre11 R76A	NotI, HindIII	3xHA Tag	pRS315

3.1.4 Strains

Table 3.7: *Escherichia coli* strains

Strain	Genotype	Source
XL1 blue	recA1 endA1 gyrA96 thi-1 hsdR17 supE44 relA1 lac [F´ proAB lacIqZΔM15 Tn10 (Tetr)]	Stratagene, Heidelberg
Rosetta (DE3)	F– ompT hsdSB(rB– mB-) gal dcm (DE3) pRARE2 (CamR)	Novagen, Madison USA
B834(DE3)	F– ompT hsdSB(rB– mB-) met gal dcm (DE3)	Novagen, Madison USA

Table 3.8: *Saccharomyces cerevisiae* strains

Strain	Genotpye	Origin
W303	*Mata/α; ura3-1, trp1-1, his3-11,15; leu2-3, 112; ade2-1; can1-100; GAL+*	Britta Coordes (lab of Katja Strässer, Gene Center)
W303 - Δmre11	*mre11delta::KanMX4, Mata/α; ura3-1, trp1-1, his3-11,15; leu2-3, 112; ade2-1; can1-100*	Ilaria Guerini (lab of Prof. Steve Jackson, Cambridge)

3.2 Media and antibiotics

E. coli strains were cultivated in Luria bertani medium containing the respective antibiotics

Luria bertani (LB) medium (1L)

Bacto tryptone	10g
Yeast extract	5g
NaCl	5g
2M NaOH	1.3 ml
+/- agar	15g

Millipore H_2O added to 1L

Antibiotic stock solutions: (used as 1:1000 dilutions)

ampicillin	100 mg/ml in water
kanamycin	50 mg/ml in water
chloramphenicol	34 mg/ml in ethanol
tetracycline	10 mg/ml in ethanol

The *S. cerevisiae* strain W303 Δmre11 was cultured in either full medium (YPD), or depending on transformed plasmids, in synthetic SDC media (SDC (-Ura) for pRS416 or SDC (-Ura, -His) for pRS315 plasmid):

YPD medium (for 1L)

10g	yeast extract
20g	Bacto-Peptone
20g	Glucose

Millipore H_2O added to 1L

SDC medium (1L)

6.75 g	Yeast Nitrogen Base w/o AA
20g	Glucose
0.6g	complete synthetic mix (including all essential AA except the auxotrophy markers leucine, tryptophane, histidine, uracil and adenine
10ml	Adenine + 20mM NaOH (2mg/ml in H_2O)
10ml	Histidine (2mg/ml in H2O)
10ml	Leucine (10mg/ml in H2O) (not added for .SDC-Leu)
10ml	Tryptophan (5mg/ml in H2O)
10ml	Uracil (2mg/ml in H20) (not added for .SDC-Ura)
	Millipore H_2O added to 1L

3.3 Methods

3.3.1 Molecular biology methods

If not stated differently molecular biology standard procedures were carried out according to protocols by Sambrook, J. and Russell (Sambrook and Russell 2001). Commercially available kits and enzymes were used following the manufacturer's instructions.

3.3.1.1 Molecular cloning

Constructs for the expression of *S. pombe* Mre11 and Nbs1 were designed with help of the secondary structure prediction programs JPRED (Cole et al. 2008), PSIPred (Bryson et al. 2005), (Jones 1999) and HHPred (Soding et al. 2005) as well as by alignment of sequences from different species using the program ClustalW (Larkin et al. 2007).
PCR primer were designed with a melting temperature (Tm) preferencially above 60 °C. For this purpose the program GeneRunner was used (http://www.generunner.net/). The cloning primers contained restriction sites for specific endonucleases with an overhang sequence between 5 and 7 bases to assure efficient cleavage.

Full length constructs of Mre11 and Nbs1 were amplified by PCR from cDNA using Phusion Flash Master Mix (Finnzymes, Espoo, Finnland). A typical PCR reaction contained 10-100 ng template DNA and 50 pmol of each primer in 20µl of 1x PCR Mix. The following PCR program was used:

1) 98 °C → 30 s

2) 98 °C → 10 s

3) 50-60 °C → 15 sec

(depending on melting temperature of used primers)

4) 72 °C 20 s / 1kb

repeat 2) – 4) 30 times 72 °C 120s

PCR products were separated in agarose gels using a Gel Extraction Kit (Metabion, Martinsried, Germany), digested with the corresponding restriction enzymens and ligated into the vector of interest.

3.3.1.2 Site Directed Mutagenesis by Overlap Extension PCR

All Mre11 or Nbs1/Xrs2 mutants described in this thesis were genererated by site directed mutagenesis using Overlap extension PCR as described in Sambrook and Russell (Sambrook and Russell 2001). For the PCR reactions Phusion Flash Master Mix was used (Finnzymes, Espoo, Finnland). Briefly described, the procedure consists of two PCR steps: In the first PCR step, two fragments are generated which contain either the region 5´ or 3´ of the mutation site. The primer pair for each reaction consists of a cloning primer hybridizing to either the 5´ or 3´ end of the gene and the corresponding mutagenesis primer which hybridizes to the opposite strand at the site of mutation. Thereby two fragments with compatible ends around the mutation site are generated. This allows hybridization of the fragments and subsequent extension in the second PCR step, which yields the full length mutagenesis product. After 5 PCR cycles, the amount of full length PCR product is further amplified by the addition of the cloning primers and additional 30 PCR cycles (see below):

1) 98 °C → 30 s

2) 98 °C → 10 s

3) 50-60 °C → 15 sec (depending on melting temperature of used primers)

4) 72 °C 20 s / 1kb

repeat 2) – 4) 5 times

5) Addition of 25 pmol forward and reverse cloning primers

6) 98 °C → 10 s

7) 50-60 °C → 15 sec (depending on melting temperature of used primers)

8) 72 °C 20 s / 1kb

repeat 6) – 8) 25-30 times followed by a final elongation step at 72 °C for 120-180 sec.

All following following cloning steps were carried out similar to cloning with normal PCR products (3.3.1.1).

3.3.1.3 Transformation in E. coli

For transformations chemically competent *E. coli* were used by performing the following standard protocol (*E. coli* host strains are listed under 3.1.4): 10 µl ligation mixtures or 50-400 ng of purified plasmid were added to 70 µl of competent cells and incubated on ice for 15 min. Cells were then heat shocked for 1 min at 42 °C, followed by 2 min of incubation on ice, addition of 800 µl LB medium and subsequent incubation on a thermo shaker at 37 °C for 45 to 60 min to establish antibiotic resistance. Afterwards cells were plated on LB agar plates containing the respective antibiotics and incubated overnight at 37 °C.

3.3.2 Protein biochemistry methods

3.3.2.1 Protein expression in E. coli

To achieve overexpression of recombinant proteins, the plasmid containing the gene of interest was transformed into E. coli Rosetta (DE3) (Novagen, Schwalbach, Germany). The transformation was carried out analogous to 3.3.1.3, but with the addition of 34 mg/ml Chloramphenicol. For pre-cultures 50 ml LB medium were inoculated with several colonies from a fresh transformation plate (not older than 1 week) and grown overnight at 37 °C in a shaking incubator. The next day 3L LB medium were inoculated 1:100 with the pre-culture and grown at 37 °C to oD_{600} 0.6 - 0.8. The culture was then cooled to 18 °C and further incubated for additional 45 minutes in the shaker. Then protein production was induced by addition of 0.2 mM IPTG. The culture was further shaken overnight at 18 °C. Cells were harvested the next morning, frozen in liquid nitrogen and stored at 20 °C until further use.

3.3.2.2 Recombinant selenomethionine expression in E. coli

Expression of selenomethionine containing Nbs^{mir}-$Mre11^{cd}$ fusion protein (3.3.3.1 and 4.2.1) was performed in *Escherichia coli* B834 Rosetta (DE3) in a shaking culture of minimal medium containing 50 mg/L selenomethionine with 250 µM IPTG at 18 °C overnight. All amino acids were reagent-grade L-enantiomers purchased from Sigma (Deisenhofen, Germany). After dissolving the components (Table 3.9) in 2000 ml FPLC grade water, solution A was autoclaved, cooled to RT and supplemented with 200 ml filter-sterilized

solution B plus 125 mg selenomethionine (Calbiochem, Schwalbach, Germany). Expression was carried out analogous to native proteins (3.3.2.1).

Table 3.9: LeMaster's medium (Hendrickson et al. 1990)

Compounds for autoclavable solution A (2000 ml)	
Alanine 1.0 g	Serine 4.166 g
Arginine hydrochloride 1.16 g	Threonine 0.46 g
Aspartic acid 0.8 g	Tyrosine 0.34 g
Cystine 0.066 g	Valine 0.46 g
Glutamic acid 1.5 g	Adenine 1.0 g
Glutamine 0.666 g	Guanosine 1.34 g
Glycine 1.08 g	Thymine 0.34 g
Histidine 0.12 g	Uracil 1.0 g
Isoleucine 0.46 g	Sodium acetate 3.0 g
Leucine 0.46 g	Succinic acid 3.0 g
Lysine hydrochloride 0.84	Ammonium chloride 1.5 g
Phenylalanine 0.266 g	Sodium hydroxide 1.7 g
Proline 0.2 g	Dibasic potassium phosphate 21.0 g
Compounds for non-autoclavable solution B (200ml)	
Glucose 20.0 g	Concentrated sulfuric acid 16.0 µl
Magnesium sulphate 0.5 g	Thiamine 10.0 mg
Iron sulphate 8.4 g	

3.3.2.3 Purification of GST-labelled proteins

Cells from 3-12 L expression culture were resuspended in buffer A (Table 3.10) and lysed by sonication followed by centrifugation at 30,000 x g, 4 °C for 45 min. The supernatant was loaded onto a Glutathion-Sepharose affinity column (GE Healthcare) and washed with 5-10 column volumes of buffer A. Afterwards a high salt wash using 5-10 column volumes of buffer B was performed and the column then equilibrated again with buffer A. The GST-fusion proteins was eluted in buffer C containing 20 mM reduced Glutathione. Proteolytic cleavage was achieved by addition of Prescission protease (GE Healthcare, to cleave off the GST tag) or Tobacco Etch Virus (TEV) protease (in cases where the $Nbs1^{mir}$-$Mre11^{cd}$ fusion

protein was cleaved) to the protein solution and overnight incubation at 10 °C. The prepared protein was dialysed overnight against 1L of buffer D. The dialysis procedure was repeated twice the next day for additional 2x one hour with fresh buffer to remove residual glutathione. The cleaved GST was removed by passing the dialyzed solution fractions again through a Glutathione-Sepharose column. The flowthrough was collected and further purified by size exclusion chromatography on a S200 column (GE Healthcare). The elution fractions were analysed by SDS-gel electrophoresis (3.3.2.5) and fractions containing the protein of interest were pooled and concentrated (Amicon spin concentrators, Millipore). Proteins used for crystallization were prepared with specific size exclusion buffers listed in Table 3.12. Proteins which were later used for biochemical assays in various buffers, were purified by size exclusion chromatography using buffer D. Proteins, which were not used directly after purification were stored flash frozen in small aliquots of 100 µl at -80 °C. All mutant proteins were purified in the same way as the native proteins. Also the selenomethionine labelled Nbs1^{mir}-Mre11^{cd} protein was purified similarly, but with 5 mM ß-Mercaptoethanol in buffers A-D.

Table 3.10: Buffers for purification of GST-labelled proteins

Buffer A (Lysisbuffer)		**Buffer B (High salt buffer)**		**Buffer C (elution buffer)**	
50 mM	Hepes/NaOH pH7.5	20 mM	Hepes/NaOH pH7.5	50 mM	Hepes/NaOH pH7.5
500 mM	NaCl	1 M	NaCl	500 mM	NaCl
4 mM	EDTA	2 mM	EDTA	20 mM	Glutathione (reduced)
2 mM	ß-Mercaptoethanol	2 mM	ß-Mercaptoethanol	4 mM	EDTA
				2 mM	ß-Mercaptoethanol

Buffer D (Dialysis and size exclusion chromatography buffer)	
20 mM	Hepes/NaOH pH7.5
500 mM	NaCl
2 mM	EDTA
2 mM	ß-Mercaptoethanol

3.3.2.4 Purification of His-tag labeled proteins

Cells were lysed similar to the GST-labelled proteins (3.3.2.3) but with the usage of a Ni-NTA specific, 20mM imidazol containing buffer A (Table 3.11). The supernatant was loaded

onto a Ni-NTA agarose beads (QIAGEN) containing gravity flow column, which had been equilibrated with Ni-NTA buffer A. The beads were first washed extensively with Buffer A, then with the high salt buffer B, and finally reequilibrated with buffer A. The protein was eluted from the column using buffer C. The elution fraction were concentrated with a centrifugal filter unit (Amicon spin concentrators, Millipore) and loaded onto a Superdex S200 26/60 size exclusion column (GE Healthcare) equilibrated in buffer D. Fractions containing the protein of interest were identified by SDS-PAGE (3.3.2.5), pooled and concentrated. The protein concentration was determined with the calculated theoretical extinction coefficient at 280 nm. Proteins which were not used directly after purification were stored flash frozen in small aliquots of 100 µl at -80 °C.

Table 3.11: Buffers for purification of His-tag labelled proteins

Ni-NTA Buffer A (lysis buffer)		**Ni-NTA Buffer B (high salt buffer)**		**Ni-NTA Buffer C (elution buffer)**	
20 mM	Hepes/NaOH pH 7.5	20 mM	Hepes/NaOH pH 7.5	20 mM	Hepes/NaOH pH 7.5
500 mM	NaCl	1 M	NaCl	300 mM	NaCl
20 mM	Imidazol	20 mM	Imidazol	300 mM	Imidazol
4 mM	EDTA	2 mM	EDTA	2 mM	EDTA
2 mM	ß-Mercaptoethanol	2 mM	ß-Mercaptoethanol	2 mM	ß-Mercaptoethanol

Buffer D (size exclusion chromatography buffer)	
20 mM	Hepes/NaOH pH 7.5
300 mM	NaCl
2 mM	EDTA
2 mM	ß-Mercaptoethanol

3.3.2.5 Discontinous Polyacrylamide Gel Electrophoresis (SDS-PAGE)

Protein samples were analysed by discontinuous polyacrylamide gel electrophoresis (SDS-PAGE) (Laemmli 1970) with a vertical Mini-PROTEAN 3 System (BioRad). Protein samples were mixed with Laemmli buffer and denaturated 1-5 min at 95 °C. Depending on the molecular weight of the analysed protein, a separating gel with 6 to 15% acrylamide was used. Gels were run at 200V in 1x TGS buffer, stained afterwards with Coomassie staining solution and destained in water.

4x lower buffer: 3 M Tris (pH 8.5), 0.4% (w/v) SDS

4x upper buffer: 0.5 M Tris (pH 6.8), 0.4% (w/v) SDS

4x Laemmli buffer: 0.11 M Tris (pH 6.8), 16% (v/v), 4% (w/v) SDS,
5% (v/v) β-mercaptoethanol, 0.05% (w/v) bromophenol blue

10x TGS buffer: 0.5 M Tris (pH 8.3), 1.9 M glycin, 1% (w/v) SDS

Coomassie stain: 50% (v/v) ethanol, 7% (v/v) acetic acid, 0.2% (w/v),
Coomassie Brilliant Blue R250

3.3.2.6 Western blot analysis

Protein samples were first fractionated by SDS-PAGE according to Laemmli (Laemmli 1970) with a Mini Protean III system (Biorad, München) (3.3.2.5). Gels were then blotted to a Nitrocellulose membrane (Roth, Karlsruhe, Germany) using a Mini Trans-Blot Cell system with a transfer buffer containing 50 mM TRIS/HCl pH 8.3, 0.19 M glycine, 0.1 (w/v) % SDS and 20 % methanol. Three layers of Whatman paper, followed by the nitrocellulose membrane, the SDS-PAGE gel and another three layers of Whatman paper, all presoaked in blotting buffer, were assembled in the blotting machine. Transfer of proteins to the membrane occurred at 100V for 60 min at 8 °C. The nitrocellulose membrane was blocked with TBST+M buffer (50 mM Tris/HCl pH 7.5, 150 mM NaCl, 0.1% Tween 20, 4% milk powder) for 45 min. The first antibody was diluted in TBST+M buffer and incubated overnight at 8 C. Next the membrane was washed with TBST+M buffer for 3x 15 min and incubated with a Horseradish Peroxidase (HRP) coupled secondary antibody in TBST+M buffer at RT for 2h. Afterwards, the membrane was washed 3x 15 min in TBS-T buffer without milk powder. All used antibodies and the respective dilutions are listed under 3.1.1.
The immunostained proteins were detected by addition of Pierce ECL Western Blotting Substrate solution (Thermo Scientific, Bonn) to the blotting membrane and subsequent exposure with a light sensitive Hyperfilm™ ECL™ (GE Healthcare). The films were developed with a Kodak X-Omat M35 developing machine.

3.3.2.7 Analytical size exclusion chromatography

To analyse the complex formation of different Mre11 and Nbs1 protein constructs from *S. pombe*, 10 nmol Mre11 and 7.5 nmol Nbs1 proteins were mixed and dialysed against the chromatography running buffer containing 20 mM Hepes pH 7.5, 100 mM KCl, 5% glycerol, 2mM ß-mercaptoethanol and either 1 mM $MnCl_2$ or 2 mM EDTA. A volume of 350 µl protein sample was loaded at a flow rate of 0.5 ml/min onto a Superdex S200 10/300 GL column (GE Healthcare), pre-equilibrated with running buffer. Elution fractions were analyzed for Mre11 and Nbs1 by SDS-PAGE and Coomassie staining (3.3.2.5).

3.3.2.8 Limited Proteolysis

A stock solution of 1mg/ml proteinase K dissolved in H_20 was diluted to 1:10, 1:100, 1:1000, 1:3000, 1.6000 and 1:10000 with 2 mM HCl (pH ≈ 3). For each sample 45 µl of a 1 mg/ml protein solution in 20 mM Tris/HCl pH 7.5, 150 mM NaCl, 2 mM ß-Mercaptoethanol was mixed with 5 µl of the corresponding dilution of proteinase K. The samples were incubated at RT for 1 h and stopped by addition of 1 µl PMSF-saturated isopropanol and 16.6 µl of 4x SDS-sample buffer. An appropriate amount of sample was analyzed by SDS-PAGE (3.3.2.5). Protein bands of interest were cut out and sent to the Zentrallabor für Proteinanalytik (ZfP - Prof. Dr. Axel Imhof, München) for MALDI peptide mass fingerprint analysis.

3.3.2.9 Nuclease activity assay

Mre11 nuclease activity was tested using a 6-FAM- 5` labelled 60mer poly(dT) oligonucleotide (Table 3.2). For each reaction, 10 nM DNA was incubated with 5 µM of Mre11 (residues 1-413) or Mre11 (residues 1-413) H134S proteins in 10 µl buffer containing 20 mM Hepes pH 7.5, 100 mM KCl,.5% glycerol, 5 mM $MnCl_2$ and 2 mM Mercaptoethanol at 37 °C for 2 h. The reaction was stopped by addition of 3 µl loading buffer (10mM Tris, pH 8.0 16.6% formamide, 16.6% glycerol, 5mM EDTA) and incubated at 95 °C for 5 min. Reaction products were resolved on a denaturating 18% acrylamide gel in 1x TBE buffer containing 8M Urea. Gels were imaged with a Typhoon 9400 fluorescence scanner (GE Healthcare) using the green-exited (532nm) fluorescence mode.

3.3.2.10 EMSA (electrophoretic mobility shift assay)

Binding of different *S. pombe* Mre11 and Nbs1 constructs to DNA was analyzed by electrophoretic mobility shift assays (EMSAs). The binding of proteins to DNA can be visualized by a mobility shift in native gel electrophoreses. Protein-DNA complexes posses normally a lower charge/mass ratio than free DNA and therefore migrate slower in the gel. The DNA is visualized by a covalently coupled fluorescence label. The samples contained the DNA substrate at a concentration of 50 nM and the protein in different excess concentrations (0/1.5/3/6/12 µM for Mre11 and 0/0.5/5/50 µM for Nbs1 constructs) and in a total volume of 10 µl. The assay buffer contained 20 mM Hepes/NaOH pH 7.5, 100 mM KCl, 10% Glycerol, 1 mM $MnCl_2$ and 2 mM ß-Mercaptoethanol. The protein samples had been equilibrated by dialysis against the assay buffer before use. After addition of protein to the DNA, the samples were mixed and incubated for 30 min at RT. Afterwards they were analyzed with a 0.5% (w/v) agarose gel in 1x TB buffer (90 mM Tris, 90 mM boric acid, pH 8 without adjustment). The gel was run at 4 V/cm and 8 °C for 2 h and visualized with a Typhoon 9400 fluorescence scanner (GE Healthcare).

3.3.3 Structural biology methods

3.3.3.1 Crystallization

All proteins were crystallized at 20 °C using the hanging drop vapour diffusion technique. Initial crystals were obtained in commercial 96-well format sitting drop screens using the Matrix Hydra II 96-channel microdispenser (Thermo Scientific) for dispensing of reservoir solutions and protein drops. The initial screens were set up with a reservoir volume of 50 µl and a dropsize of 0.5 µl reservoir + 0.5 µl protein solution. Initial crystals were optimized manually in refinement screens by varying the composition of the reservoir solution as well as the protein concentration. The refinement screens contained a reservoir volume of 500µl with 2 µl reservoir + 2 µl protein solution drops. The protein preparation buffers, protein concentrations, screen compositions and cryo protectants for all crystallised proteins are listed in Table 3.12. Cryocooling for data collection was achieved by soaking the crystals for 30 sec in mother liquor solution containing the cryo protectant and flash freezing in liquid nitrogen.

Table 3.12: Crystallization conditions for Nbs1^{mir}Mre11^{cd} complexes and Mre11^{cd}

	preparation buffer	protein concen-tration	crystallization solution	cryo reagent
Nbs1^{mir}Mre11^{cd} SeMet	20 mM Hepes pH 7.5 200 mM NaCl 1 mM $MnCl_2$ 2 mM ß-Mercaptoethanol	10 mg/ml	400 mM ammonium citrate pH 6.0 20% w/v PEG 3350	15 % D(-) -2,3butanediol
Nbs1^{mir}Mre11^{cd}	20 mM Hepes pH 7.5 200 mM NaCl 1 mM $MnCl_2$ 2 mM ß-Mercaptoethanol	9 mg/ml	100 mM Tri-Na-Citrate pH 5.0 200 mM ammonium sulfate 13% w/v PEG 4000	15 % D(-) -2,3butanediol
Nbs1^{mir}Mre11^{cd} (+50 Mn^{2+})	20 mM Hepes pH 7.5 200 mM NaCl 1 mM $MnCl_2$ 2 mM ß-Mercaptoethanol	8 mg/ml	400 mM ammonium citrate pH 6.0 20% w/v PEG 3350 50 mM $MnCl_2$	15 % D(-) -2,3butanediol
Non-fused Mre11^{cd}Nbs1^{mir}	20 mM Hepes pH 8.0 200 mM NaCl 1 mM $MnCl_2$ 2 mM ß-Mercaptoethanol	8 mg/ml	200 mM ammonium citrate pH 5.5, 14 % w/v PEG 3350 50 mM $MnCl_2$	20% glycerol
Mre11^{cd}	20 mM Hepes pH 7.5 300 mM NaCl 0.1 mM EDTA 1 mM $MnCl_2$ 2 mM ß-Mercaptoethanol	22 mg/ml	100 mM Hepes pH 8.1 9% w/v PEG 8000 200 mM NaCl.	12% D(-) -2,3butanediol

3.3.3.2 Data collection, structure solution and model building

Diffraction data were collected at the PXI beamline at the SLS (Villigen, Switzerland) or at beamline ID23-1/2 at the ESRF (Grenoble, France) as indicated in Table 4.1. Single-wavelength anomalous dispersion (SAD) data to 2.8 Å were collected at the selenomethionine

peak wavelength at the beamline ID23-2 on selenium-containing crystals. All data were integrated and scaled with XDS (Kabsch 1993). The structure of the $Nbs1^{mir}$-$Mre11^{cd}$ fusion protein was determined by SAD phasing methods using SHARP and autoSHARP (Global Phasing, Cambridge), which located 8 selenomethionine and 2 manganese sites within the asymmetric unit. An initial model was built by alternate rounds of automatic model building using the programs ARP/warp (Langer et al. 2008) and Buccaneer (Cowtan 2006). The resulting model was used for molecular replacement with the program Phaser (McCoy 2007) against the native dataset. The model was completed by manually model building in the resulting electron density using the program COOT (Emsley and Cowtan 2004) and refined to 2.4 Å. Phases for the non-fused $Mre11^{cd}$-$Nbs1^{mir}$ complex and apo-$Mre11^{cd}$ were obtained by molecular replacement with Phaser using the monomeric $Mre11^{cd}$ model derived from the $Nbs1^{mir}$-$Mre11^{cd}$ fusion protein model. Prior to refinement, 5-10 % of the reflections were randomly omitted for monitoring the free R-value. All models were refined by iterative cycles of bulk solvent correction, overall anisotropic B factor refinement, positional, TLS group refinement with Phenix (Zwart et al. 2008) and manual model building with COOT. Initial NCS restraints were gradually removed in the final cycles of the refinement, to allow some structural variations. Especially for refinement of flexible loop regions within the structures the refinement program autoBUSTER (Global Phasing, Cambridge) was used during the last steps of the refinement process. Data collection and model statistics are summarized in Table 4.1. All figures were prepared with PYMOL (DeLano Scientific).

3.3.3.3 Small angle x-ray scattering

Synchrotron radiation small angle X-ray scattering (SAXS) data were collected at the EMBL X33 beamline at the DORIS storage ring (DESY, Hamburg, Germany) using a MAR345 two-dimensional image plate detector. Scattering patterns from solutions of $Mre11^{cd}$ at concentrations of 5 mg/ml were measured in the corresponding preparation buffers. Various programs of the ATSAS (Konarev et al. 2006) software package were used to process and evaluate the SAXS data. PRIMUS was used for initial data analysis. The radius of gyration R_g was determined by fitting the measured scattering data with the Guinier equation ($s \times R_G < 1.3$) and the program GNOME was used to determine P(r)-functions. CRYSOL was utilized to compute theoretical SAXS-curves from crystallographic coordinate files for data comparison.

3.3.4 Yeast specific methods

3.3.4.1 Yeast transformation

For transformation of Mre11 coding plasmids into the W303 Δmre11 strain, 50 ml of yeast culture were grown to an OD_{600} of 0.5 to 0.8 in YPD and pelleted by centrifugation at 3600 rpm (Rotanda 46R centrifuge) and room temperature (RT) for 3 min. After washing with 10 ml of H_2O, the pellet was washed once with 500 µl of solution I (10 mM Tris-HCl, pH 7.5, 1 mM EDTA, 100 mM Li-acetate) and resuspended in 250 µl solution I. 3 µg DNA and 5 µl of single stranded carrier DNA (DNA of salmon of herring testis, 2 mg/ml) were mixed with 50µl of cells in solution I and incubated with 300 µl solution II (10 mM Tris-HCl, pH 7.5; 1 mM EDTA; 100 mM Li-acetate; 40% w/v PEG 4000) on a turning wheel at RT for 30 min. The samples were heat shocked at 42 °C for 10 min, followed by 3 min of incubation on ice. 1 ml of H_2O was added, the sample centrifuged, the pellet resuspended in 50 µl H_2O and plated on a selective plate. To transform yeast cells grown on plate, one loop of logarithmically grown cells was resuspended in 30 µl of 100 mM Li-acetate and vortexed. The rest of the transformation was done according to the protocol described above.

3.3.4.2 Plate survival assays

One loop of freshly growing cells from a plate was resuspended in 1 ml H_2O. Five 10 fold dilutions were prepared and 6 µl of each dilution spotted onto the corresponding plates: SDC (-Ura), SDC (-Ura) + 0.2/1/5 µg/ml Camptothecin (CPT), SDC (-Ura) + 0.005% methyl methanesulfonate (MMS), SDC (-Ura) + 50 or 200 mM hydroxyurea (HU), YPD, YPD + 0.2/1/5 µg/ml CPT, YPD + 0.005 % MMS, YPD + 50 or 200 mM HU.
The compositions of SDC (-Ura) and YPD media are listed under 3.2.

3.3.4.3 Co-immunoprecipitation

The interaction of different *S. cerevisiae* Mre11 mutants with Rad50 and Xrs2 was analyzed performing a modified co-immunoprecipitation protocol by (Strahl-Bolsinger et al. 1997): W303 Δmre11 cells containing a P527 ScMre11 plasmid, coding for the respective c-myc-tagged Mre11 mutant protein (Table 3.6), were cultivated in SDC (-Ura) medium. 50 ml of

medium were freshly inoculated with an overnight culture to a starting oD_{600} of 0.2 - 0.3 and shaked at 30 °C until an OD_{600} of 0.7. Cells were pelleted by centrifugation at 3600 rpm for 3min (Rotanda 46R), washed twice with TBS (20 mM Tris-HC1 at pH 7.6, 200 mM NaC1), and resuspended in 400 µ1 lysis buffer (50mM Hepes pH 7.5, 140mM NaCl, 10% Glycerin, 0.5% NP-40, 1mM PMSF, 2mM benzamidine hydrochloride, 2 µM Pepstatin, 0.5 µM Leupeptin, 3.3 µM Chymostatin). Then, 400 µ1 glass beads were added and the cells lysed by vortexing on an Eppendorf 5432 shaker for 40 min. The tubes were then punctured on the bottom, and the lysate collected in a 15 ml falcon tube by centrifugation at 1000rpm for 1min. The lysate was transferred into an 1.5 ml Eppendorf tube and clarified by centrifugation at 4 °C and 13000 rpm for 5 min and 15min. The supernatant was transferred into a fresh Eppendorf tube, followed by addition of 5µg α-cMyc antibody (3.1.1) and 20 U of DNAse I (New England Biolabs). The samples were incubated for 3h at 8 °C on a turning wheel to allow formation of Mre11-cMyc-antibody complexes. Then, 50µl of Protein G Dynabeads (Invitrogen), preequilibrated with lysis buffer, were added (beads in suspension) and the incubation was continued for 1h. Then the beads were washed three times for 5 min with 1.4 ml lysisbuffer and subsequently resuspended in 60 µl 1.5x Laemmli buffer (3.3.2.5). The Co-immunoprecipitates were analysed by SDS-PAGE (3.3.2.5) followed by western blot analysis (3.3.2.6). For western blot analysis of IP inputs, whole cell extracts were prepared using TCA-mediated protein precipitation as described before (Janke et al. 2010).

3.3.4.4 Indirect immunofluorescence

An exponentially grown yeast culture (10ml with OD_{600} of 0.5 – 1.0) was mixed with 1 ml of 37% HCOH to fix the cells and incubated on a turning wheel at 30 °C for 90 min. The cells were pelleted by centrifugation at 3000 rpm and RT for 5 min (Rotanda 46R centrifuge), washed twice with spheroblasting premix (1.2 M sorbitol, 0.1 M K-phosphate buffer, pH 7.4, 0.5 mM $MgCl_2$), resuspended in 1 ml spheroblasting premix and stored at 4 °C up to 18h. Afterwards, the cells were pelleted and resuspended in 200µl of spheroblasting premix, containing 100 µg of 100T zymolyase and incubated in a 30 °C waterbath for 30 min. Following spheroblasting, the cells were pelleted by centrifugation at 2000 rpm and RT (table top centrifuge) for 4 min and resuspended in at least 10x the volume of the cells in spheroblasting premix. Then, one drop of the suspension was pipetted on a fluorescence microscopy slide, which had been precoated with polylysine. After 5 min of incubation the

drops were pipetted off and the immobilized cells washed with 1 drop of blocking buffer (1% BSA powder in PBS (phosphate buffered saline, 2.7 mM KCl, 7.9 mM Na_2HPO_4, 1.5 mM KH_2PO_4, 137 mM NaCl). The cells were fixed by incubation of the slide with methanol in a staining jar at -80 °C for 6 min followed by 30 sec incubation in -80 °C cold acetone. Next, the slides were dried at RT and incubated with 100 µl blocking buffer for 10 min. The solution was removed and the cells incubated with 20 µl of the first antibody solution (antibody diluted in 1% BSA in PBS) at RT for 2 h. Then the slides were washed to remove the antibody for 3x 1 min incubations with 10 µl blocking buffer additionally containing 0,1 % Triton-X at RT. Afterwards, 20 µl of the second antibody diluted in blocking buffer was added to the cells followed by incubation in the dark for 1 h. Finally, the cells were washed 3x with blocking buffer plus 0,1 % Triton-X. For staining of cell nuclei the slides were put in a jar containing SSC buffer (300 mM NaCl; 30 mM Na-citrate, pH 7.0) and 5µl of DAPI (10mg/ml) in the dark for 10 min. Afterwards the slides were washed with a 1:4 dilution of SSC buffer at RT for 5 min in the dark and dried. Finally the cells were covered with 80% glycerol and sealed with the cover slide.

The stained cells were analyzed using a DMI 6000 B fluorescence microscope (Leica Microsystems, Wetzlar). The signal of the Alexa Fluor 488 coupled antibody was detected at an emission wavelength of 519 nm and the DAPI signal at an emission wavelength of 461 nm. The excitation wavelength was at 495 nm for Alexa Fluor 488 and 358 nm for DAPI. The signal intensity was 3 for Alexa Fluor 488 and 2 in the case of DAPI. A gain of 3.5 (Alexa Fluor 488) or 3.3 (DAPI) was used for signal detection. Fluorescence signals were analyzed with the LAS AF Lite software (Leica Microsystems, Wetzlar) and the pictures arranged using ImageJ (NIH, Bethesda, USA).

3.3.5 Bioinformatical methods

3.3.5.1 Structure based sequence alignments

Protein sequences of Mre11 from eukaryotic organisms *Schizosaccharomyces pombe* (SpMre11), *Saccharomyces cerevisisae*, *Danio rerio* and *Homo sapiens* were aligned with ClustalW (Larkin et al. 2007). The archaeal Mre11 sequence from *Pyrococcus furiosus* (PfMre11) was added after calculating a pairwise alignment of PfMre11 and SpMre11 with the program FATCAT (Ye and Godzik 2004) using the pdb-coordinates of PfMre11 (Protein

data base entry 1II7) and SpMre11^{cd} as input files. The PfuMre11/SpMre11 alignment was further revised by comparison of the overlaid structures with Pymol (DeLano Scientific).

4. RESULTS

4.1 Cloning and expression of Mre11 and Nbs1 from *S. pombe*

The coding genes for full length Mre11 and Nbs1 from the fission yeast *Schizosaccharomyces pombe* were amplified by PCR using a cDNA library and cloned into *E. coli* expression vectors according to 3.3.1.1. Full length Mre11 (aa 1-649), could be purified but was prone to aggregation and degradation over time. Full length Nbs1 (aa 1-613), also expressed in *E. coli*, was mostly unsoluble and could be purified only in minor amounts (data not shown). However, an Mre11-Nbs1 mutant complex consisting of Mre11 aa 1-478 and Nbs1 aa 474-613 could be co-expressed and purified in mg amounts (3.3.2.4 and Table 3.5). Even though this complex was extensively tested for crystallization, it did not yield crystals in any condition. Furthermore, it was already degraded by proteolysis during the preparation. Thus, to identify stable fragments of Mre11 and Nbs1, suitable for crystallization, a limited proteolysis analysis was performed. For this purpose, the Mre11 aa 1-478 / Nbs1 aa 474-613 complex was incubated with different concentrations of Proteinase K. Nevertheless, no stable Nbs1 fragment shorter than aa 474-613 could be identified. For Mre11, however, a stable fragment of approximately 45 kDa was identified and further analyzed by a MALDI trypsin fingerprint (3.3.2.8 and Figure 4.1). Here, peptides in the N-terminal region of Mre11 between residues 1-412 were found, which matched also the observed molecular weight of the fragment. Based on this observation a new construct of Mre11 was cloned which contained aa 1-413 (Table 3.5). The Mre11 construct aa 1-413 could be expressed and prepared in high purity and with a yield of several mg protein. However, albeit remaining stable after purification, it did not crystallize in any tested screen. A secondary structure analysis with JPRED (Cole et al. 2008) predicted the first 17 residues of *S. pombe* Mre11 to be unstructured. Therefore, a construct consisting of aa 15-413 was generated from which the structure could later be determined (Table 3.5, Figure 4.2). The Mre11 fragment aa 15-413 contained, based on structure aligments with the archaeal Mre11 homologue from *Pyrococcus furiosus*, both the nuclease and the DNA capping domain. It was therefore further named $Mre11^{cd}$ (cd = catalytical domain).

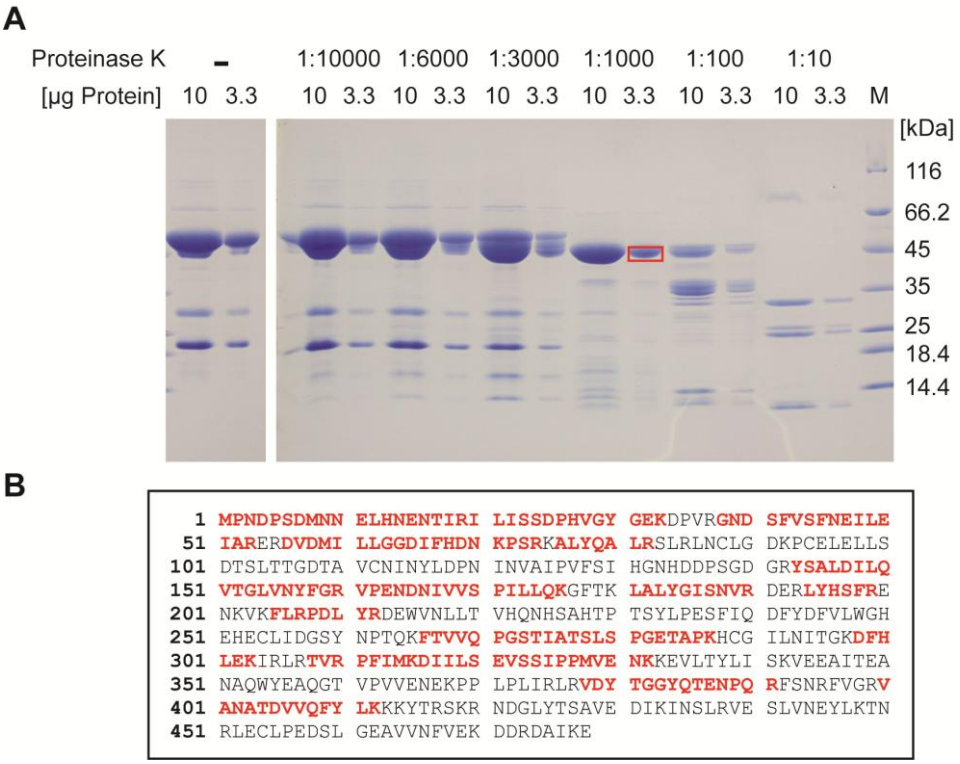

Figure 4.1: Limited proteolysis analysis of the *S. pombe* Mre11 aa 1-478 / Nbs1 aa 474-613 complex. **(A)** SDS-PAGE for limited proteolysis samples of the *S. pombe* Mre11 aa 1-478 / Nbs1 aa 474-613 complex with different concentrations of Proteinase K. 10 or 3.3 µg of protein were loaded from each sample. **(B)** Sequence of *S. pombe* Mre11 aa 1-478. Peptides, which were identified by a MALDI-TOF Trypsin fingerprint analysis are colored in red (3.3.2.8).

Since full length Nbs1 could not be produced in amounts suitable for crystallization, different constructs of the Nbs1 C-terminus, which contains the binding site for Mre11 (Ueno et al. 2003), were prepared. The largest soluble fragment, including amino acid residues 428-613 (Table 3.5), did not crystallize alone or in complex with Mre11 aa 15-413. Secondary structure predictions of *S. pombe* Nbs1 with the program JPRED (Cole et al. 2008) indicated the C-terminal region between aa 570-613 to be mainly unstructured, which could impair crystal growth. Therefore, starting from the size of fragment aa 428-613, smaller deletion constructs were generated (Table 3.5). The smallest fragment binding to Mre11, determined by size exclusion chromatography, was Nbs1 aa 474-531. It contains two conserved sequence motifs which were proposed by Ueno *et al.* (Ueno et al. 2003) to present the Mre11 interaction region and was therefore further named Nbs1^{mir}.

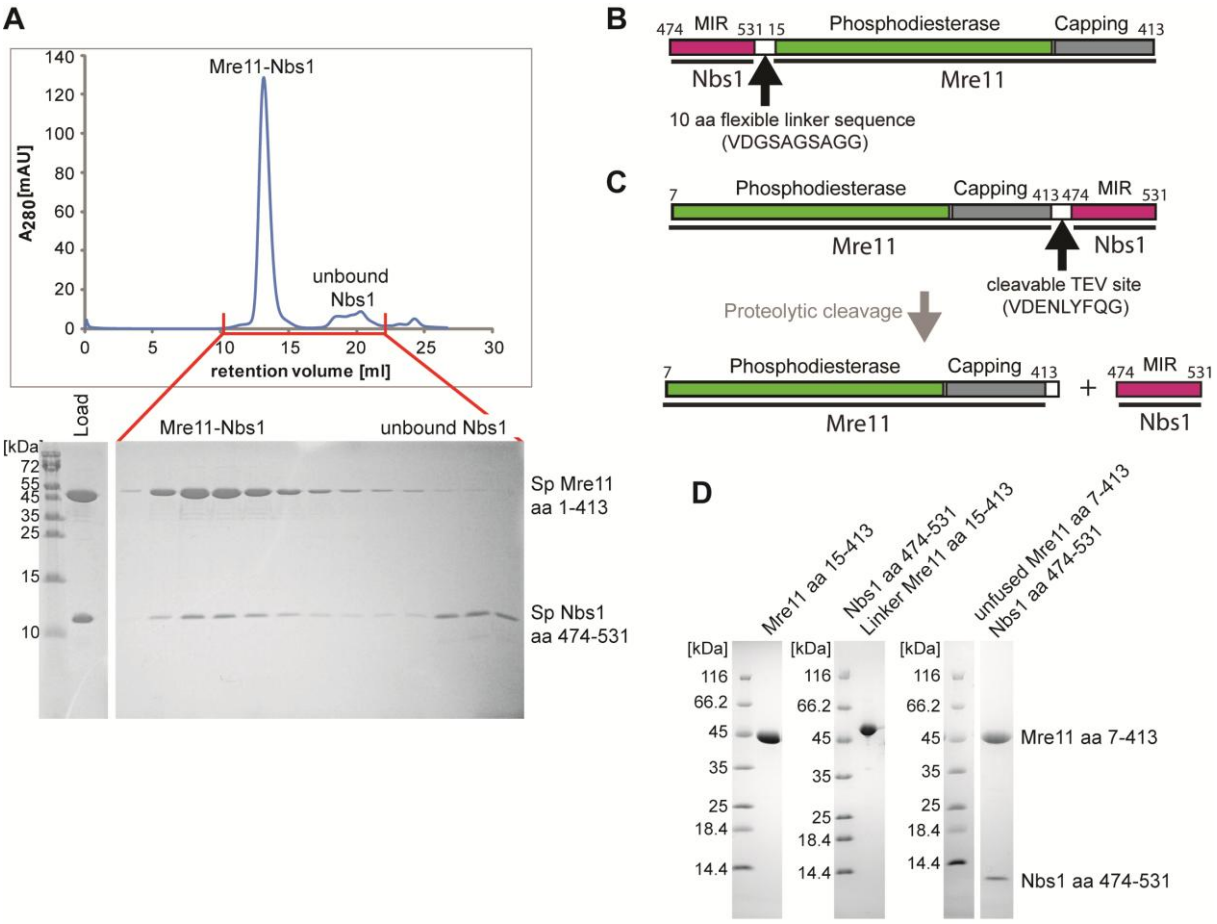

Figure 4.2: **Binding studies of Mre11 and Nbs1, construct design and protein preparations of Mre11/Nbs1 complexes for crystallization: (A)** Analytical size exclusion chromatography with a Superdex S200 10/300GL column showed that Mre11 aa 1-413 and Nbs1 474-531 form a stable complex with a 1:1 stoichiometry. **(B-C)** $Mre11^{cd}$ and $Nbs1^{mir}$ fusion proteins used for crystallization. $Nbs1^{mir}$ (aa 474-531) - $Mre11^{cd}$ (aa 15-413) (B) was directly crystallized, $Mre11^{cd}$ (aa 7-413) - $Nbs1^{mir}$ (aa 474-531) (C) was crystallized in the non-fused form after proteolytic cleavage of the linker peptide with Tobacco etch virus protease at its recognition site in the linker region between $Mre11^{cd}$ and $Nbs1^{mir}$. Mre11 is shown with the phosphodiesterase in green and the DNA capping domain in grey. The Mre11 interacting region of Nbs1 is depicted magenta. **(D)** SDS-PAGE of different protein preparations (from left to right): Mre11 aa 15-413, Nbs1 (aa 474-531) - (Mre11 (aa 15-413) fusion protein, non-fused Mre11 (aa 7-413) - Nbs1 (aa 474-531) complex.

Since none of the generated fragments initially crystallized with Mre11, a fusion protein consisting of $Nbs1^{mir}$ (aa 474-531) and $Mre11^{cd}$ (aa 15-413) was generated to facilitate crystallization (Figure 4.2 B and Table 3.5). The flexible linker, which covalently links the C-terminus of Nbs1 with the N-terminus of Mre11 consisted of the amino acid sequence GSAGSAGS. The construct could be crystallized and its structure solved (Table 3.12 and 4.3). To rule out, that the fusion influences the structure, also a reversed plus additionally

cleavable fusion protein was generated (Mre11^{cd} aa 7-413 fused to Nbs^{mir} aa 474-531). In this construct the C-terminus of Mre11 aa 7-413 was linked via a TEV protease cleavage site to the N-terminus of Nbs1 aa 474-531. After proteolytic cleavage of the linker peptide, the non-fused complex of Mre11^{cd} and Nbs^{mir} could be crystallized and its structure determined (4.2.1 and Table 3.12).

4.2 Crystallization, structure solution and refinement

4.2.1 Nbs1^{mir}-Mre11^{cd} complex

Initial crystallization screenings with the covalently fused Nbs1^{mir}-Mre11^{cd} complex yielded crystals in several different conditions (3.3.3.1). Larger three dimensional crystals grew in conditions containing citrate salts and different PEGs. They could easily be reproduced in refinement screenings with native and selenomethionine labeled proteins (Figure 4.3 A-C and Table 3.12). Crystals of the selenomethionine labeled, covalently fused Nbs1^{mir}-Mre11^{cd} complex diffracted to a limiting resolution of 2.8 Å at the ESRF ID23-1 beamline and allowed phase determination by SAD (3.3.3.2). Crystals of the native, covalently fused Nbs1^{mir}-Mre11^{cd} complex, derived from a refinement screen containing ammoniumsulfate, diffracted to a limiting resolution of 2.4 Å at the ESRF ID23-2 beamline (Figure 4.3 D and Table 4.1). All measured crystals belonged to space group $P2_12_12_1$. An initial model was built by alternate rounds of automatic model building into the experimentally derived 2.8 Å electron density derived from crystals of the selenomethionine labeled protein. The resulting model was used for a molecular replacement against the native 2.4 Å dataset and completed by manual model building in the resulting electron density (3.3.3.2). The geometry of all chains was well within an acceptable range in the final model. The final R factors were 22.0% for R_{work} and 24.2% for R_{free}. Crystallographic data and refinement statistics are summarized in Table 4.1. An example of the refined electron density can be found in Figure 4.3 E.

As described under 4.6, the structure derived from these crystals contained only one Mn^{2+} ion in the active site. An active site loop, responsible for complexing the second Mn^{2+} ion, was instead involved in complexing a sulfate molecule. Therefore, additional refinement screenings without ammonium sulfate but with high manganese chloride concentrations were set up, which yielded crystals diffracting up to 2.5 Å at the SLS PX I beamline (Table 3.12

and Table 4.1). From these crystals a structure with two Mn^{2+} ions per active site could be solved using molecular replacement (3.3.3.2).

The non-fused $Mre11^{cd}$ (aa 7-413) / (Nbs^{mir} aa 474-531) complex, which was generated to rule out that the protein fusion influences the structure, crystallized under conditions similar to the $Nbs1^{mir}$ (aa 474-531) / $Mre11^{cd}$ (aa 15-413) fusion protein (Table 3.12 and Figure 4.3 F). A densitometric analysis with ImageJ (NIH, Bethesda, USA) of Nbs1 and Mre11 bands from an SDS-PAGE gel of crystals confirmed, that both proteins were also in the non-fused complex present in an exact 1:1 stoichiometry (Figure 4.3 G).

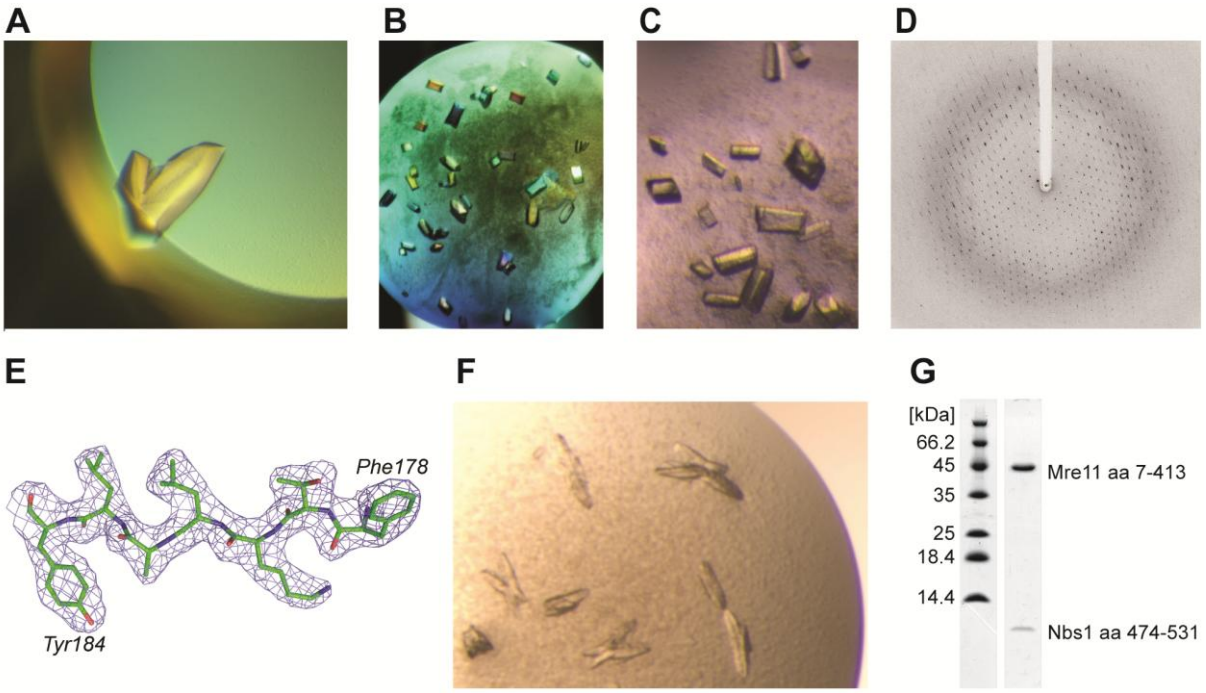

Figure 4.3: Crystallization of covalently fused or non-fused *S. pombe* $Nbs1^{mir}$-$Mre11^{cd}$ complexes and diffraction data collection: (A) Initial crystals of the native, covalently fused $Nbs1^{mir}$-$Mre11^{cd}$ complex (condition: 0.1 M Sodium citrate pH 5.6, 0.2 M ammonium sulfate, 15% w/v PEG 4000). **(B)** Crystals of the native, covalently fused $Nbs1^{mir}$-$Mre11^{cd}$ complex from a refinement screen (condition: 0.5 M ammonium citrate pH 5.5 and 20% w/v PEG 3350). **(C)** Crystals of the selenomethione labeled, covalently fused $Nbs1^{mir}$-$Mre11^{cd}$ complex from a refinement screen (condition: 0.4 M ammonium citrate, pH 6.0, 20% w/v PEG 3350). **(D)** Diffraction pattern of native crystal of covalently fused $Nbs1^{mir}$-$Mre11^{cd}$ complex. **(E)** Final $2F_o$-F_c electron density map at 1.0 σ for the refined model of $Nbs1^{mir}$-$Mre11^{cd}$. Amino acid residues 178 to 184 of Mre11 chain A are shown. Residues are presented as stick models with carbon atoms colored in green, nitrogen in blue, and oxygen in red. **(F)** Crystals of the non-fused $Mre11^{cd}$-$Nbs1^{mir}$ complex from a refinement screen containing 0.2 M Ammonium citrate, 14% w/v PEG 3350 and 50 mM $MnCl_2$ **(G)** SDS-PAGE gel of non-fused $Mre11^{cd}$-$Nbs1^{mir}$ complex crystals stained with Coomassie blue. A densitometric analysis of the Nbs1 and Mre11 bands

with ImageJ (NIH, Bethesda, USA) showed that both proteins also exhibit an exact 1:1 stoichiometry in crystals of the non-fused complex.

Table 4.1 : Crystallographic data collection and model refinement statistics

	Nbs1^{mir}-Mre11^{cd} SeMet	**Nbs1^{mir}-Mre11^{cd}**	**Nbs1^{mir}-Mre11^{cd} +50mM Mn^{2+}**	**Non-fused Mre11^{cd}-Nbs1^{mir} +50 mM Mn^{2+}**	**Mre11^{cd}**
Data collection					
Beamline	ID23-1	ID23-2	SLS PXI	ID23-2	ID23-1
Space group	$P2_12_12_1$	$P2_12_12_1$	$P2_12_12_1$	$P2_12_12_1$	$P2_12_12_1$
Cell dimensions					
a, b, c (Å)	58.9, 79.3, 218.5	60.3, 78.9, 222.7	59.3, 79.1, 223.0	59.1, 80.0 220.9	76.3, 82.3, 164.3
Wavelength	0.97925	0.8726	1.006	0.8726	1.000
Resolution (Å)	50-2.8	47.9-2.4	50-2.5	47.5-2.2	46-3.0
R_{sym}	5.5 (31.3)	5.0 (36.2)	4.1 (28.1)	5.3 (44.5)	6.1 (45.8)
$I / \sigma I$	18.06 (3.74)	27.41 (4.36)	15.74 (3.15)	24.96 (3.93)	16.02 (2.87)
Completeness (%)	96.4 (87.6)	96.4 (87.9)	89.4 (77.8)	95.8 (85.9)	92.4 (82.3)
Redundancy	3.68	7.05	2.11	7.63	3.64
Refinement					
Resolution (Å)		47.9-2.4	47.4 – 2.5	47.5-2.2	45.6 – 3.0
No. reflections		43364	36766	53869	20978
R_{work} / R_{free}		22.0/24.2	18.5 /21.8	22.2/24.0	22.2/ 28.9
No. atoms					
Protein		6720	6536	6491	5895
Water		240	162	211	-
Ligand/ions		2 Mn	4 Mn	4 Mn	4 Mn
***B*-factors (Å ^{2})**					
Protein		38.1	48.6	52.9	76.3
R.m.s deviations					
Bonds (Å)		0.012	0.010	0.014	0.008
Angles (°)		1.9	1.2	1.9	1.3

4.2.2 Apo-Mre11^{cd}

Initial crystals of apo-Mre11^{cd} could be observed in a commercial crystallization screen after 4 weeks of incubation at 20 °C (Figure 4.4 A). However, they were too small to be suitable for diffraction data collection. Subsequent refinement screenings yielded larger crystals from which diffraction data with a limiting resolution of 3.0 Å was collected at the ESRF ID23-1 beamline (Figure 4.4 B and C and 3.3.3.2). The crystals belonged to the space group $P2_12_12_1$. The structure of apo-Mre11^{cd} was solved by molecular replacement methods using the earlier solved Nbs1^{mir}-Mre11^{cd} structure as a replacement model (3.3.3.2 and 4.2.1). A high percentage of structural elements in the apo-Mre11^{cd} structure exhibited a conformation similar to Nbs1^{mir}-Mre11^{cd}. Nevertheless, especially the regions interacting with Nbs1 required extensive manual model building, due to large structural differences between the Nbs1 bound and unbound states. After several rounds of manual model building and refinement, the final R-factors were 28.9 for R_{work} and 22.2 for R_{free} (Table 4.1).

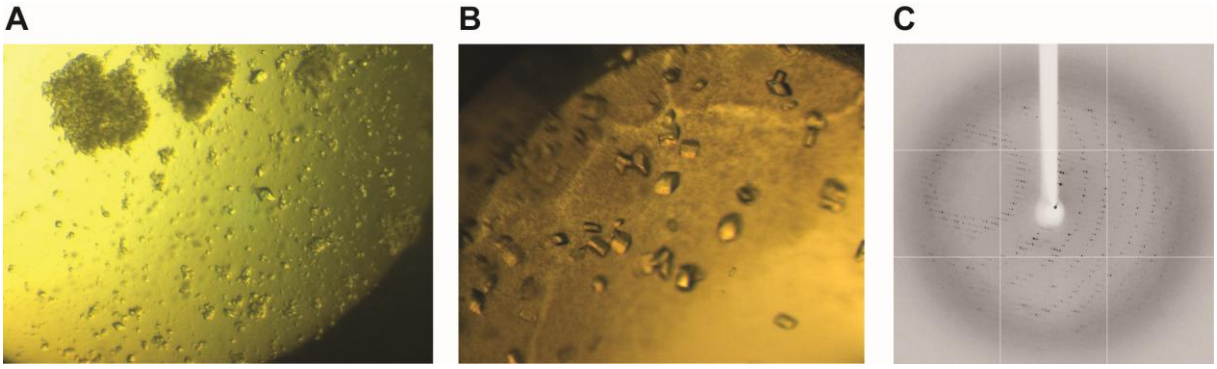

Figure 4.4: Crystallization and data collection of *S. pombe* Mre11^{cd}: (A) Initial crystals of apo-Mre11^{cd} (Condition: 0.2M sodium chloride, 0.1 M Hepes/NaOH pH 7.5, 12% w/v PEG 8000). **(B)** Crystals of apo-Mre11^{cd} from a refinement screen (condition: 0.1 M Hepes/NaOH pH 8.1, 0.2 M sodium chloride, 9% w/v PEG 8000), which were used for data collection (see C). **(C)** Diffraction pattern of Mre11^{cd} crystals from the refinement condition shown in (B).

4.3 Analysis of the apo-Mre11^{cd} structure

The structure of *S. pombe* apo-Mre11^{cd} exhibits a dimeric architecture. Two Mre11^{cd} protomers in the asymmetric unit assemble via a helix bundle interaction between the phosphodiesterase domains. Each phosphodiesterase domain is flanked by an adjacent DNA capping domain, thereby creating a broad U-shaped particle, which harbors the predicted

DNA binding cleft (seen in the archaeal *P. furiosus* Mre11-DNA structure) at its concave side (Figure 4.5 A-B) (Williams et al. 2008).

Binding of Mn^{2+} to the phosphodiesterase motifs identified two apparently functional nuclease sites at the bottom of the broad DNA groove. All Mn^{2+} coordinating residues (Asp25, His27, Asp65, His68, Asn133, His134, His222, His 250, His 252) as well as the two histidine residues (H68, H134), earlier reported to be crucial for exo- and endonuclease activity, were present in an arrangement similar to prokaryotic Mre11 (Figure 4.5 C). Furthermore, the crystallized $Mre11^{cd}$ fragment was an active ssDNA endo/exo nuclease, confirming that the crystallized $Mre11^{cd}$ fragment contained all catalytic core elements (4.9).
Even though there is only a relatively low sequence homology between eukaryotic, archaeal and eubacterial Mre11, some principal characteristics of the domain architecture are conserved among structures from the three different domains of live (Figure 4.5D). Similar to *S. pombe* Mre11, also the phosphodiesterase domains of archaeal *Pyrococcus furiosus* Mre11 and eubacterial *Thermotoga maritima* mediate the dimeric Mre11-Mre11 interaction (Hopfner et al. 2001; Lammens et al. 2011). The capping domains are attached peripheral to the phosphodisterase domain, resulting also in a U-shaped Mre11 dimer.

However, SpMre11 possesses also important differences to prokaryotic and archaeal Mre11 (Figure 4.5 D). Even though the dimer interfaces of Mre11 homologues from all three domains of live consists of a four helix bundle, with two helices from each Mre11 protomer, the assembly of these helices varies: SpMre11 displays a "parallel" helix arrangement, similar to *T. maritima* (Tm) Mre11, while the helix bundle in *P. furiosus* (Pf) Mre11 dimers is "tilted". As a result, the observed SpMre11 dimer cannot bind DNA in the same way as observed for PfMre11 (Williams et al. 2008). Furthermore, SpMre11 has a notable, large loop that extends the dimer interface distal to the DNA binding cleft. It spreads from residue 91 to 123 and is strongly conserved between eukaryotic organisms while absent in archaea and eubacteria (See also alignments below: Figure 4.7 D, Figure 4.8). Interestingly, the $N122^{SpMre11}$ residue within the loop is mutated in human A-TLD 3/4 (human: N117S). The mutation was reported to impair Nbs1 binding while still permit interaction with Rad50 (Stewart et al. 1999). Therefore, it was speculated that this eukaryotic sequence insertion might be a key interaction site for Nbs1 (Hopfner et al. 2001). Additional differences between eu- and prokaryotic Mre11 exist also in the structural composition of the capping domain. It contains an extended 40 Å long alpha helix element (helix αF) in *S. pombe* Mre11, which spans from residue 332 to 358 αF, whereas the corresponding *P. furiosus* and *T. maritima*

helices are much shorter (21 and 19 Å respectively - see also sequence alignment in Figure 4.8).

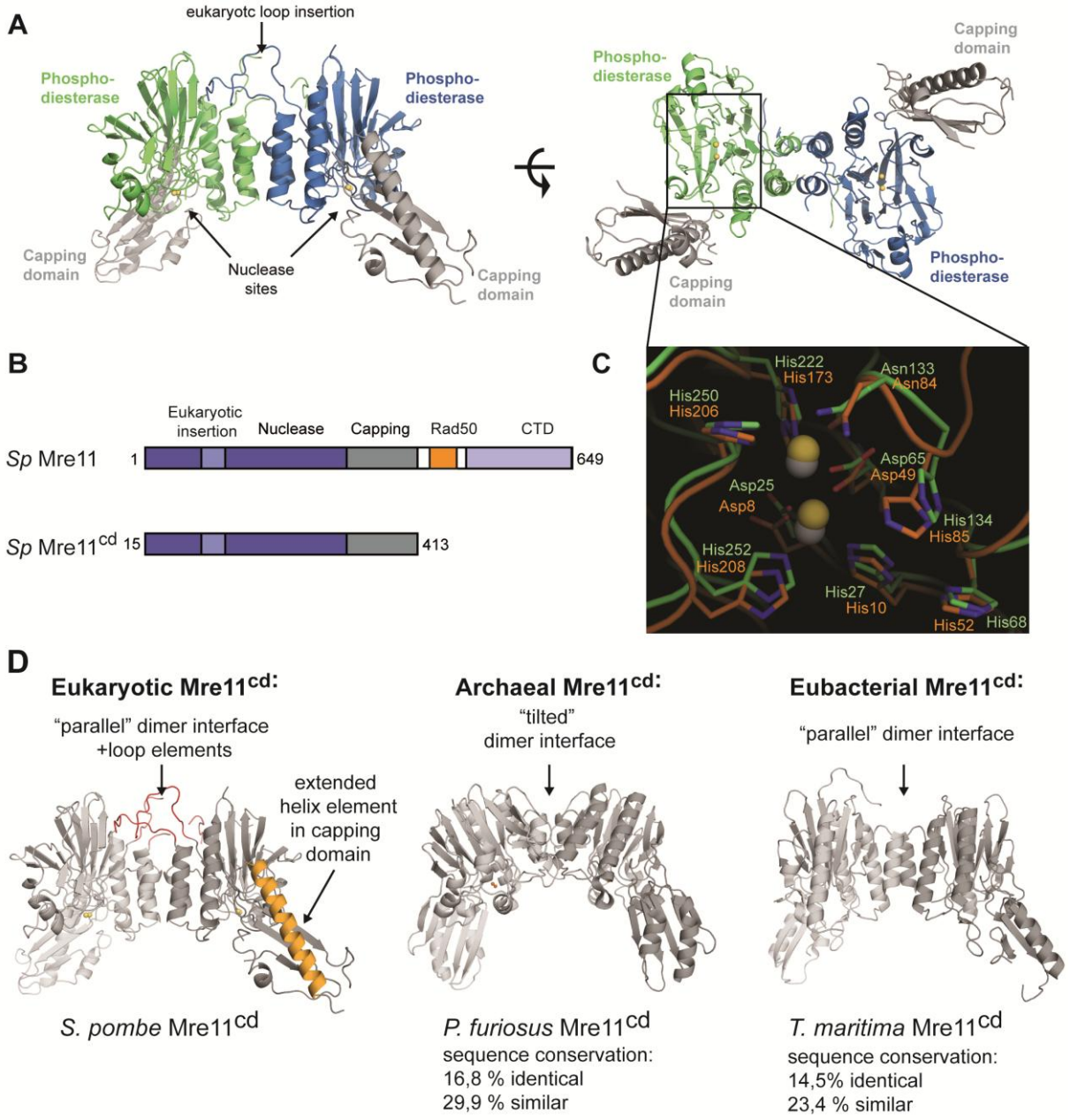

Figure 4.5: Structure of *S. pombe* apo-Mre11^{cd} and comparison with homologous Mre11 structures from *P. furiosus* and *T. maritima*: (A): Mre11^{cd} dimer (phosphodiesterase in green/cyan and DNA capping domains in grey), shown as ribbon representation from side and top view. **(B)** Domain maps of full length *S. pombe* Mre11 and the crystallized Mre11^{cd} construct (CTD stands for Mre11 C-terminal domain). **(C)** Overlay of Mre11 active sites from *S. pombe* Mre11^{cd} (protein model in green, Mn^{2+} ions shown as yellow spheres) and *P. furiosus* Mre11 (PDB entry 1II7 - protein model in orange, Mn^{2+} ions shown as grey spheres). **(D)** Comparison of the eukaryotic *S. pombe* Mre11^{cd} structure with archaeal *P. furiosus* Mre11 (PDB entry 1II7) and eubacterial *T.*

maritima Mre11 (PDB entry 2Q8U). The loop insertion in the nuclease domain of *S. pombe* (residues 91-123, here colored in red) is specific for eukaryotic Mre11 and absent in archaea or bacteria. *S. pombe* Mre11 contains furthermore an extended 40 Å long alpha helix element in the capping domain (colored in orange), which spans from residue 332 to 358.

4.4 Analysis of the Nbs1^{mir}-Mre11^{cd} complex structure

4.4.1 The structure of Nbs1^{mir}-Mre11^{cd} - An overview

The Nbs1^{mir}-Mre11^{cd} complex structure reveals that both proteins form a complex with 2:2 stoichiometry. The two Nbs1^{mir} molecules bind to the Mre11 dimer at two distinct sites (Figure 4.6 A-C). Each Nbs1^{mir} wraps around the outside of one Mre11 phosphodiesterase domain in a highly extended conformation via an α-helix and a ß-strand (interaction region 1). This first interaction region maps to the Nbs1^{mir} residues 477-498. Nbs1^{mir} becomes disordered C-terminal from interaction region 1. However, a second stretch of residues from one Nbs1 molecule, which contains a strongly conserved "KNFKxFxK motif (residues 518-526), is ordered again and binds asymmetrically across the Mre11 dimer interface, opposite from the active site cleft. This interaction region 2 is mediated by the eukaryote-specific insertion loop (residues 91-123, see also 4.3), which is further named "latching" loop.

To rule out that the protein fusion between Nbs1^{mir} and Mre11^{cd} might influence the protein structure, also a reversed plus additionally cleavable fusion protein (Mre11^{cd} 7-413 fused to Nbs^{mir} 474-531) had been generated. The non-fused complex of Mre11^{cd} and Nbs^{mir} had been crystallized and its structure determined to 2.2 Å resolution (4.2.1). Consistently, both structures are highly similar, arguing against influences of fusion and construct design (Figure 4.6 D).

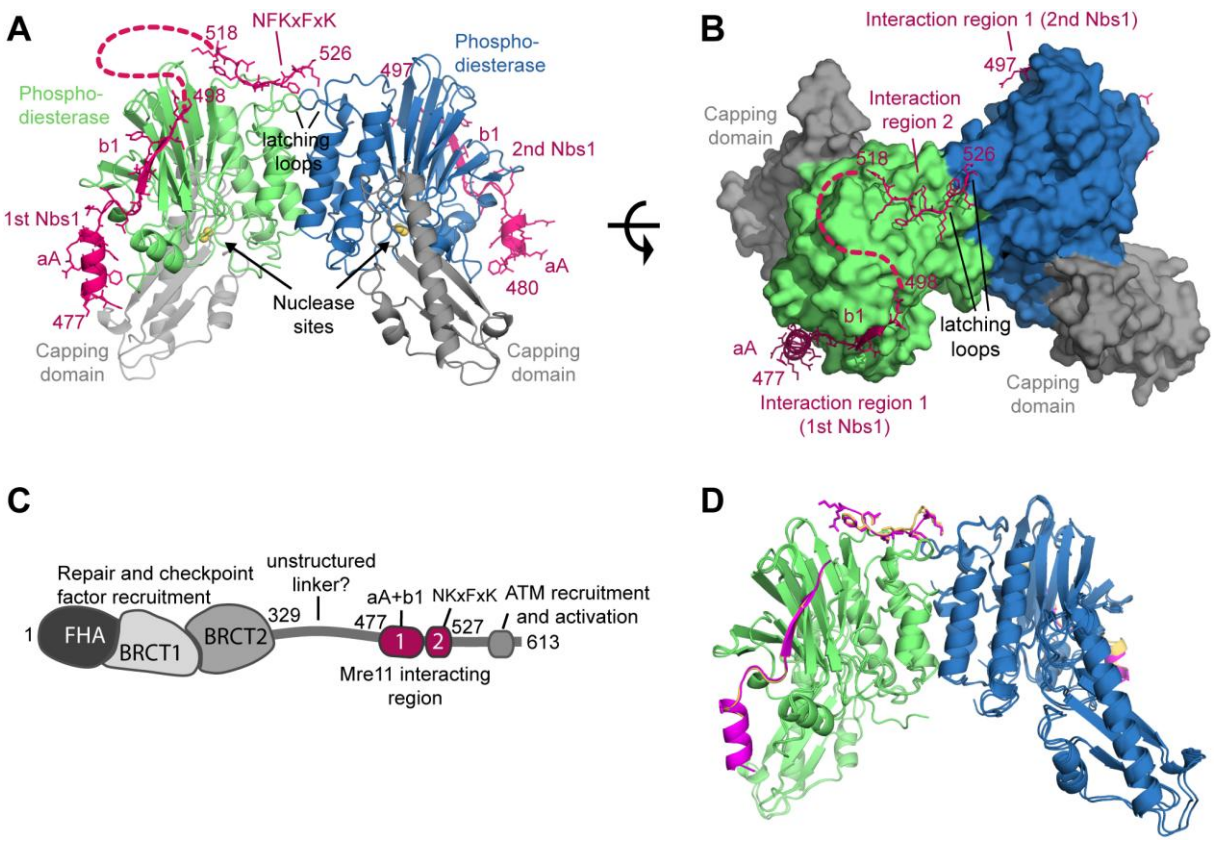

Figure 4.6: Structure of Nbs1^{mir}-Mre11^{cd} and domain map of Nbs1 (A) Structure of the two Nbs1^{mir} molecules (magenta) bound to the Mre11^{cd} dimer (phosphodiesterase in green/cyan and DNA capping domains in grey), shown as ribbon representation with highlighted secondary structures. Nbs1 binds with "interaction region 1" around the outside of the phosphodiesterase domain. One of the two Nbs1 additionally binds with "interaction region 2" to two latching loops at the Mre11 dimer interface. **(B)** Molecular surface representation of the Mre11 dimer with bound Nbs1 molecules highlights the asymmetric bridging of the Mre11 dimer by Nbs1 "interaction region 2". **(C)** Domains and motifs of *S. pombe* Nbs1. **(D)** A superposition of crystal structures of the Nbs1^{mir}-Mre11^{cd} fusion protein complex and the non-fused Mre11^{cd}-Nbs1^{mir} complex (crystallized after proteolytic cleavage) reveals highly similar structures that rule out structural artefacts of the fusion.

4.4.2 Analysis of protein interaction sites in the structure of Nbs1^{mir}-Mre11^{cd}

Each of the two Nbs1^{mir} molecules in the structure binds via interaction region 1 to the outside of one Mre11 phosphodiesterase domain. The interface residues D477^{Nbs1}-R486^{Nbs1} attach as an α-helix (αA) to an Mre11 loop emerging from the metal coordinating active site motif IV (Figure 4.7 A). This interaction would place the N-terminal FHA and BRCT module of Nbs1 (missing in this structure - Nbs1 domain map shown in Figure 4.6 C) near the entry/exit of Mre11's DNA binding cleft, suitable for recruitment of repair and checkpoint factors to DSBs

(Lloyd et al. 2009; Williams et al. 2009). Following αA, Nbs1 binds via an "S" shaped loop structure (residues $L487^{Nbs1}$-$G491^{Nbs1}$) across the short Mre11 helix element αD, which involves a hydrophobic interaction between the highly conserved residues $F238^{Mre11}$ and $L490^{Nbs1}$. Subsequent to the "S" loop, Nbs1 is attached as a third strand ($\beta1^{Nbs1}$ $S492^{Nbs1}$-) to a two-stranded β-sheet of Mre11. All in all, the interaction region 1 is partially polar, but it contains a few hydrophobic anchor points.

The two $Nbs1^{mir}$ molecules become unstructured C-terminal from the interaction region 1. Only one of the two chains is ordered again between residues 518-526 and binds as interaction region 2 across both Mre11 latching loops. Thereby it breaks the pseudo-twofold symmetry of the Mre11:Nbs1 complex (Figure 4.6 A-B). The contacts to Mre11 are mediated by the highly conserved "KNFKxFxK" motif of Nbs1 via a hydrogen bonding and π-stacking network (Figure 4.7 B and sequence alignments Figure 4.7 C-D). In particular, residue $K519^{Nbs1}$ binds the backbone of $G177^{Mre11}$, $N520^{Nbs1}$ binds the backbone of $C94^{Mre11}$ and stabilizes the conformation of KNFKxFxK, $F521^{Nbs1}$ stacks with $E97^{Mre11}$, while $K522^{Nbs1}$ and $K526^{Nbs1}$ bind to backbone carbonyls plus side chain oxygens of both $N122^{Mre11}$ from the two Mre11 protomers. Most notably, $F524^{Nbs1}$ inserts in a π-stacking interaction between two peptide bonds and the two $N122^{Mre11}$ carboxamide groups from each of the two Mre11 protomers and appears to "probe" the Mre11 dimer conformation. The importance of this interaction is indicated by the extremely high conservation of the entire motif among the otherwise poorly conserved Nbs1/Xrs2 orthologs (Figure 4.7 D).

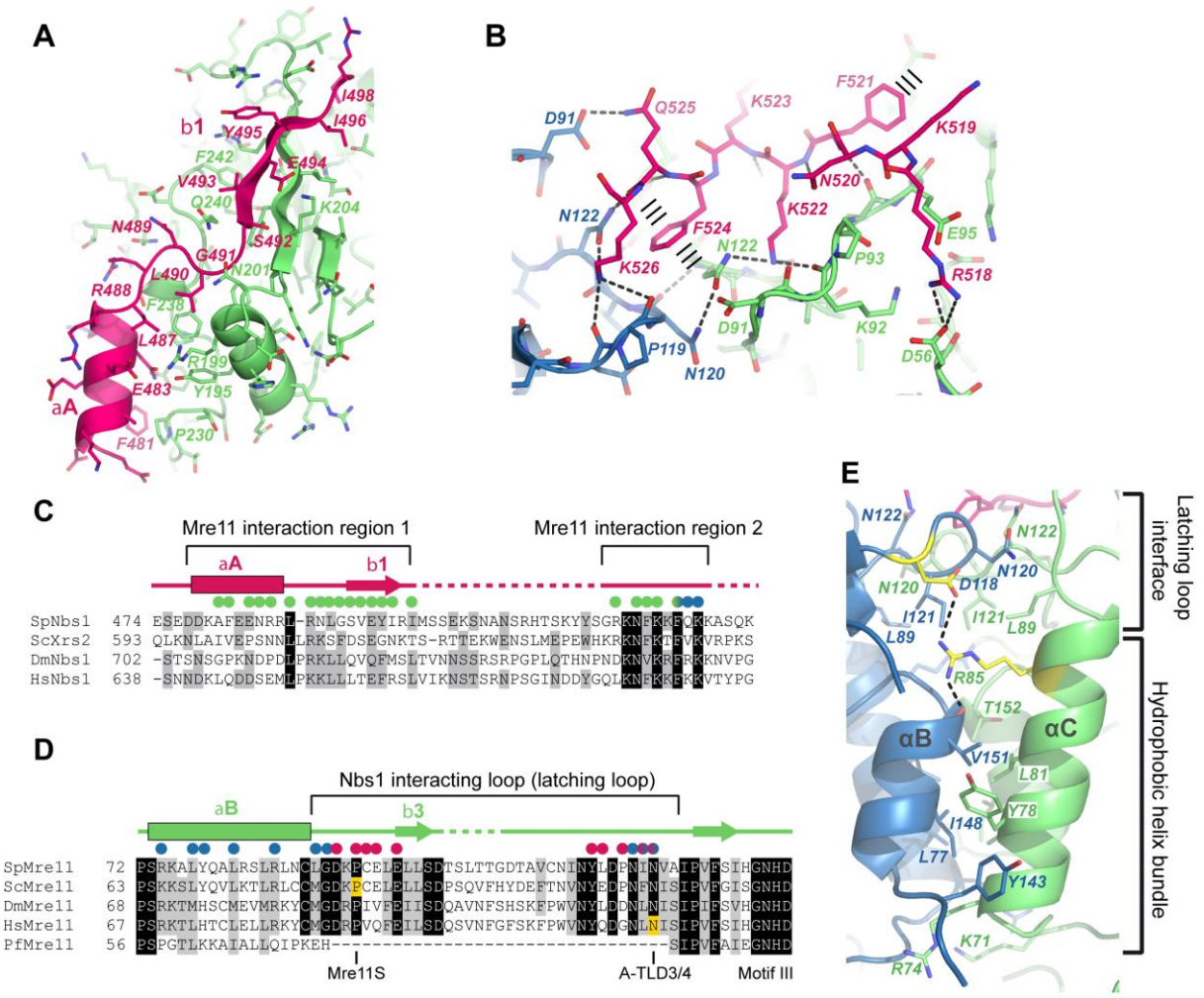

Figure 4.7: Details of the Mre11-Nbs1 and Mre11 dimer interfaces: (A) Details of interaction region 1. Mre11 interaction region 1 of Nbs1 (magenta) binds to the outside of Mre11's phosphodiesterase domain (cyan) with two secondary structure elements (αA and ß1) in a partially polar, partially hydrophobic interface. Key residues from both interaction partners are annotated. **(B)** Interaction region 2 of Nbs1 (magenta) contains the highly conserved NFKxFxK motif and binds asymmetrically across the Mre11 dimer (cyan/green) via a network of hydrogen bonds and π-stacking interactions (highlighted). **(C)** Sequence alignment of the Mre11 interaction region of Nbs1 from *Schizosaccharomyces pombe* (Sp), *Saccharomyces cerevisiae* (Sc), *Drosophila melanogaster* (Dm) and *Homo sapiens* (Hs). Conserved (grey) and highly conserved (black) residues are shaded. The secondary structure is shown on top. Residues involved in direct interaction with the Mre11 dimer are shown as green (one Mre11 protomer), blue (the other protomer) or green/blue (both protomers) spheres (3.3.5.1). **(D)** Structure based sequence alignment of eukaryotic Mre11's (see C) with prokaryotic Mre11 from *Pyrococcus furiosus* (Pf) around the eukaryotic Mre11 specific latching loop. Conserved (grey) or highly conserved (black) residues are shaded. Secondary structure, nuclease motif III and A-TLD3/4 plus Mre11S mutation sites are highlighted. Many highly conserved residues of the eukaryote-specific latching loop are involved in Nbs1 (magenta spheres), or Mre11 dimer (blue spheres) contacts (3.3.5.1). (E) Details of the Mre11 dimer interface in the $Nbs1^{mir}$-$Mre11^{cd}$ structure. The Mre11 monomers are colored in blue and green, while $Nbs1^{mir}$ is colored in pink. The dimer interface can be distinguished into two different regions, the hydrophobic

four helix and the latching loop interface. Both motifs are connected with each other via salt bridges between the conserved residues $R85^{Mre11}$ and $D118^{Mre11}$ (colored in yellow).

Another remarkable feature of the $Nbs1^{mir}$-$Mre11^{cd}$ structure is the Mre11 dimer interface (Figure 4.7 E). It can be divided into two different sub-regions. The first part of the interface is build up by the conserved four helix bundle, which is composed of helices αB and αC from each monomer. The lower end of the helix bundle exposes some positively charged residues ($K71^{Mre11}$, $R74^{Mre11}$) into the predicted concave DNA binding groove, whereas the main dimer interactions are mediated by conserved hydrophobic interfaces between αB and αC. Here, residues $L77^{Mre11}$, $Y78^{Mre11}$, $L81^{Mre11}$, $Y143^{Mre11}$ and $I148^{Mre11}$ are involved (Mre11 sequence alignment - Figure 4.8). The second part of the Mre11 interface is mainly build up by the Mre11 latching loops in the presence of $Nbs1^{mir}$ and is absent in the apo-$Mre11^{cd}$ structure (4.3).

The $Nbs1^{mir}$ engaged latching loops are connected to the basal four helix bundle interface via two higly conserved salt bridges. Here, arginine residue $R85^{Mre11}$ from helix αB of each Mre11 monomer binds to its neighbouring residue $D118^{Mre11}$ from the latching loop of the other monomer. The latching loops interact with each other via a “kissing” loop conformation, which involves hydrophobic packing of L89 and I121 as well as a network of side chain and backbone hydrogen bonds via residues $N120^{Mre11}$, $I121^{Mre11}$ and $N122^{Mre11}$.

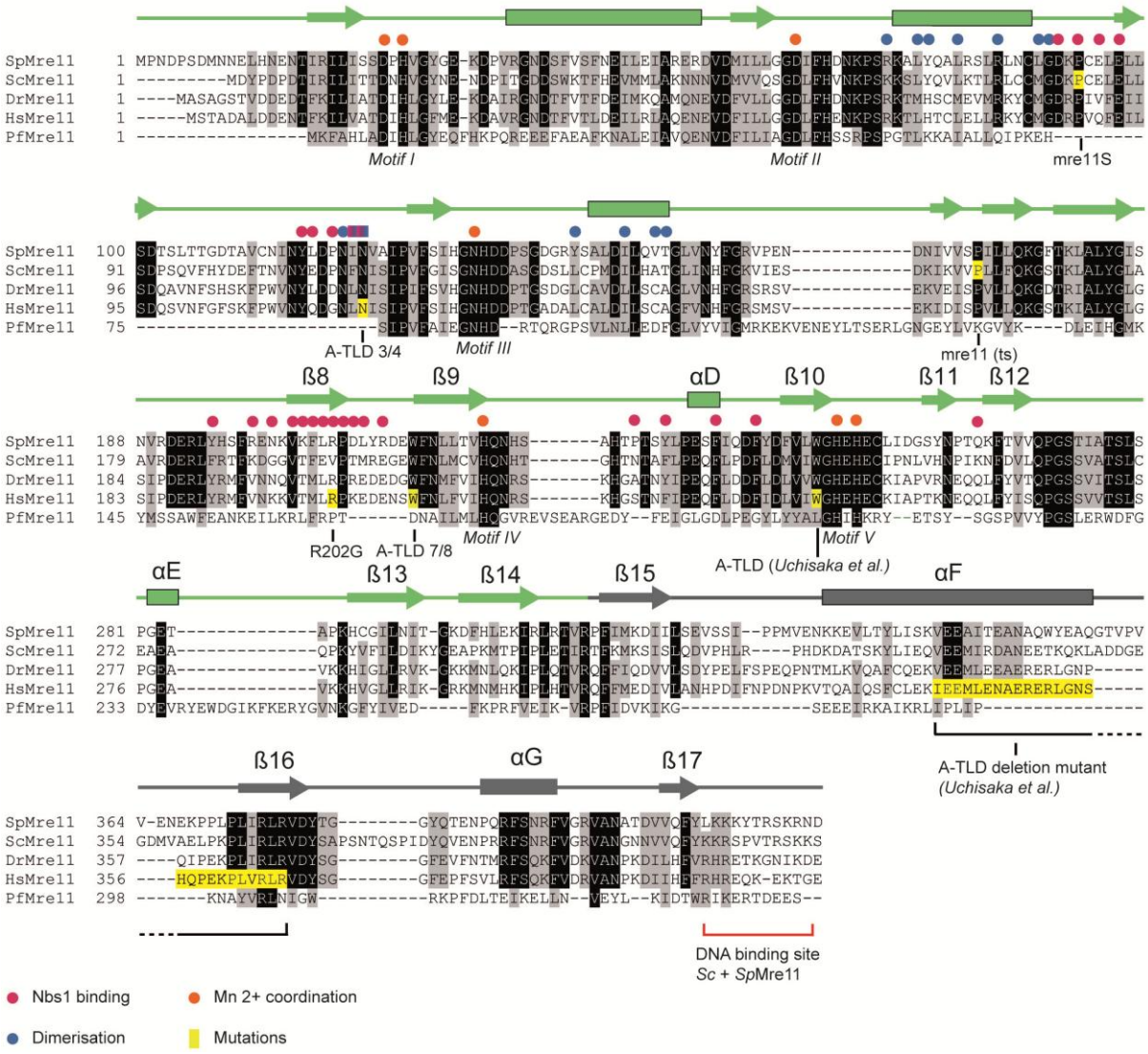

Figure 4.8 Structure based sequence alignment and functional motifs of Mre11: Sequence alignment of the nuclease modules of Mre11 species from *Schizosaccharomyces pombe* (Sp), *Saccharomyces cerevisiae* (Sc), *Danio rerio* (Dr), *Homo sapiens* (Hs) and *Pyrococcus furiosus* (Pf). Conserved (grey) or highly conserved (black) residues are shaded (3.3.5.1). The secondary structure is shown on top of the alignment. Phoshopdiesterase motifs are annotated. Spheres represent residues implicated in Nbs1 interaction (magenta), Mre11 dimer interaction (blue) and metal coordination (orange). Phosphodiesterase motifs and the DNA binding site of *S. cerevisiae* (*Sc*) ans *S. pombe* (*Sp*) Mre11 are indicated. Mutation sites in ataxia telangiectasia like disease (A-TLD, see main text), breast cancer (R202G) (Bartkova et al. 2008), S. cerevisiae Mre11S (Nairz and Klein 1997) and Mre11(ts) (Chamankhah et al. 2000) are shown in yellow and are annotated.

4.5 Conformational impact of Nbs1^{mir} binding on the Mre11^{cd} dimer configuration

A comparison of the apo-Mre11^{cd} and Nbs1^{mir}-Mre11^{cd} structures reveals that Nbs1^{mir} binding appears to substantially influence the Mre11^{cd} dimer and latching loop conformations: The latching loops are mostly disordered and "swapped" between the two Mre11 protomers in the apo-Mre11^{cd} structure. Nbs1^{mir} binding leads to a disorder to order transition and to geometrically rearranged latching loops, which form a network of interactions with both, the Mre11 phosphodiesterase domain "core" and Nbs1^{mir} (Figure 4.9 A-B). Furthermore, Nbs1 binding increases the Mre11 dimer interface to a large extent and promotes a dimeric "kissing loop" conformation of the two Mre11 molecules by bridging both N122^{Mre11} residues via π-stacking interactions.

Figure 4.9 C shows an overlay of monomers from apo-Mre11^{cd} and Nbs1^{mir}-Mre11^{cd} structures. Here, a more detailed view of the Nbs1 induced conformational rearrangements within one Mre11 molecule can be seen: The latching loop, which orients towards the second Mre11 molecule in apo-Mre11, is flipped in an almost 180° rotation towards the basal phosphodiesterase core in the Nbs1 bound state. Interestingly, it is thereby directly connected to the Mre11 dimer helix αC, which rotates by 15° towards a more tilted orientation in respect to the Mre11 dimer axis. Also binding of the Mre11 interaction region 1 of Nbs1^{mir} leads to conformational changes in Mre11, albeit not as pronounced as the changes seen for the latching loops and Mre11 interacting region 2. A small eukaryotic loop insertion element, consisting of residues 209-214, moves to cap the beta sheet interaction between ß8 of Mre11 and b1 of Nbs1^{mir}.

Remodeling of the latching loops and the hydrophobic Mre11 helix bundle also induces a global change of the Mre11 dimer configuration: An alignment of Nbs1^{mir}-Mre11^{cd} to just one apo-Mre11 protomer, reveals a 30° rotation shift in the Mre11 dimer angle of Nbs1^{mir}-Mre11^{cd} towards a more compact conformation with a narrower DNA binding cleft (Figure 4.9 D). From this can be concluded, that the Mre11 dimer interface possesses an intrinsic flexibility, which would allow the adoption of different conformations depending on the functional state of Mre11.

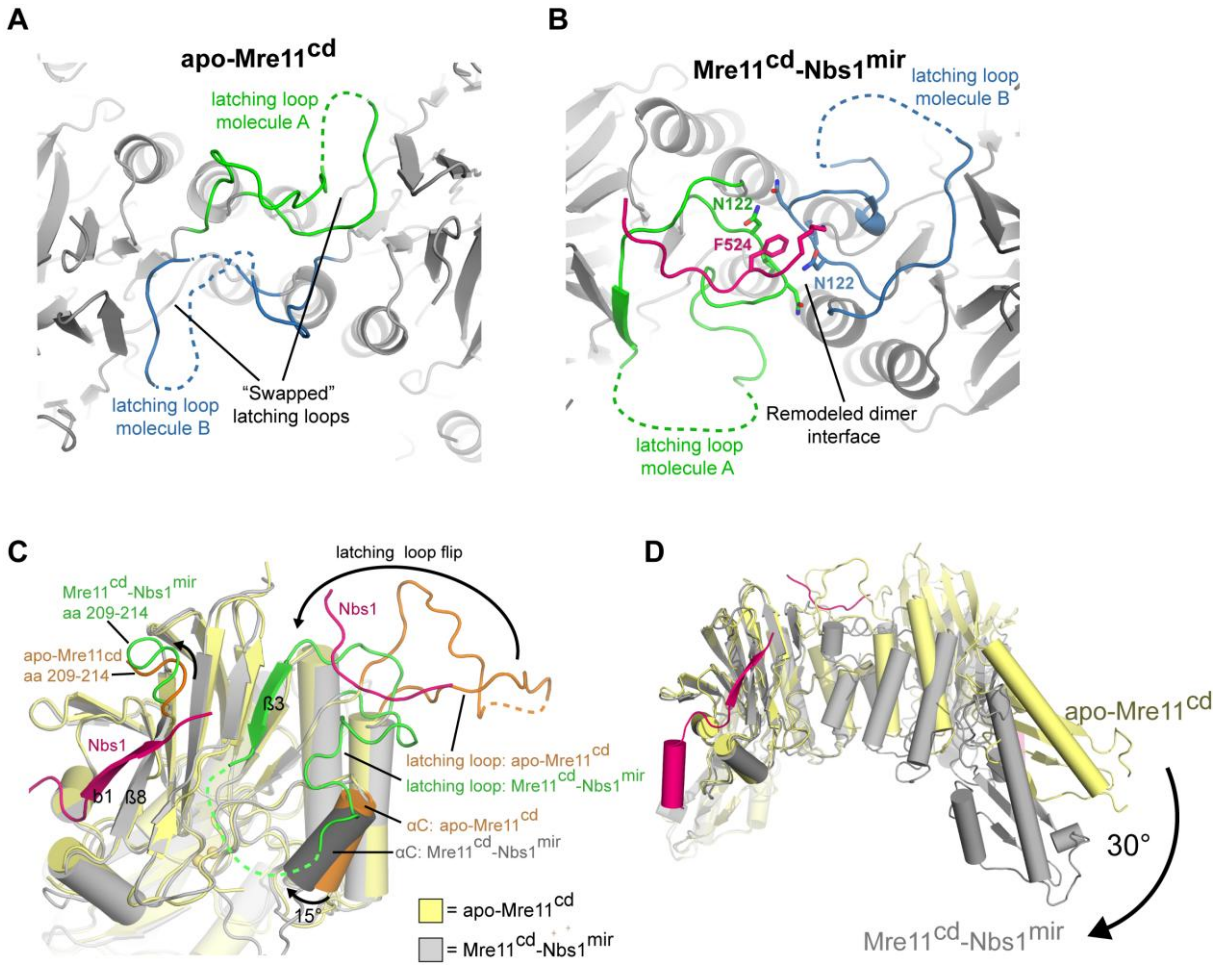

Figure 4.9: Conformational impact of Nbs1 binding on the Mre11 dimer configuration: (A) A top view of apo-Mre11^{cd} along the Mre11 dimer axis shows the latching loops indicated in green (molecule A) and blue (molecule B). The latching loops are "swapped" between the molecules A and B. They appear highly flexible and lack any secondary structure. **(B)** A top view of Nbs1^{mir}-Mre11^{cd} similar to (A) on the latching loop conformation in presence of the bound Mre11 interaction region 2 of Nbs1. Nbs1 binding orders the latching loops and promotes a dimeric "kissing loop" interaction between the latching loops by bridging both N122^{Mre11} via its phenylalanine residue F524^{Nbs1}. **(C)** Nbs1 binding causes several conformational rearrangements in Mre11. An overlay of Mre11 monomers from apo-Mre11^{cd} and Nbs1^{mir}-Mre11^{cd} structures is shown. The latching loop of apo-Mre11^{cd} reaches towards the neighboring Mre11^{cd} molecule. In Nbs1^{mir}-Mre11^{cd} it is flipped by an almost 180° turn and interacts with both Nbs1 and the basal Mre11 phosphodiesterase core. Direct binding of the latching loop induces a 15° rotation of helix αC towards a more tilted orientation in respect to the Mre11 dimer axis. A small loop element consisting of residues 209-214 gets positioned to bind cooperatively with ß8 to the beta-strand b1 of Nbs1^{mir}. **(D)** An overlay of apo-Mre11^{cd} and Nbs1^{mir}-Mre11^{cd} by aligning of Nbs1^{mir}-Mre11^{cd} to just one apo-Mre11 protomer reveals a distinct macromolecular change. The dimer angle of Nbs1^{mir}-Mre11^{cd} is rotated by 30°, in comparison to apo-Mre11^{cd}, towards a more compact and "closed" conformation.

4.6 Comparison of Nbs1^{mir}-Mre11^{cd} structures with different metal coordinating states

The structure of Nbs1^{mir}-Mre11^{cd}, derived from crystals grown without additional Mn^{2+} ions in the crystallization condition contained only one Mn^{2+} ion in the active site. Therefore, additional refinement screenings with high $MnCl_2$ concentrations were performed. These crystals yielded a structure with an active site containing two Mn^{2+} ions (4.2.1). By comparison of both structures an interesting observation regarding a potential regulation mechanism of the Mre11 catalytic site could be made. Apparently, each nuclease domain contains both a metal binding site of high and low affinity (Figure 4.10). In the initially solved Nbs1^{mir}-Mre11^{cd} structure, where only one Mn^{2+} ion was present in the active site, the phosphodiesterase motif III (residues N133 and H134) and a C-terminally adjacent loop element, spanning residues 135-142, were flipped into an inactive conformation. Sodium citrate, which is included in the crystallization condition, might titrate out the Mn^{2+} ion with the lower affinity. Addition of higher concentrations of Mn^{2+} resulted in binding of Mn^{2+} to the lower affinity site. Coordinating of the second Mn^{2+} by N133 rearranges the entire loop, yielding a structure with both Mn^{2+} ions present in a catalytically active arrangement similar to the DNA bound *P. furiosus* Mre11^{cd} structure (Williams et al. 2008). A switchable phosphodiesterase motif III loop might play a role in the allosteric communication between DNA binding and active site structure, *e.g.* for the co-processing factor CtIP/Sae2 to stimulate the Mre11 nuclease activity (Lengsfeld et al. 2007; Sartori et al. 2007).

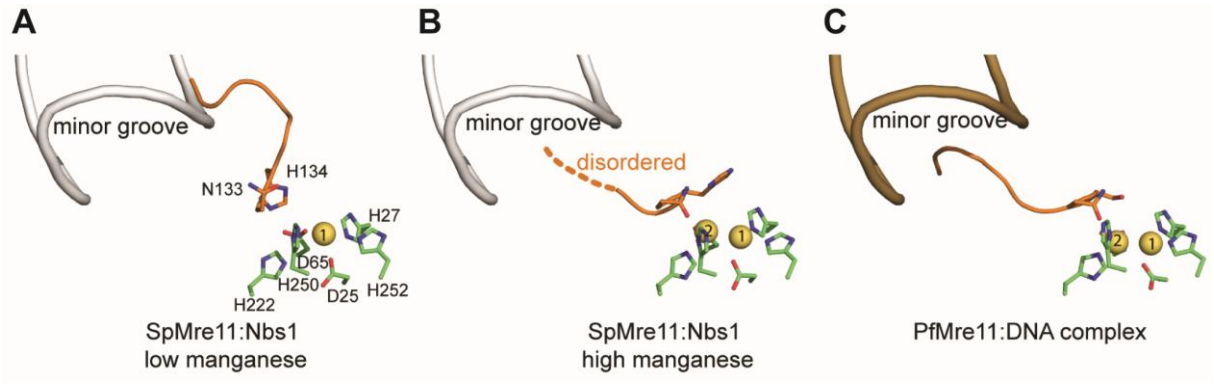

Figure 4.10: Manganese coordination states of different *S. pombe* Nbs1^{mir}-Mre11^{cd} structures and a comparison with the *P. furiosus* active site: Comparison of the manganese coordination site of *S. pombe* Nbs1^{mir}-Mre11^{cd} in the presence of low (< 1 mM) **(A)** and high (50 mM) Mn^{2+} **(B)** with the coordination site of DNA bound *P. furiosus* Mre11^{cd} **(C)** (PDB entry 3DSD) (Williams et al. 2008). Coordinating residues are shown

as green and color-coded sticks, the metals are shown as yellow spheres. One high affinity metal binding site (1) is coordinated even at low manganese concentrations. Binding of a second manganese ion (2) at high concentrations and its coordination by N133 flips a loop (orange) that might bind to the minor groove of a DNA hairpin (brown cartoon model). The corresponding position of DNA (not present in the *S. pombe* structures) is indicated as a grey model. These results suggest an allosteric interaction between DNA binding and active site formation in eukaryotic Mre11.

4.7 SAXS analysis of Mre11^{cd} and comparison with Nbs1^{mir}-Mre11^{cd}

The crystallized *S. pombe* Mre11^{cd} protein (4.3) was also analyzed by small angle x-ray scattering (SAXS), to verify that the conformation seen in the crystal structure is also present in solution. For this purpose, the experimentally derived angle scattering pair distributions (Figure 4.11 A) and scattering intensity plots (Figure 4.11 B) of Mre11^{cd} were compared with curves theoretically calculated from the crystal structures of apo-Mre11^{cd} and Nbs1^{mir}-Mre11^{cd}.

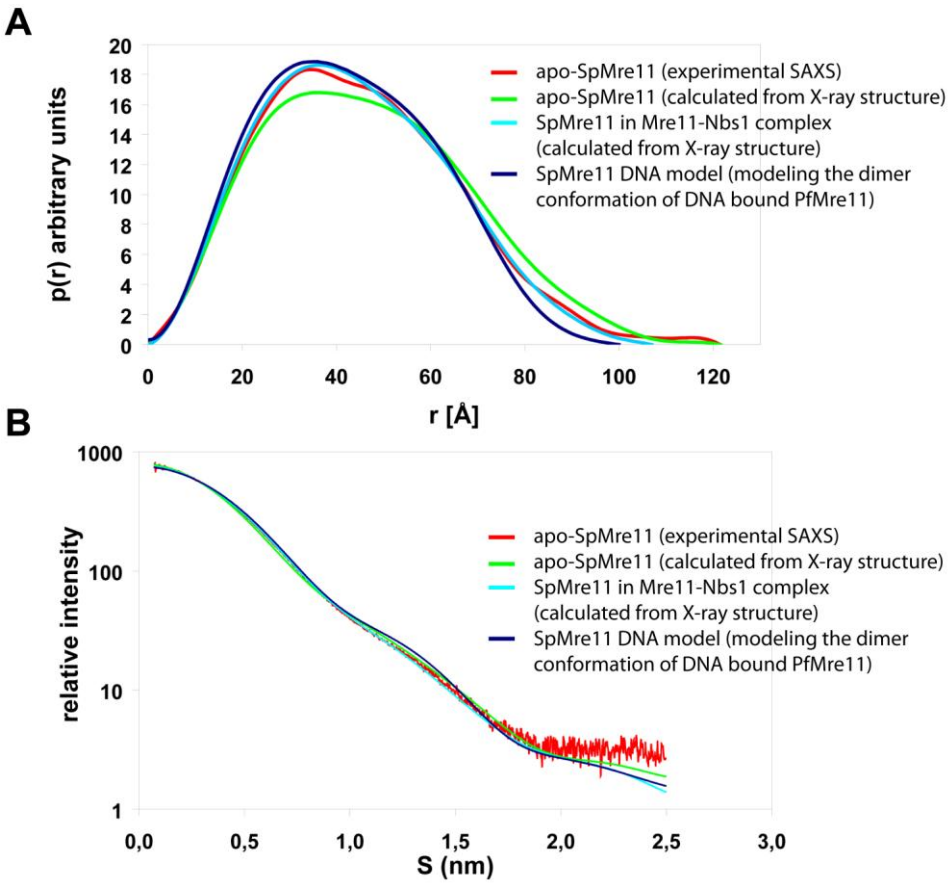

Figure 4.11: Small angle X-ray scattering analysis of Mre11^{cd}. Small angle scattering pair distribution (A) and scattering intensities (B) as derived by the scattering experiment for *S. pombe* Mre11^{cd} (SpMre11^{cd}, colored in red) or calculated from

various structural models: Crystal structure of SpMre11^{cd} dimer (green); crystal structure of the SpMre11 dimer in the Sp Nbs1^{mir}-Mre11^{cd} complex (light blue, Nbs1^{mir} coordinates omitted); model of the SpMre11^{cd} dimer with a dimer angle corresponding to the DNA bound P. furiosus Mre11^{cd} dimer (PfMre11^{cd}, dark blue).

Furthermore, a theoretical model of the DNA bound *S. pombe* Mre11^{cd} conformation was generated by superposition of Mre11^{cd} protomers on the structure of DNA bound *P. furiosus* Mre11 (3.3.3.3) (Williams et al. 2008). The P(r) function of apo-Mre11^{cd} measured with SAXS is quite distinct from the model of the DNA bound state, which contains more short vectors due its more compact dimeric shape. The apo-Mre11 P(r) function is rather in a range between the crystal structures of apo-Mre11^{cd} and Nbs1^{mir} bound Mre11^{cd}. This suggests that in solution, the *S. pombe* Mre11^{cd} dimer might be flexible and flip between the two conformations observed in the apo-Mre11^{cd} and Nbs1^{mir}-Mre11^{cd} structures. Nbs1 binding would then stabilize one of the two conformations.

4.8 Structural and biochemical characterization of the Mre11-Nbs1 interface and disease causing Mre11 mutations

4.8.1 Analysis of A-TLD and NBS-like disease mutations

The structures of apo-Mre11^{cd} and Nbs1^{mir}-Mre11^{cd} allowed for the first time a structural analysis of the molecular basis for several human Ataxia-telangiectasia like disease (A-TLD) and Nijmegen breakage syndrome like (NBS-like) disease causing Mre11 mutations (Figure 4.12 A). Most remarkably, the human equivalent of N122^{SpMre11} - the residue that sandwiches the Nbs1 phenylalanine in the Mre11 dimer interface - is mutated in A-TLD 3/4 (N117S^{HsMre11}) (Stewart et al. 1999) (Figure 4.12 B). W210C^{HsMre11} leads to A-TLD 7/8 (Fernet et al. 2005), and the equivalent *S. pombe* W215^{SpMre11} residue caps the three stranded shared ß-sheet between Mre11 and Nbs1 (Figure 4.12 C). Thus, A-TLD 7/8 likely affects the Nbs1 interaction at interaction region 1. The same structural region is mutated in yeast *mre11*(ts), which also exhibits compromised MRX complex formation (Chamankhah et al. 2000). Most recently, a compound heterozygous mutation consisting of W243R^{HsMre11} (W248^{SpMre11}) and a deletion mutation Del(340-366) have been associated with A-TLD. In Del(340-366) a part of the central long capping domain helix is deleted (Uchisaka et al. 2009) (Figure 4.12 A). Such a severe truncation likely destabilizes the protein, explaining the

decreased Mre11 levels in these patients. The point mutation in the other allele maps to W248^{SpMre11}, which forms the hydrophobic core of the structural region linking the nuclease active site and contact site to αA^{Nbs1} (Figure 4.12 D). Consequently, W243^{hMre11}->R could affect both nuclease activity as well as Nbs1 binding.

Until recently A-TLD was the only hereditary disease known to be caused by mutations in the *Mre11* gene. However, a new patient study reported the compound heterozygous mutation D113G^{HsMre11} to be linked with a so far unreported NBS-like disease (NBSLD) (Matsumoto et al. 2011). In the *S. pombe* Nbs1^{mir}-Mre11^{cd} structure, the homologous D118^{SpMre11} residue is involved in Mre11 dimer formation by connecting the latching loop to the basal helical dimer interface via a highly conserved salt bridge with R85^{SpMre11} from the neighboring Mre11 protomer (Figure 4.12 E). R85 furthermore hydrogen bonds to the C-terminal turn of helix αB of the opposing Mre11 protomer. Since this bond is not seen in apo-Mre11, R85 is likely a key residue in determining the Mre11 dimer angle in the presence of Nbs1.

Taken together, A-TLD and NBSLD mutations do not cluster to one particular site, but affect the Nbs1 binding site at different interaction regions. Since Nbs1 binds as an extended peptide at multiple sites, the structural results of this thesis could explain the observation that A-TLD mutations in Mre11 retain residual Nbs1 binding activity (Stewart et al. 1999) and are hypomorphic to a null mutation.

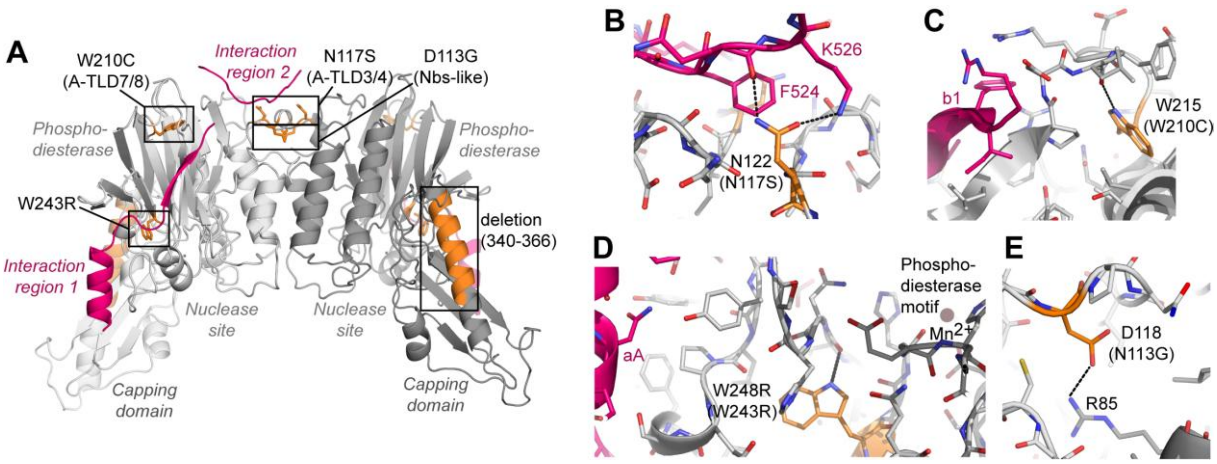

Figure 4.12: Structural basis for A-TLD and NBS-like disease causing mutations (A) A-TLD mutation sites (orange sticks) are found throughout the Mre11 dimer (light/dark grey cartoon model). All point mutations are located in places that are critical for the interaction with Nbs1 (magenta cartoon model). **(B)-(D)** Details of A-TLD mutation sites. A-TLD associated residues (orange sticks) are found either in direct contact with Nbs1 (B) or stabilize structural elements that interact with Nbs1 (C, D). **(E)** Details of NBS-like disease causing mutation site D113G (homologous to D118 in *S. pombe*).

4.8.2 Structural and biochemical link between Nbs1 interaction and the nuclease active site of Mre11

The structure of $Nbs1^{mir}$-$Mre11^{cd}$ showed that Nbs1 binds to Mre11 as an elongated peptide chain via multiple interacting residues. To characterize the impact of mutations in prominent Mre11-Nbs1 interface residues and A-TLD causing mutations on the stability of the Mre11-Nbs1 interaction, binding experiments using analytical size exclusion chromatography were carried out (3.3.2.7). For this purpose, several mutants of *S .pombe* Mre11 aa 1-413 and Nbs1 aa 428-613 constructs were generated (Figure 4.13 A and Table 3.5). The mutations $F524E^{SpNb1}$ and the double mutants $K522E^{SpNbs1}$ / $K526E^{SpNbs1}$ target key interactions in the Mre11-Nbs1 interface 2 (Figure 4.7 B). Furthermore, three conserved residues of *S. pombe* Mre11 were mutated to the corresponding human A-TLD causing mutations, namely $N122S^{SpMre11}$ ($N117S^{HsMre11}$ / A-TLD 3/4), $W215C^{SpMre11}$ ($W210C^{HsMre11}$ / A-TLD 7/8) and $W248R^{SpMre11}$ ($W243R^{HsMre11}$) (Stewart et al. 1999; Fernet et al. 2005; Uchisaka et al. 2009). Remarkably, all mutant proteins were still able to form stable Mre11-Nbs1 complexes in size exclusion chromatography, but this ability depended strongly on the presence of Mn^{2+} in the chromatography buffer. In fact, while Wt Nbs1 (aa 428-613) interacted both in the presence and absence of Mn^{2+}, KNFKxFxK motif mutants $F524E^{SpNbs1}$ and $K522E^{SpNbs1}$/ $K526E^{SpNbs1}$ interacted in the presence but not in the absence of Mn^{2+} (Figure 4.13). Similarly, the A-TLD like mutations $N122S^{SpMre11}$, $W215C^{SpMre11}$ and $W248R^{SpMre11}$ interacted with Wt Nbs1 (aa 428-613) in the presence but not absence of Mn^{2+}. Since a mutation in the phosphodiesterase motif was found to disrupt MRX also *in vivo* (Bressan et al. 1998), it can be concluded that 1) Mn^{2+} binding to the active site stabilizes the $Nbs1^{mir}$ interaction, likely by solidifying the phosphodiesterase fold and dimer structure due to coordination of phosphodiesterase motifs and 2) that A-TLD mutations as well as mutations in the Nbs1 part of the interface reduce but not completely abolish the ability of $Nbs1^{mir}$ to interact with Mre11. Taken together, these structural and biochemical results suggest that the hypomorphic phenotype of A-TLD stems from a functionally perturbed, but not completely abolished interaction of $Nbs1^{mir}$ with the phosphodiesterase dimer of Mre11. This is due to the interaction being mediated by an extended stretch of multiple, independent interaction sites, rather than by a single, strong interaction site.

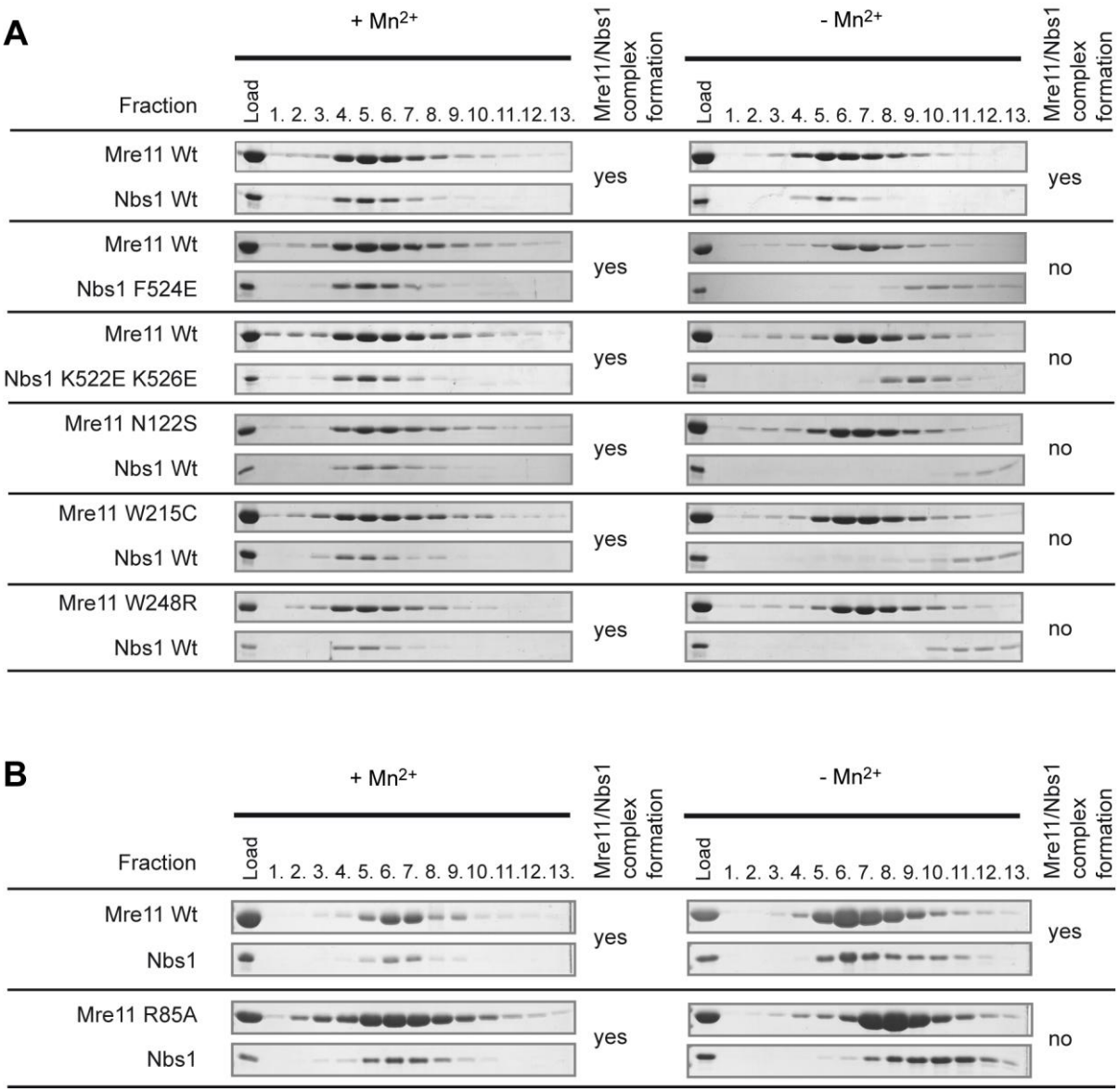

Figure 4.13: Analytical size exclusion experiments with *S. pombe* mutant proteins. (A) Interaction studies of Nbs1 (aa 428-613) with Mre11^{cd} (aa 1-413), analyzed by co-migration on gel filtration. Shown are SDS-PAGE bands from gel filtration fractions for both Mre11^{cd} and Nbs1 (aa 428-613). Wild type (Wt) Nbs1 (aa 428-613) co-migrates and hence interacts with the Mre11^{cd} dimer in both absence and presence of Mn^{2+}. Mutations in Nbs1 (KNFKxFxK motif) and Mre11 (A-TLD sites) evidently reduce but not abolish affinity and lead to loss of interaction in the absence but not in the presence of Mn^{2+}. The data also show that Mn^{2+} strengthens the interaction of Mre11^{cd} with Nbs1, presumably by stabilizing the phosphodiesterase fold. **(B)** Interaction studies with the Mre11 R85A mutation that disrupts the salt bridge between R85 and D118 in the Mre11 dimer interface. The experimental approach is similar to Figure (A) but here a longer Mre11 construct was used (aa 1-421). Also the Mre11 R85 mutant protein shows a reduced but not abolished affinity to Nbs1 with a loss of interaction in the absence but not in the presence of Mn^{2+}.

In addition, the Mre11 mutant protein aa 1-421 R85A^{SpMre11} was tested for binding of Nbs1 aa 428-613 (Figure 4.13 B). The mutation disrupts the salt-bridge, which connects the latching loops with the hydrophobic helix bundle in the dimer interface of the Nbs1^{mir}-Mre11^{cd} complex structure. The mutant protein was also binding to Nbs1 only the presence of Mn^{2+} ions but not in an EDTA containing buffer, indicating that the disruption of the dimer salt bridge weakens the Mre11-Nbs1 interface 2.

4.9 Biochemical analysis of Mre11 and Nbs1 from *S. pombe*

So far, atomic resolution data regarding the binding mechanism of Mre11 to DNA substrates, is only available from two archaeal *P. furiosus* Mre11-DNA complex structures (Williams et al. 2008). Eukaryotic Mre11 mediates more diverse functions and is only partially sequence conserved to *P. furiosus*. Thus, a crystal structure of a eukaryotic Mre11 homologue in complex with DNA would be of great value for the functional characterization of the eukaryotic MRN complex on a molecular level. To find a suitable DNA substrate for crystallization, the DNA binding properties of different *S. pombe* Mre11 and Nbs1 constructs were studied by electrophoretic mobility shift assays (EMSAs) (3.3.2.10). Deletion mutant studies with the homologous *S. cerevisiae* protein had early indicated that eukaryotic Mre11 possesses two distinct DNA binding sites. A region containing the last 50 C-terminal amino acids is especially important for meiotic repair but dispensible for mitotic repair functions. In contrast, deletion of a basic region between residues aa 410 - 420 of ScMre11 (KKRSPVTRSKK) abolishes mitotic as well as meiotic repair *in vivo* and Mre11 nuclease activity *in vitro* (Furuse et al. 1998; Usui et al. 1998). This region corresponds to the *S. pombe* residues aa 411-421 (LKKKYTRSKRN). The crystallized Mre11 construct aa 15-413, which was derived from a limited proteolysis approach, lacks part of this sequence element. The Mre11 fragment aa 1-413 is still an active nuclease (Figure 4.14 A, 3.3.2.9) and degrades a 60mer poly(dT) ssDNA specifically, as seen by comparison with a control reaction where the nuclease deficient mutant Mre11 H134S mutant was tested (Williams et al. 2008). However, the nuclease deficient mutant construct Mre11 aa 1-413 H134S did not bind significantly to any tested dsDNA or ssDNA substrate (Figure 4.14 B, here shown for a 5´-6FAM labeled 60mer poly(dT) ssDNA). In contrast, the Mre11 construct aa 15-421 H134S, which contains the complete DNA binding motif, binds to both dsDNA and ssDNA. It is binding for example to the 60mer poly(dT) ssDNA substrate with an affinity comparable to full length Mre11 (aa

1-649) for the tested concentrations. Therefore, also *S. pombe* Mre11 depends on the complete basic DNA binding sequence element between residues 411-421 to bind efficiently to DNA *in vitro*. However, neither the Mre11 aa 15-413 nor the aa 15-421 construct did crystallize in complex with DNA so far.

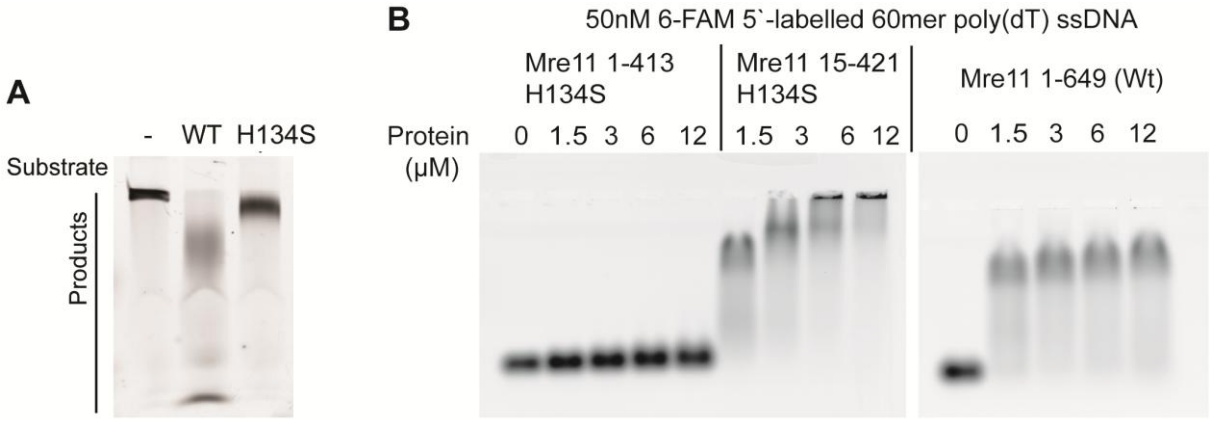

Figure 4.14: Analysis of Mre11^{cd} nuclease acitivity and DNA binding properties of different *S. pombe* Mre11 constructs. (A) Degradation of a 6-FAM 5`-labelled 60mer poly(dT) single-stranded oligo-nucleotide (Table 3.2) in the presence of wild type SpMre11^{cd} (1-413) (Wt), but not in the absence of Mre11 (-) or presence of a predicted nuclease deficient variant (His134->S), shows specific nuclease activity of Mre11^{cd}. Experiment carried out by Carolin Möckel (AG Hopfner) (3.3.2.9). **(B)** Electrophoretic mobility shift assays (EMSAs) with Mre11 aa 1-413 H134S, Mre11 15-421 H134S and Mre11 1-649 reveal that *S. pombe* Mre11 contains (similar to *S. cerevisiae*) a DNA binding region at the C-terminal end of the cap domain. Residues 414-421 are crucial for DNA binding to the tested 6-Fam labeled 60mer poly (T) ssDNA substrate. Mre11 15-421 binds to the DNA at the tested concentrations with an affinity similar to the also tested Mre11 aa 1-649 construct.

It was reported before that human Nbs1 has a stimulatory role for nucleotide dependent dsDNA binding of Mre11-Rad50 (Lee et al. 2003). In addition, the homologous *S. cerevisiae* protein Xrs2 binds also as a single protein without Mre11-Rad50 to different DNA substrates (Trujillo et al. 2003). The Mre11 interaction region of Nbs1, which was crystallized with Mre11 (aa 474-531) contains a strongly conserved basic KNFKxFxK motif (4.4.2). In fact the region between Nbs1 residues 518-531 includes 6 basic residues, which prompted the question if it might be involved in DNA binding. To answer this question different Nbs1^{mir} constructs were analysed with EMSAs. The Nbs1 aa 474-531 peptide contains the complete basic KNFKxFxK motif, whereas this region is lacking in Nbs1 aa 474-517. Indeed, Nbs1 aa 474-531 was interacting with both a 13mer blunt end dsDNA hairpin and a 60mer poly(dT) ssDNA oligo (Table 3.2), whereas Nbs1 aa 474-517 exhibited no significant DNA interaction

(Figure 4.15). This raises the possibility that the KNFKxFxK motif, which mediates bridging of the Mre11 dimer via interaction region 2 in the Mre11^{cd}Nbs1^{mir} structure, might be involved in direct binding of DNA during the sensing and processing of DSBs by the MRN complex. A model regarding this role of Nbs1 will be discussed later (5.6).

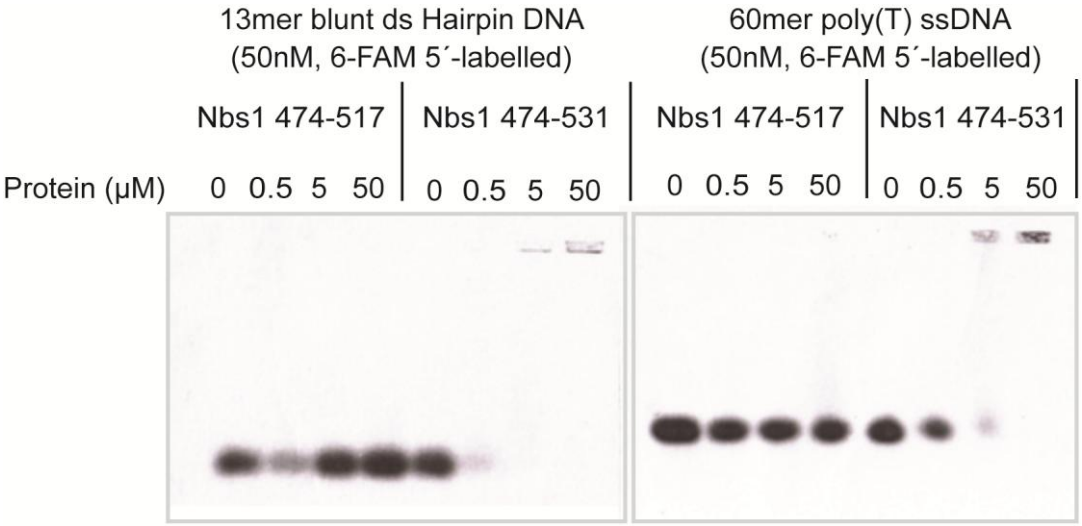

Figure 4.15: Analysis of DNA binding properties of different *S. pombe* Mre11 and Nbs1 constructs by electrophoretic mobility shift assays (EMSAs): A DNA binding site within the crystallized Nbs1 construct aa 474-531 maps to the region between amino acid residues 518-531, which contains the conserved KNFKxFxK motif that bridges the Mre11 dimers via the Mre111 interactions region 2 (4.4).

4.10 Structure guided *in vivo* analysis of Mre11 from *S. cerevisiae*

Several functional motifs in Mre11 revealed by the crystal structure of *S. pombe* Nbs1^{mir}-Mre11^{cd} were studied *in vivo*, using the budding yeast *S. cerevisiae* as a model organism. The structure of Nbs1^{mir}-Mre11^{cd} raised different questions: How stable is the interaction of Mre11 and Nbs1 (Xrs2 in *S. cerevisiae*) and how do point mutations in different regions of the Mre11-Nbs1/Xrs2 interface affect the functionality of the complex? How important is the dimeric configuration of Mre11 and which roles play the Nbs1/Xrs2 interacting latching loops apart from mediating the interaction to Nbs1/Xrs2? In addition, also the active site adjacent loop element which might play regulatory roles (4.6) and a potential phosphorylation motif of Mre11 were targeted by mutational analysis in *S. cerevisiae.* For this purpose, Mre11 point mutations were introduced into a pRS416 plasmid containing the coding sequence for a myc-

tagged version of Mre11 (D´Amours and Jackson 2001). The plasmid was then transformed into a *S. cerevisiae* W303 Δmre11 strain for *in vivo* studies.

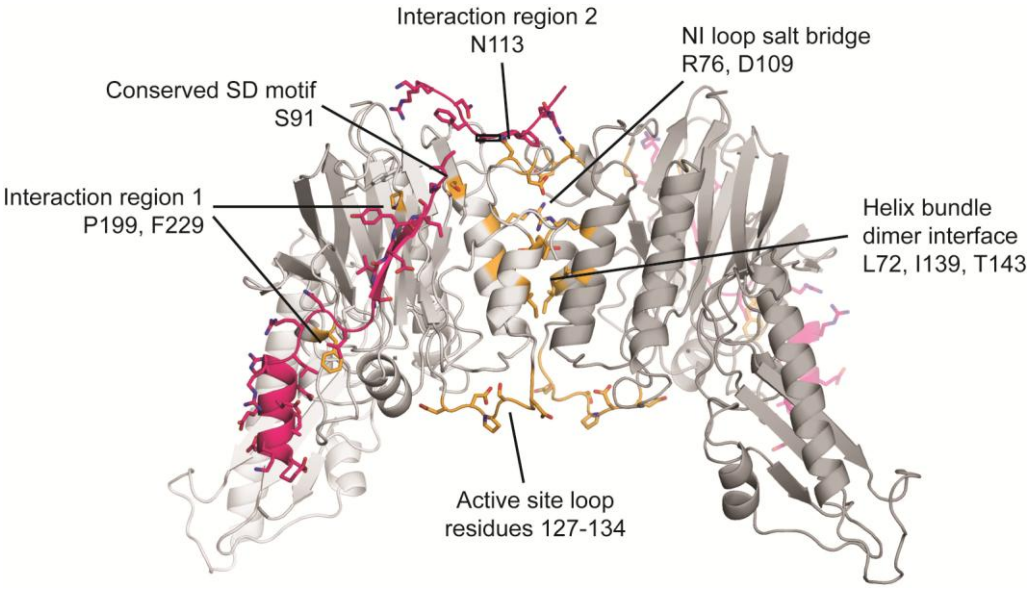

Figure 4.16: Overview of *S. cerevsiae* Mre11 mutations studied *in vivo:* Mutated residues are highlighted (orange) in the homologous *S. pombe* $Nbs1^{mir}$-$Mre11^{cd}$ structure (Mre11 colored in grey and Nbs1 in pink). The studies concentrated on several different functional regions in Mre11: The interaction regions 1 (P199, F229E) and 2 (N113), latching loop salt bridge (R85, D109) in the Mre11 dimer interface, the dimer helix bundle (L72, I139,T143), an active site adjacent loop element (residues 127-134) and a potential serine-aspartate phosphorylation site (S91).

4.10.1 Mutational analysis of functional motifs in *S. cerevisiae* Mre11 by plate survival assays

All generated *S. cerevisiae* mutations were tested for sensitivity different genotoxic agents by plate survival assays (Figure 4.17 and 3.3.4.2). These included the Topoisomerase I poison Camptothecin (CPT), the DNA alkylating chemical methyl methanesulfonate (MMS) and the DNA replication inhibitor hydroxyurea (HU).

A sequence alignment of several eukaryotic Mre11 proteins had shown that *S. cerevisiae* Mre11 contains a highly conserved serine-aspartate motif at position $S91^{ScMre11}$ (Figure 4.7 D). Since the MRN(X) complex is phosphorylated by different kinases during the repair of DSBs, it was plausible that this motif might represent a phosphorylation site for *e.g.* the CK2 kinase (Kim 2005; Di Virgilio et al. 2009). However, a $S91A^{ScMre11}$ mutation did not

lead to any visible growth defect on CPT or HU plates, although a phosphorylation mimicking S91E^{ScMre11} mutation showed a mild sensitivity (Figure 4.17 A). The mutation maps to the latching loops and is in close proximity to the Nbs1/Xrs2 interaction site observed in the *S. pombe* structure. Since Nbs1/Xrs2 mediates the nuclear transport of Mre11-Rad50, the observed defect might stem from a disrupted Mre11-Xrs2 interaction, which could exclude Mre11-Rad50 from the nucleus. Indeed, an SV40 T large antigen nuclear localization sequence (NLS) fused to Mre11 was shown to rescue the mitotic repair defect of a Δxrs2 mutant, revealing that an Mre11-Rad50 complex is sufficient for mitotic repair when present in the nucleus (Tsukamoto et al. 2005). To test the hypothesis, that the growth defect of S91E^{ScMre11} is caused by an exclusion from the nucleus, Mre11 constructs were generated, which possess a SV40 T large antigen nuclear NLS at the C-terminus of Mre11. Clearly, the NLS on S91E^{ScMre11} rescued the growth defect of the mutant strain. Even though it cannot be excluded that S91^{ScMre11} is indeed a phosphorylation site, the growth defect observed for the S91E^{ScMre11} mutation is rather caused by a weakened Mre11-Xrs2 interaction than by the influence of the phosphorylation mimicking.

Next, a loop element, comprising residues 127-134, which connects the phosphodiesterase motif III with the dimer mediating helix αC of Mre11 was studied (Figure 4.17 A). Interestingly, this loop possessed two different conformations in the conserved *S. pombe* structure, depending on the metal coordination state of the active site. Therefore, it might regulate the nuclease function of Mre11 (4.6). Mutations of the aspartate residue D127^{ScMre11}, which is strongly conserved among eukaryotic organisms, to either alanine or arginine had different outcomes. Whereas the D127A^{ScMre11} mutation exhibited only a very slight defect on 200 mM HU, the D127R^{ScMre11} mutation displayed a significant growth defect on both CPT and HU plates. The defect was even stronger with a D127R^{ScMre11} / D131R^{ScMre11} double mutant which also targets a second aspartate residue in this loop. Instead of an aspartate, the homologous archaeal *P. furiosus* (Pf) Mre11 protein contains an arginine residue at the position of D127^{ScMre11}, which mediates a major contact with the DNA backbone in the *Pf*Mre11-DNA complex structure (Williams et al. 2008). This indicates that DNA binding of eukaryotic Mre11 must be different from archaeal Mre11, at least regarding this motif. However, it might also be that the loop is coordinated by Rad50 in a conformation which allows DNA binding. Anyway, the sequence integrity of this loop is crucial for the repair ability of *S. cerevisiae* Mre11 and exchanging the whole loop element in *S. cerevisiae* to the sequence of the *Pf*Mre11 loop caused a strong growth defect similar to an *mre11* deletion

(Figure 4.17 A: mre11Δ 127-133 replaced by RTQRG and mre11 Δ 127-134 replaced by RTQRGP).

A conserved hydrophobic four helix bundle mediates the lower part of the bipartitive Mre11 dimer interface in the crystal structure of *S. pombe* Nbs1^{mir}-Mre11^{cd}. The integrity of the corresponding four helix bundle in *S. cerevisiae* was targeted by mutations which should distort the interface (L72F^{ScMre11}, I139F^{ScMre11}, T143I^{ScMre11}) or even disrupt it (L72R^{ScMre11}). From the first class of mutations only L72F^{ScMre11} exhibited a mild growth defect on HU plates, whereas I139F^{ScMre11} and T143I ^{ScMre11} showed a growth phenotype similar to wildtype Mre11. This indicates that the introduction of bulky hydrophobic residues does not strongly impair the functionality of Mre11 in mitotic repair. Instead, the helix bundle disrupting mutation L72R^{ScMre11} showed a growth defect similar to mre11Δ, indicating that like *S. pombe* Mre11 also *S. cerevisiae* Mre11 depends on a stable dimer interface in order to be DNA repair proficient (Williams et al. 2008).

The region, which in *S. pombe* Mre11 mediates binding to the helix-ß-strand motif of Nbs1^{mir} via interaction region 1 (4.4), was probed in *S. cerevisiae* by mutation of two conserved Mre11 residues (P199A^{ScMre11} and F229E^{ScMre11}). However, both mutations did not cause any significant growth defects on CPT or HU plates. This observation fits with studies of Xrs2 deletion mutants which showed this region in Xrs2 (interaction region 1) to be dispensable for resistance to MMS and only crucial for meiotic repair functions or telomere maintenance (Tsukamoto et al. 2005).

The functional characterization of the salt bridge motif consisting of R76^{ScMre11} and D109^{ScMre11} (R85 and D109 in *Sp*Mre11), which is linked to human NBSLD (Matsumoto et al. 2011) was of special interest for this study. The *S. pombe* Mre11 dimer possesses an intrinsic flexibility as seen by the different dimer angels in the apo-Mre11^{cd} and Nbs1^{mir}-Mre11^{cd} structures. Such a flexible interface might be important for all Mre11 dimer associated activities such as nuclease activity. The salt bridges between both Mre11 protomers could allow dynamic rearrangements of the Mre11 dimer interface necessary for DNA binding and signaling.

One approach to study the role of the R76-D109^{ScMre11} salt bridge was to exchange it to hydrophobic residues. Since a hydrophobic interface might not dissociate as easily as a salt bridge mediated interface, such mutations might “freeze” the Mre11 dimer interface in the conformation seen in the Nbs1^{mir}-Mre11^{cd} crystal structure and thereby inactivate the MRX complex (Figure 4.17 A). Indeed, all hydrophobic mutations tested in *S. cerevisiae* rendered

the yeast cells highly sensitive to CPT and HU (R76M, R76M D109F, R76M D109L, R76M D109M, R76F D109M). However, immunofluorescence studies showed that these mutations also lead to a delocalisation of Mre11 from the nucleus, strongly indicating that they affect the interaction with Xrs2 (data not shown). Interestingly, an additional $D109N^{ScMre11}$ mutation in the $R76M^{ScMre11}$ strain rescued partially the growth defect of $R76M^{ScMre11}$. This indicates that the charge of $D109^{ScMre11}$ might have a negative effect on the complex stability if not counteracted by a basic residue at position $R76^{ScMre11}$. If both residues are mutated to polar instead of hydrophobic residues ($R76Q^{ScMre11}$ / $D109N^{ScMre11}$), Mre11 exhibited no sensitivity to HU and CPT, indicating that a polar nature of the Mre11 dimer interface is more important than the charge provided by the R76-$D109^{ScMre11}$ salt bridge.

The impact of an arginine side chain deletion on the functionality of *S. cerevisiae* Mre11 was studied with an $R76A^{ScMre11}$ mutation. In addition, also an $R76K^{ScMre11}$ mutation was generated, which preserves the positive charge of the arginine residue. Both the $R76A^{ScMre11}$ and the $R76K^{ScMre11}$ mutation were characterized in more detail to uncover the importance of the conformational integrity of the latching loops for the general functionality of the MRX complex. For comparison, the latching loop mutation $N113S^{ScMre11}$, which is homologous to the well characterised A-TLD3/4 mutation $N117S^{HsMre11}$ (Stewart et al. 1999), was studied. $N117S^{HsMre11}$ was shown to reduce the binding of Mre11 to Nbs1, which can be explained by the *S. pombe* $Nbs1^{mir}$-$Mre11^{cd}$ structure, where this residue mediates a key interaction with Nbs1 via interaction region 2. Dilution plate assays with selective minimal medium (SDC -ura) revealed strong sensitivity to methyl methanesulfonate (MMS) and hydroxyurea (HU) for both $N113S^{ScMre11}$ and mre11Δ (Figure 4.17 B) consistent with previous reports (D'Amours and Jackson 2001; Lee et al. 2002). In addition, also a strong sensitivity towards the Topoisomerase 1 inhibitor camptothecin was found. A comparable growth defect could be observed for the $R76A^{ScMre11}$ mutant, indicating that the salt bridge, which connects both Mre11 protomers in the Mre11 dimer, is critical for mitotic repair functions. The DNA damage sensitivity caused by xrs2Δ can be rescued by adding a nuclear localization sequence to Mre11 (Tsukamoto et al. 2005), and an NLS also rescues the repair defect of the $S91E^{ScMre11}$ latching loop mutation (Figure 4.17 A). Therefore, it was tested whether an NLS could also rescue the DNA damage sensitivity observed for $R76A^{ScMre11}$ and $N113S^{ScMre11}$ proteins.

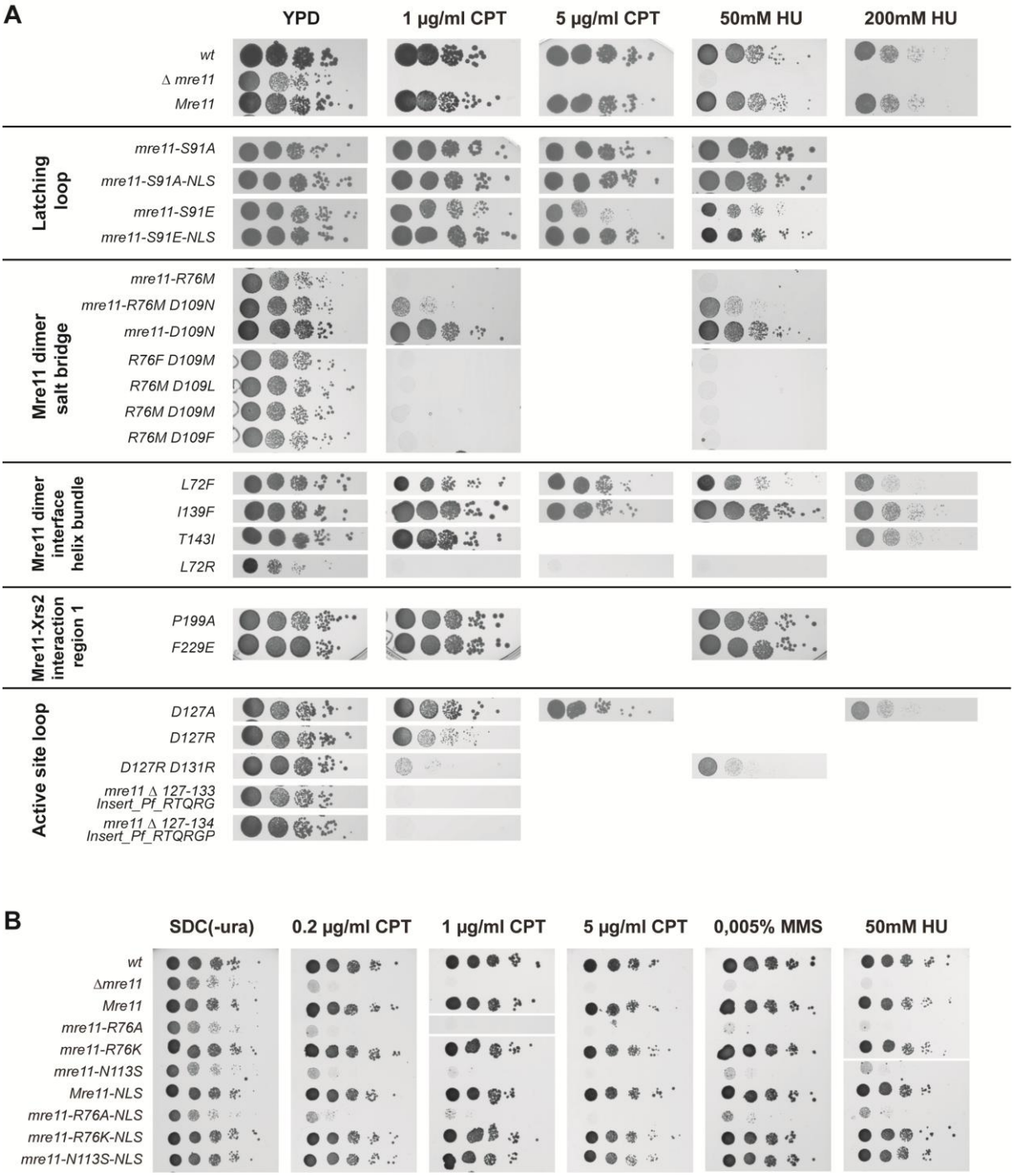

Figure 4.17: Mutational analysis of functional motifs in *S. cerevisiae* Mre11 by plate survival assays with camptothecin (CPT), methyl-methanesulfonate (MMS) and hydroxyurea (HU). (A) Plate survival assays with YPD agar plates. The following motifs in Mre11 were targeted by mutations: Latching loop (S91A, S91A-NLS, S91E, S91E-NLS), Mre11 dimer salt bridge (R76M, R76M D109N, D109N, R76F D109M, R76M D109L, R76M D109M, R76M D109F), Mre11 dimer interface helix bundle (L72F, I139F, T143I, L72R), Mre11-Xrs2/Nbs1 interaction region 1 (P199A, F229E), active site loop between phosphodiesterase motif III and Mre11 dimer interface helix αC (D127A, D127R, D127R D131R, mre11Δ127-133 replaced by the *P. furiosus* RTQRG loop sequence and mre11 Δ127-134 replaced by the *P. furiosus* RTQRGP loop sequence). **(B)** Plate survival assays with SDC (-Ura) agar plates: The R76A and N113S mutations both exhibit growth defects similar to

Δmre11, whereas the R76K mutation displays no visible defect. C-terminal tagging of the mutants with the SV40 large T antigen nuclear localization sequence (NLS) reconstitutes Wt-like resistance of N113S but not of R76A.

Like for S91E^{ScMre11} also here a SV40 T large antigen NLS was fused to the C-terminus of Mre11 and the DNA damage resistance monitored with plate dilution assays (Figure 4.17 B). The NLS rescued the N113S^{ScMre11} mutation, but not the R76A^{ScMre11} mutation, which still exhibited a strong growth defect when treated with different DNA damage causing agents. Therefore, a defect in the Xrs2 interaction alone cannot explain the severe phenotype of Mre11 R76A^{ScMre11}.

4.10.2 Indirect immunofluorescence reveals nuclear localization defects of different latching loop targeting mutations

Xrs2/Nbs1 is required for the transport of Mre11-Rad50 to the nucleus (Carney et al. 1998; Tsukamoto et al. 2005). In addition, the human A-TLD3/4 causing N117S^{HsMre11} mutation was shown to induce a partial exclusion of Mre11 from the nucleus, probably caused by a weakened Nbs1 interaction (Stewart et al. 1999). Therefore, the cellular localization of NLS-tagged and untagged R76A^{ScMre11}, R76K^{ScMre11} and N113S^{ScMre11} mutants was monitored by indirect immunofluorescence microscopy to control if the mutations cause a nuclear delocalization of Mre11 (Figure Figure 4.18) (3.3.4.4).

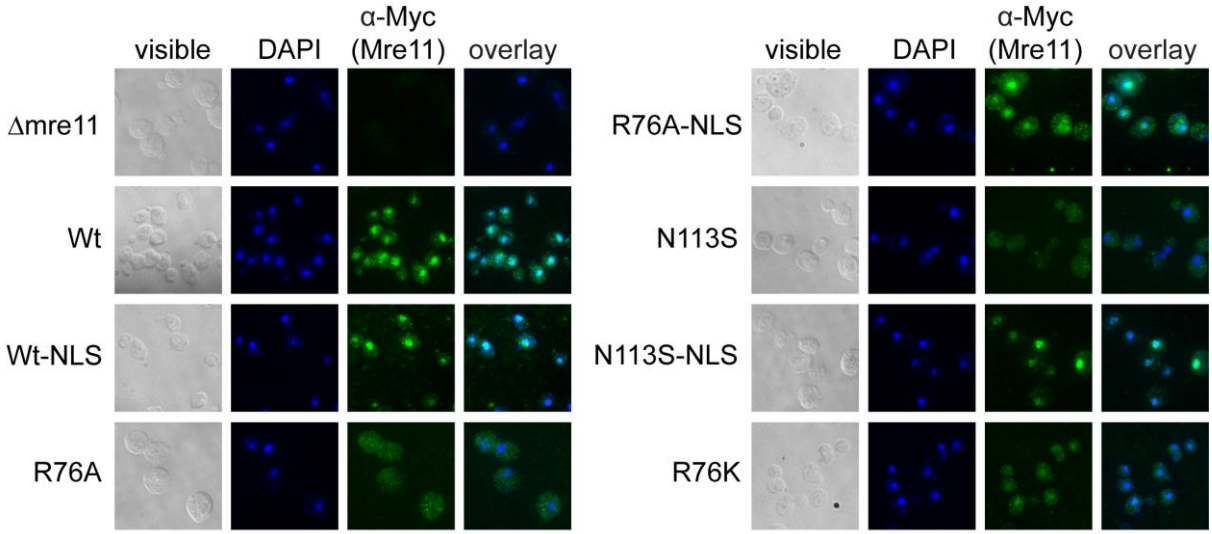

Figure 4.18: Cellular localization of *S. cerevisiae* Mre11 mutants by indirect immunofluorescence. Fixed yeast cells are immunostained by subsequent incubation with a monoclonal mouse α-c-Myc antibody and an

Alexa Fluor 488 conjugated goat α-mouse antibody. Nuclear localization is strongly decreased in the case of R76A^{ScMre11} and N113S^{ScMre11} while partly reduced for R76K^{ScMre11}. NLS-tagged R76K and N113S mutants show a nuclear accumulation similar to Wt Mre11, while R76A-NLS accumulates at least in the majority of cells comparable to Wt Mre11.

Here, it could be seen that the homologous N113S^{ScMre11} mutation, as well as R76A^{ScMre11}, resulted in a strongly decreased nuclear accumulation of Mre11, consistent with the severe phenotypes of these mutations. On the other hand, the repair competent mutant R76K^{ScMre11} also displayed a partially decreased nuclear accumulation. Therefore, a decreased nuclear accumulation of Mre11 does not necessarily lead to repair defects. The NLS relocated all mutant proteins to the nucleus. However, the R76A-NLS^{ScMre11} mutation possesses still a severe repair defect (4.10.1). This raised the question to which degree nuclear mislocalisation really accounts for the DNA damage sensitivity observed in R76A^{ScMre11} and N113S^{ScMre11} mutant strains.

4.10.3 Analysis of *S. cerevisiae* Mre11-Rad50-Xrs2 complex integrity and Mre11 dimer interaction for different Mre11 latching loop targeting mutations

To test if the integrity of the MRX complex was affected by the latching loop targeting mutations R76A^{ScMre11}, R76K^{ScMre11} and N113S^{ScMre11}, co-immunoprecipitations (Co-IPs) of the myc-tagged Mre11 strains were performed (Figure 4.19) (3.3.4.3). Here, protein levels of Mre11, Rad50 and Xrs2 were relatively equal in cell lysates from Wt and mutant proteins, ruling out misfolding or degradation as the main cause for the observed phenotype. Like its human homologue, the Mre11 N113S^{ScMre11} mutant was still able to form a stable complex with Rad50 in Co-IPs (Stewart et al. 1999). Also for Mre11 R76K^{ScMre11} a normal Rad50 interaction was observed, whereas this interaction was partly reduced but not abolished in Co-IPs with the Mre11 R76A^{ScMre11} mutant strain.

In contrast to Wt Mre11, however, Xrs2 was not detectable in immunoprecipitates from R76A^{ScMre11}, R76K^{ScMre11} and N113S^{ScMre11} mutant strains. This observation is in agreement with the observed cellular mislocalisation of Mre11 R76A^{ScMre11} and Mre11 N113S^{ScMre11} (4.10.2). However, R76K^{ScMre11} displayed no phenotype in plate survival assays with different genotoxic agents and showed a reduced but significant nuclear accumulation (4.10.1 and

4.10.2). This means that R76K ^{ScMre11} must possess a residing ability to bind Xrs2, which is strong enough for a nuclear "piggy back" transport but too weak to be detectable in Co-IPs.

In conclusion, the phenotype of Mre11 N113S^{ScMre11} can be explained as a mislocalisation defect. The mutant is still competent in the Xrs2 independent mitotic repair functions of Mre11-Rad50 and can be rescued by addition of a NLS to Mre11 (4.10.1). In contrast, the R76A^{ScMre11} mutation clearly impairs also the mitotic repair ability of Mre11-Rad50. Mre11 R76A^{ScMre11} still binds to Rad50, even though at a partially decreased level. Therefore, the dramatic sensitivity to genotoxic agents like HU or CPT can unlikely be explained by a fold instability of Mre11 or loss of Rad50 binding, as it was reported for mutations with global repair defects like Mre11-58 (Usui et al. 1998).

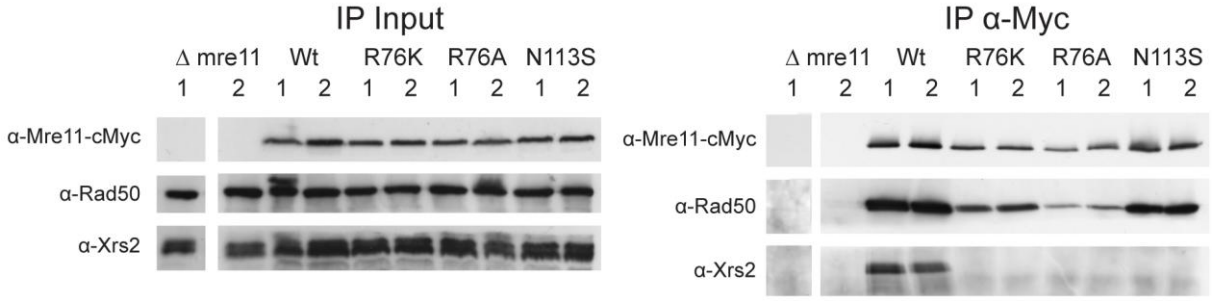

Figure 4.19: Analysis of Mre11-Rad50-Xrs2 complex integrity by co-immunoprecipitation for different *S. cerevisiae* Mre11 mutations. Mre11-Rad50-Xrs2 complex formation defects caused by the R76A, R76K and N113S mutations, which target the Mre11 latching loops, were detected by co-immunoprecipitation (3.3.4.3). Cell extracts were prepared in buffer containing 150 mM NaCl and immunoprecipitated with an α-c-Myc antibody against Mre11. Proteins were visualized by Western blotting with α-myc (Mre11), α-Rad50, and α-Xrs2 antibodies, respectively. All tested latching loop targeting mutations caused a defect in Xrs2 binding, underlining the crucial role of the latching loops for this function. Both R76 mutations showed reduced levels of immunoprecipitated Mre11, indicating a reduced dimer stability. The ratio of co-immunoprecipitated Rad50 per Mre11 was slightly reduced only in the case of Mre11 R76A.

Since R76^{ScMre11} maps to the dimer interface of Mre11, it was analyzed whether the R76A^{ScMre11} mutant has a defect in dimerization, which could explain its severe phenotype. Williams et al. showed with mutational studies that the hydrophobic four helix bundle is crucial for Mre11`s dimer integrity (Williams et al. 2008). The impact of the latching loop mediated Mre11 dimer interaction, which is likely to be affected by the R76A^{ScMre11} mutation, however, is still unknown. To answer this question, a second plasmid, coding for a C-

terminally HA-tagged Mre11, was introduced into the myc-tagged mre11 shuffle strain to create "mixed" dimer complexes. The myc-tagged Mre11 was then immunoprecipitated and the dimer integrity analyzed using an antibody against HA-tagged Mre11 (Figure 4.20) (3.3.4.3 and 3.3.2.6). Indeed, dimer formation was severely reduced in the R76A^{ScMre11} strain compared to Wt. This underlines that the Mre11 latching loops not only play a crucial role in binding to Nbs1/Xrs2, but also in stabilizing Mre11 dimers in *S. cerevisiae*. In summary, single point mutations in the Mre11-Xrs2 and the Mre11 dimer interface were identified, which specifically disrupt these protein-protein interactions, thereby causing distinct phenotypes.

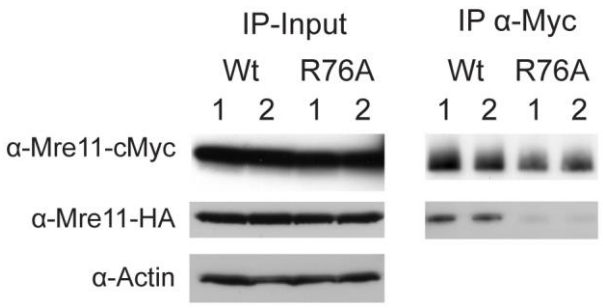

Figure 4.20: Analysis of Mre11 dimer stability of *S. cerevisiae* Mre11 Wt and R76A by co-immunoprecipitation. ScMre11 dimeric assembly is disrupted by the latching loop destabilizing R76A mutation. Mixed Mre11 dimers, consisting of two monomers with different affinity tags were created by introducing two plasmids, carrying the Mre11 Wt or R76A gene with a C-terminal 3xHA tag or 13xmyc tag, respectively, into an *S. cerevisiae* W303 Δmre11 strain. Dimer assembly was tested by co-immunoprecipitation of myc-tagged Mre11 with a monoclonal α-c-Myc antibody and visualization of dimer assembly by western blot analysis using antibodies against myc and HA-tagged Mre11.

5. DISCUSSION

All living organisms depend on surveillance mechanisms, which protect the stability of their genomes from hazardous DNA damages. They therefore possess various repair pathways which sense and repair DNA lesions and thereby maintain the genomic stability of the cell. The efficient repair of DNA double strand breaks (DNA DSBs) is of special importance for the cell, since unrepaired DSBs are highly cytotoxic and may induce chromosomal aberrations and cancerogenic diseases. The Mre11-Rad50-Nbs1 (MRN) complex is a central component of the DNA DSB repair machinery. The complex senses and binds as one of the first factors to DSBs. It then works as an effector molecule, which recruits other repair proteins to the break. MRN also actively processes DNA ends via its nuclease activity to facilitate repair of the lesion. Furthermore it is involved in DNA damage signal transduction by recruiting and activating the cell cycle checkpoint kinase ATM which then may promote cell cycle arrest or apoptosis. The enzymatic core, consisting of the Mre11 nuclease dimer and two adjacent Rad50 ABC-ATPases, is found in eukaryotes, archaea, bacteria and viruses. However, only the eukaryotic complex contains with Nbs1 a third compound. Nbs1 possesses no enzymatic activities. Instead it is a regulatory protein which mediates eukaryote specific functions of the complex in DSB repair and signaling via interactions to Mre11 and in the human complex also to Rad50 (Assenmacher and Hopfner 2004; Williams et al. 2010; Stracker and Petrini 2011). Nbs1 is crucial for the activation of ATM by the MRN complex *in vivo* (Berkovich et al. 2007). Furthermore it was shown *in vitro* to influence the DNA binding specificity of Mre11-Rad50 and to stimulate nucleolytic DNA hairpin processing by the complex (Paull and Gellert 1999; Lee et al. 2003; Trujillo et al. 2003). However, it is only poorly understood on a molecular level how Nbs1 carries out these functions and no atomic structures of eukaryotic Mre11 or Rad50 in complex with Nbs1 are reported so far. Therefore, the aim of this work was to analyze the structural and functional interplay between Nbs1 and Mre11 in detail. For this purpose crystal structures of the catalytic core module of Mre11 alone and in complex with the interaction region of Nbs1 were solved and biochemically characterized.

5.1 Preparation and crystallization of *S. pombe* apo-Mre11^{cd} and Nbs1^{mir}-Mre11^{cd}

To gain insights into the structure of the eukaryotic Mre11-Rad50-Nbs1 complex, different eukaryotic organisms where screened for soluble protein constructs. Here, the main focus was

to find constructs of Mre11 and Nbs1 suitable for crystallization. It turned out that especially protein fragments from the fission yeast *Schizosaccharomyces pombe* could be expressed in a soluble form in *Escherichia coli* in mg amounts which allowed extensive crystallization screenings (4.1). Mre11 and Nbs1 from *S. pombe* are relatively compact in size compared to their human protein homologs. *S. pombe* Mre11 has a size of 649 amino acid residues compared to 708 residues for human Mre11. Likewise *S. pombe* Nbs1 comprises only 613 amino acids whereas its human counterpart is 754 residues long. However, important structural elements like the Mre11 nuclease domain or the Mre11 interaction region of Nbs1 are conserved (see also domain maps in Figure 2.3). Albeit full length *S. pombe* Mre11 could be purified recombinantly from *E. coli*, it was prone to proteolytic degradation over time and did not crystallize. A secondary structure prediction with the program JPRED (Cole et al. 2008) showed that extensive areas of the C-terminal part of the protein lack secondary structure elements, which explains the proteolytic degradation of the protein preparations. Furthermore the C-terminus is involved in binding to Rad50 and might therefore be instable when this binding partner is absent (Lammens et al. 2011). Since no soluble Rad50 construct could be obtained, the aim was to crystallize the catalytic N-terminal part of Mre11. For this purpose a limited proteolysis approach in combination with a secondary structure analysis was applied. Based on this data a new construct containing residues 15-413 was generated (4.1). Alignments with Mre11 from the archaeal organism *P. furiosus* indicated that it included the complete nuclease core, which is composed of a phosphodiesterase domain and an adjacent DNA capping domain (Hopfner et al. 2001). Therefore the construct was named $Mre11^{cd}$ (cd = catalytic domains). The protein was tested in crystallization screenings and yielded crystals diffracting to a limiting resolution of 3.0 Å. The structure of $Mre11^{cd}$ was later solved by molecular replacement methods using the $Nbs1^{mir}$-$Mre11^{cd}$ complex structure (4.2.2).

Full length Nbs1 from *S. pombe* could not be expressed and purified in amounts suitable for crystallization. Of special interest for this work was the C-terminal region of Nbs1, which contains the binding sites for Mre11 and the checkpoint kinase ATM/Tel1. Indeed, a C-terminal fragment containing residues 428-613 could be purified in mg amounts (4.1). However it did not crystallize alone or in complex with $Mre11^{cd}$ and was prone to proteolytic degradation. The N-terminal part of *S. pombe* Nbs1, which contains the Forkhead and two BRCT domains was already crystallized by Williams *et al.* (Williams et al. 2009). The authors also characterized the C-terminal region, comprising residues 330-613, by proteolysis and SAXS studies to be mainly unstructured. This likely explains why the construct 428-613 did

not crystallize. Therefore, different shorter deletion constructs of Nbs1 were purified and tested for binding with Mre11^{cd}. By this approach, the core interaction motifs of Nbs1 for Mre11 were narrowed down to the region between residues 474-531. This region contains two conserved sequence elements which had been proposed before to be important for Mre11 binding (Ueno et al. 2003). The construct was further named Nbs1^{mir} (mir = Mre11 interaction region) (4.1). Since Mre11^{cd} aa 15-413 and Nbs1 aa 474-531 did not crystallize initially, a fusion protein was generated, which connected both proteins by an eight residues long linker, to facilitate crystallization (Figure 4.2 B). The Nbs1^{mir}-Mre11^{cd} fusion protein could be crystallized and native crystals diffracted to a limiting resolution of 2.4 Å (4.2.1). The structure was solved by SAD using data from crystals of the selenomethionine labeled complex, which diffracted to 2.8 Å resolution (4.2.1).

5.2 The eukaryotic Mre11 dimer resembles the principal domain architecture of prokaryotic Mre11 but exhibits additional structural characteristics

The structure of Mre11^{cd} revealed a dimeric molecule with the principle domain architecture similar to previously reported archaeal Mre11 from *P. furiosus* and bacterial Mre11 from *T. maritima* (4.3) (Hopfner et al. 2001; Lammens et al. 2011). The dimeric contacts are mediated by the two central phosphodiesterase domains via two helices from each protomer, which form a hydrophobic four helix bundle. Each phosphodiesterase domain is flanked by a DNA capping domain. Thereby also *S. pombe* Mre11^{cd} builds a U shaped particle with a predicted DNA binding region at its concave site. Alignments showed high sequence conservation between *S. pombe* and human Mre11 for the crystallized region with 47.9% identical and 33.7% conserved residues. Therefore, the structural architecture of *S. pombe* Mre11^{cd} is presumably also representative for higher eukaryotic organisms. Overlays of the *S.pombe* Mre11^{cd} structure with the *P. furiosus* and *T. maritima* Mre11 structures showed that all active site residues are identical (4.3). This indicates that the catalytic mechanism of Mre11 is conserved between the three domains of live.

However, there are also important structural differences between the eukaryotic *S. pombe* Mre11^{cd} structure and archaeal or bacterial Mre11 structures. Most prominently, *S. pombe* Mre11 contains a conserved 33 amino acid long insertion loop element between residues 91-123, which is specific for eukaryotic organisms. It maps to the top of the Mre11 dimer

mediating four helix bundle on the opposite site of the predicted DNA binding cleft and is highly conserved among eukaryotes (4.3 and 4.4.2). The Nbs1^{mir}-Mre11^{cd} structure revealed that this loop element, which is further named latching loop, is mediating a key interaction with Nbs1 (4.4).

Also the capping domain of *S. pombe* Mre11 differs in its architecture from bacteria and archaea. In particular, it contains an extended 40 Å long alpha helix (helix αF), between residues 332 and 358, which is much shorter in archaea or bacteria (4.3). The function of this helix is not understood at the moment. One possibility is that it might be important for the interaction with Rad50, since the capping domain was observed to bind to Rad50 in the bacterial *T. maritima* Mre11-Rad50 complex structure (Lammens et al. 2011). Interestingly, the *S. pombe* Mre11^{cd} structure contains a conserved surface exposed tyrosine residue Y338^{SpMre11} at one end of the helix near the region of the putative Rad50 binding site. Mutation of the corresponding Y328^{ScMre11} residue in *S. cerevisiae* renders cells strongly sensitive to the genotoxic agents MMS, HU and CPT without affecting the protein levels of Mre11 (Lammens et al. 2011). This indicates that the extended eukaryotic capping domain helix might indeed be involved in binding Rad50.

5.3 Nbs1 binds to the Mre11 dimer via multiple contacts and controls its dimeric configuration

The structure of Nbs1^{mir}-Mre11^{cd} revealed that Mre11^{cd} and Nbs1^{mir} build a complex with 2:2 stoichiometry (4.4.1). The possibility of a structural artifact, caused by the fusion protein, was ruled out by an additional construct of Mre11^{cd} and Nbs1^{mir} with a cleavable TEV protease recognition site linker, which was cleaved during the purification procedure before the size exclusion chromatography step. Consistently, the structure of the non-fused Mre11^{mir}-Nbs1^{cd} complex is highly similar to the fusion protein structure in all aspects of stoichiometry and conformation (4.4.1).

A main characteristic of the Nbs1^{mir}-Mre11^{cd} structure is that Nbs1 interacts with Mre11 not via a compact region but instead as an extended peptide at multiple sites. Each of the two Nbs1^{mir} peptides binds to one Mre11^{cd} protomer. This so called interaction region 1 consists of a long stretched α-helix and ß-strand motif between residues 477-498 of Nbs1 (4.4.2). C-terminal to the interaction region 1, both Nbs1^{mir} chains are disordered. However, one of the two peptides is ordered again between residues 518-526 to bind the Mre11 dimer at

interaction site 2 via a highly conserved KNFKxFxK motif. Interestingly, this interaction is asymmetric and it breaks the two fold symmetry of the complex. The KNFKxFxK motif binds across the central Mre11 dimer cleft, which is build up by the two latching loops. It thereby sterically excludes binding of the second Nbs1 molecule to the latching loops. The significance of the observed interaction is underlined by the high sequence conservation on both sides of the interface. The KNFKxFxK motif is one of a few sequence elements of the poorly conserved Nbs1 C-terminus which is conserved between all eukaryotic organisms (4.4.2). The most interesting finding is that the corresponding human residue of $N122^{SpMre11}$ is mutated in A-TLD 3/4 ($N117S^{HsMre11}$) (Stewart et al. 1999). The two $N122^{SpMre11}$ residues coordinate the central phenylalanine residue $F524E^{SpNbs1}$ from both sides via π-stacking. Consistently, the $N117S^{HsMre11}$ and $N122^{SpMre11}$ mutations were reported to reduce the affinity of Mre11 to Nbs1 in human and *S. pombe* cell extracts, respectively (Lee et al. 2003; Porter-Goff and Rhind 2009). The revealed interface between Mre11 and Nbs1 also corresponds well to the interaction region of *S. cerevisiae* Xrs2 to Mre11 in two-hybrid studies (Desai-Mehta et al. 2001). In addition point mutations in $F521^{Nbs1}$, $K522^{Nbs1}$ and/or $K526^{Nbs1}$ lead to compromised or abolished Mre11 interaction and resemble xrs2Δ phenotypes in formation of meiotic breaks in *S. cerevisiae* (Shima et al. 2005). Thus, the identified Mre11-Nbs1 interaction can be explained and is supported by a broad spectrum of *in vitro* and *in vivo* data.

By bridging both Mre11 molecules Nbs1 appears to "tether" the Mre11 dimer to determine its dimeric configuration. A comparison of $Nbs1^{mir}$-$Mre11^{cd}$ with apo-$Mre11^{cd}$ showed significant conformational differences between both structures (4.5). Binding of the KNFKxFxK motif orders the latching loops, which are unstructured and "swapped" between the Mre11 protomers in the apo-$Mre11^{cd}$ structure. Besides, both structures also exhibit global conformational differences. Superposition of apo-$Mre11^{cd}$ and $Nbs1^{mir}$-$Mre11^{cd}$ revealed a difference in the Mre11 dimer angle of 30° towards a more compact conformation in the $Nbs1^{mir}$-$Mre11^{cd}$ structure. Therefore, the *S. pombe* Mre11 dimer possesses an intrinsic flexibility, which allows the adoption of different dimer conformations. Furthermore, the binding of Nbs1 coordinates the latching loops and thereby determines a distinct dimeric conformation. A model, which links the Nbs1 dependent Mre11 dimer configuration to DNA DSB signaling, is discussed in the last chapter of the discussion (5.6).

5.4 The extended structure of the Mre11-Nbs1 interface may explain the hypomorphic character of A-TLD causing mutations

Several mutations in the human *Mre11* gene were reported to cause the genetic disease Ataxia-telangiectasia like disorder (A-TLD), which is characterized by genomic instability, neurodegeneration and for one subtype also by mental retardation and lung carcinoma (Stewart et al. 1999; Fernet et al. 2005; Uchisaka et al. 2009). In addition, a heterozygous Mre11 mutation was recently reported to be linked to a Nijmegen-breakage syndrome (NBS) like disease (2.6) (Matsumoto et al. 2011).

The structure of *S. pombe* Nbs1^{mir}-Mre11^{cd} now allows for the first time a structural analysis of the mutations causing the diseases (4.8.1). The most prominent finding regards the A-TLD subtype 3/4, which is caused by a mutation of an asparagine residue N117S^{HsMre11} (Stewart et al. 1999). The corresponding *S. pombe* residue N122^{SpMre11} is mediating a key interaction with Nbs1 residue F524 at interaction region 2. Therefore, a weakened Nbs1 interaction very likely contributes to the repair and signaling defects seen in A-TLD 3/4. This is also in agreement to Co-IP studies with the human protein, where the interaction was found to be strongly reduced in cells derived from patients with ATLD 3/4 (Stewart et al. 1999). The mutation W210C^{HsMre11} (W215C^{SpMre11}), which leads to A-TLD 7/8 (Fernet et al. 2005), on the other hand appears to have an impact on the interaction region 1, since W215C^{SpMre11} caps the three stranded shared ß-sheet between *S. pombe* Mre11^{cd} and Nbs1^{mir}. W215^{SpMre11} is not surface exposed. Hence, the mutation may also destabilize the overall fold of the protein and thereby impair its functionality. This is also the case for the W243R^{HsMre11} and Del(340-366) mutations, which very likely destabilize the Mre11 protein fold (Uchisaka et al. 2009).

The impact of the NBS-like disease causing mutation D113G^{HsMre11} is more difficult to evaluate, since it occurs as a heterozygous mutation (Matsumoto et al. 2011) (4.8.1). The mutation in the second allele maps to a non-coding region and causes a splicing defect. This results in a low level expression of Wt Mre11 from the second allele. However, it also means that here a small population of Mre11 is fully functional and might be responsible for the relatively high ATM activation levels in NBS-like disease compared to A-TLD. Therefore, it cannot be clearly distinguished, to which degree the D113G^{HsMre11} mutation contributes to the observed phenotype. The *S. pombe* Nbs1^{mir}-Mre11^{cd} crystal structure revealed that D109^{SpMre11}, the corresponding residue of D113G^{HsMre11}, mediates an important Mre11 dimer interface contact (4.4.2). It maps to the latching loop and is positioned by arginine residue

R85^{SpMre11}, which protrudes from the interface helix F of the neighboring Mre11 protomer. An R76A^{ScMre11} mutation of the corresponding arginine residue in *S. cerevisiae* caused a null phenotype of Mre11 (4.10.1). Likewise, also the aspartate to glycine mutation of D113G^{HsMre11} likely destabilizes the fold of the latching loops and disturbs the interaction to Nbs1. Hence, it is suggested, that the D113G^{HsMre11} mutation renders the protein strongly dysfunctional.

The influence of A-TLD causing mutations on the Mre11-Nbs1 interaction was also further studied *in vitro* by binding assays using analytical size-exclusion chromatography and recombinant, purified *S. pombe* Mre11 aa 1-413 and Nbs1 aa 428-613 (4.8.2). The binding experiments showed that all of the tested mutations retain the ability to bind to Mre11. However, the mutations weaken the Mre11-Nbs1 interaction. The Wt Mre11 protein fragment interacted in the presence of Mn^{2+} as well as in EDTA containing buffer with Nbs1. However, EDTA completely disrupted the Mre11-Nbs1 interaction of all A-TLD mutants. Coordination of Mn^{2+} ions by the active site residues likely stabilizes the phosphodiesterase domain fold. Since EDTA removes the Mn^{2+} ions from the active site, it weakens the Mre11 fold stability and thereby also the Mre11-Nbs1 interaction. The additive effects of folding destabilization by removal of Mn^{2+} from the active site plus the weakening influence of A-TLD causing mutations on the Mre11-Nbs1 interface finally result in a disruption of the Mre11-Nbs1 complex in analytical size exclusion chromatography. The experiment suggests that A-TLD causing mutations lead to a partially weakened but not abolished Mre11-Nbs1 interaction. This can be explained by the structure of *S. pombe* Nbs1^{mir}-Mre11^{cd}, since Nbs1 interacts with Mre11 as an extended peptide via multiple independent contacts. The single A-TLD point mutations therefore presumably disrupt only a part of the interface. As a result, A-TLD mutations render the complex partially dysfunctional, thereby causing the hypomorphic disease phenotype.

5.5 The latching loops of *S. cerevisiae* Mre11 are crucial for the general functionality of the Mre11-Rad50-Xrs2 complex

Different motifs found in the *S. pombe* Nbs1^{mir}-Mre11^{cd} structure where studied *in vivo*, using the budding yeast *S. cerevisiae* as a model organism (4.10). Mre11 proteins from both organisms share a high sequence conservation for the crystallized Mre11 nuclease core

(51.3% identical + 28.4 % similar residues). Therefore, the *S. pombe* structure can be used as a guiding model for the mutational analysis of conserved functional residues in *S. cerevisiae.*

One interesting observation of the *S. cerevisiae* studies was the MMS and CPT sensitivity, caused by mutations in the loop element, which connects the phosphodiesterase motif III of the active site with the Mre11 dimer interface helix αC (4.10.1). A recently published structure of the archaeal *Methanococcus jannaschii* Mre11-Rad50 complex bound to ATPγS showed the corresponding archaeal loop to interact with Rad50 in the nucleotide bound state of the complex (Lim et al. 2011). This could also be the function of the eukaryotic loop. Exchange of the *S. cerevisiae* loop by the sequence from the archaeal organism *P. furiosus* led to severe growth defects on MMS and CPT plates similar to mre11Δ. This can likely be explained by sequence and charge differences of both loops. It contains two arginine residues in *P. furiosus*, but two aspartate residues in *S. cerevisiae* and *S. pombe* (Figure 4.8). One theory would be that coordination of the eukaryotic loop by Rad50 in the nucleotide and DNA bound state renders the active site accessible for DNA ends. Another indication for this theory comes from the observation, that the active site of *S. pombe* Mre11 contains binding sites of high and low Mn^{2+} affinity. When crystallized with low Mn^{2+} concentrations, only one Mn^{2+} is bound and the discussed loop element is flipped in a conformation where it could sterically block binding of DNA to the active site (4.6). Rad50 could therefore be directly involved in the allosteric regulation of the eukaryotic Mre11 nuclease function by ordering the active site via coordination of the Mre11 active site loop element.

The main focus of the *S. cerevisiae in vivo* studies was on the mutational analysis of the Mre11-Nbs1/Xrs2 interface and the functional role of the Mre11 latching loops (4.10.1). Here mutations in *S. cerevisiae* Mre11 residues, which mediate binding to Nbs1 via interaction region 1, exhibited no growth defects in the presence of MMS and CPT. This is in agreement with the observation that the complete deletion of the corresponding interaction region 1 region in *S. cerevisiae* Xrs2 does not impair mitotic repair but it is instead crucial for the meiotic function of the complex (Tsukamoto et al. 2005). However, analysis of interaction region 1 mutations for spore viability by the group of Steve Jackson showed also no meiosis defect (unpublished results - Laboratory of Steve Jackson, Cambridge). This might be explained by the extended conformation of Nbs1 in the $Nbs1^{mir}$-$Mre11^{cd}$ structure (4.4). Single point mutations are probably not strong enough to disrupt the complete interaction region 1 and therefore preserve the meiotic function of MRX.

The interaction region 2, observed between the *S. pombe* Mre11^{cd} latching loops and Nbs1^{mir} (4.4), appears to also be crucial for the interaction of *S. cerevisisae* Mre11 and Xrs2. The mutations S91E^{ScMre11} and N113S^{ScMre11}, which both map to the latching loop of *S. cerevisiae* Mre11, render the cells sensitive to genotoxic agents like HU and CPT (4.10.1). A control experiment with the corresponding NLS-tagged Mre11 mutants showed a rescue of the resistance against HU and CPT. Xrs2 contains the only NLS within the Mre11-Rad50-Xrs2 complex and is therefore crucial for the nuclear localization of the complex. However, when Mre11 is tagged by an NLS, Xrs2 is not needed for the resistance to genotoxic agents (Tsukamoto et al. 2005). Hence, the defects of S91E^{ScMre11} and N113S^{ScMre11} can be explained by a disturbed Mre11-Xrs2 interaction which leads to a cellular delocalization of Mre11-Rad50.

In contrast, the R76A^{ScMre11} mutation targets not only the Xrs2 interface but also the overall stability of the latching loops (4.10.1). R76^{ScMre11}, which protrudes from the dimer interface helix αC, coordinates the latching loops via a salt bridge to the latching loop residue D109^{ScMre11} (4.4.2). Remarkably, the corresponding human residue of D109^{ScMre11} is mutated in human NBS-like disease (Matsumoto et al. 2011). Co-immunoprecipitation (Co-IP) studies and indirect immunofluorescence analysis of the Mre11 R76A^{ScMre11} mutant strain revealed an abolished interaction of Mre11 and Xrs2 (4.10.2 and 4.10.3). However, the repair defect, monitored by sensitivity to MMS; HU and CPT, could not be rescued by the addition of a NLS to Mre11 R76A (4.10.1). The mutation therefore also impairs the function of Mre11 apart from weakening the interaction to Xrs2. Co-IP analysis of two Mre11 alleles with different affinity tags revealed, that the R76A^{ScMre11} mutation is strongly impairing the stability of Mre11 dimers (4.10.3). This might explain the severe mitotic repair defect of the NLS tagged R76A^{ScMre11} mutant strain, since Mre11 is only functional *in vivo* as a dimeric molecule (Williams et al. 2008).

In summary, single point mutations in the Mre11-Xrs2 or the Mre11 dimer interfaces were identified, which specifically disrupt these protein-protein interactions, thereby causing mitotic repair defects. The *in vivo* analysis of *S. cerevisiae* Mre11 (4.10) verified the interactions between Mre11 and Nbs1 determined by the *S. pombe* Nbs1^{mir}-Mre11^{cd} crystal structure (4.4). The latching loops are not only crucial for the interaction to Xrs2 *in vivo*. They also are important for the stability of the Mre11 dimer (4.10.3). In this aspect the eukaryotic Mre11 protein architecture strongly differs from bacterial and archaeal Mre11, where the

dimer interface is solely composed of the conserved hydrophobic four helix bundle (Hopfner et al. 2001; Lammens et al. 2011).

5.6 A model for Mre11 dimer and Nbs1 mediated DSB signaling

The asymmetric interaction of Nbs1 with the Mre11 dimer suggests a functional link between Mre11 dimer conformation and DSB signaling. It was already discussed how Nbs1 structurally orders the Mre11 dimer interface (5.3). Superposition of *S. pombe* (*Sp*)Mre11^{cd} with the *Sp*Nbs1^{mir}-Mre11^{cd} complex additionally revealed an unexpected flexibility in the Mre11 dimer angle by approx. 30° (4.5). Such alterations in the Mre11 dimer angle could indeed be linked to DSB recognition as a comparison of both structures with the crystal structure of *P. furiosus (Pf)*Mre11^{cd} bound to DNA shows (Figure 5.1) (Williams et al. 2008) . The DNA complex of *Pf*Mre11^{cd} revealed that DNA ends are bound across both Mre11 protomers and therefore need a particular Mre11 dimer orientation (Figure 5.1 A).

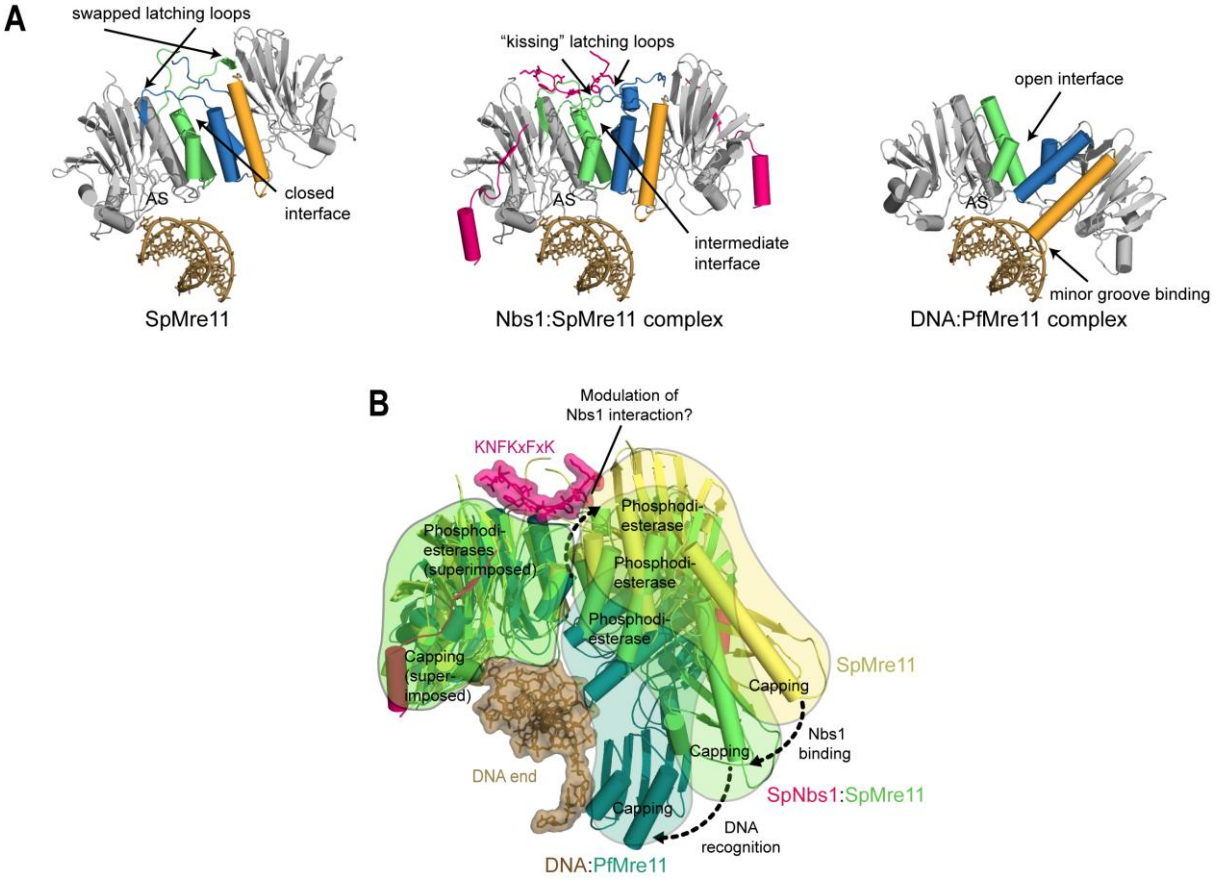

Figure 5.1: Structural variability in the Mre11 dimer and model for DNA double-strand break signaling. **(A)** Overlay of *S. pombe* Mre11^{cd} (yellow) with the Nbs1^{mir}-Mre11^{cd} complex (green with magenta Nbs1) and

DNA bound dimer of *P. furiosus* Mre11^{cd} (blue with brown DNA) reveals that the Mre11 dimer pivot angle is highly variable. All three structures are superimposed via one Mre11 protomer, respectively. DNA binding with multiple interaction sites, as observed in the PfMre11-DNA complex, requires a substantial structural change in the Mre11-Nbs1 complex that could be the basis of damage sensing and signaling, by modulating the interaction of Nbs1 with the Mre11 dimer interface. **(B)** In apo-*Sp*Mre11^{cd} (top panel, shown as cartoon model with omitted capping domains), two phosphodiesterase domain closely interact via two helix pairs (green and blue), one from each protomer. In the absence of Nbs1, the latching loops are swapped between protomers and partially disordered, allowing the dimer interface to be closed. Middle panel: Nbs1 (magenta) orders the latching loops into a "kissing" conformation and changes the mre11 dimer pivot angle by slightly opening the interface. This brings a DNA binding helix (orange) of one protomer into closer proximity to the DNA bound to the other protomer (modeled after the PfMre11:DNA complex). Lower panel: full DNA binding, as seen in the DNA-PfMre11 complex (protein data bank entry 3DSD), is achieved after further opening the dimer interface, allowing the other protomer to assist in binding the minor groove (orange helix).

Superimposing *Sp*Nbs1^{mir}-Mre11^{cd} with *Pf*Mre11^{cd}-DNA reveals now another large pivot motion of the Mre11 dimer by approx. 30° (Figure 5.1 A, B). In fact, to form the dsDNA binding interactions of the *Pf*Mre11^{cd}:DNA complex, *Sp*Mre11^{cd} protomers must rotate by approx. 30° from the conformation observed in the Nbs1 complex and even 60° from the conformation seen in the absence of Nbs1.

The revealed conformational flexibility in the Mre11 dimer, its evident coupling to Nbs1 binding, and expected conformational changes upon DNA binding, suggest an intriguing but simple, testable model for DSB signaling (Figure 5.2). Since most DNA binding residues are conserved between archaeal and eukaryotic Mre11, it is plausible that DSB recognition will induce an Mre11 dimer orientation as seen in the *Pf*Mre11^{cd}-DNA complex (Figure 5.1 A, B). Such a conceivable conformational change will likely affect the latching loops by the underlying rigid body movements of the phosphodiesterase domains and hence modulate the interaction with the Nbs1 molecules at this region. This is plausible because the observed differences between Nbs1 bound and free Mre11 suggest that latching loop structure, Mre11 dimer angle and Nbs1 interaction are coupled.

Moreover, the Hopfner group and others showed that bacterial and archaeal Mre11-Rad50 bind to DNA as an ATP dependent clamp, and DNA binding involves large conformational rearrangements in both proteins (Lammens et al. 2011; Lim et al. 2011). Such a DNA and ATP induced conformational switch of Mre11-Rad50 could be the driving force for a rotation of Mre11 dimers and remodeling of the Mre11-Nbs1 interaction. Interestingly, mutational studies showed that the activation of ATM depends on nucleotide binding by Rad50 (Lee and

Paull 2005; Dupre et al. 2006). Therefore, ATM could be activated by reading out the ATP and DNA bound conformation of MRN via multiple interfaces with MRN.

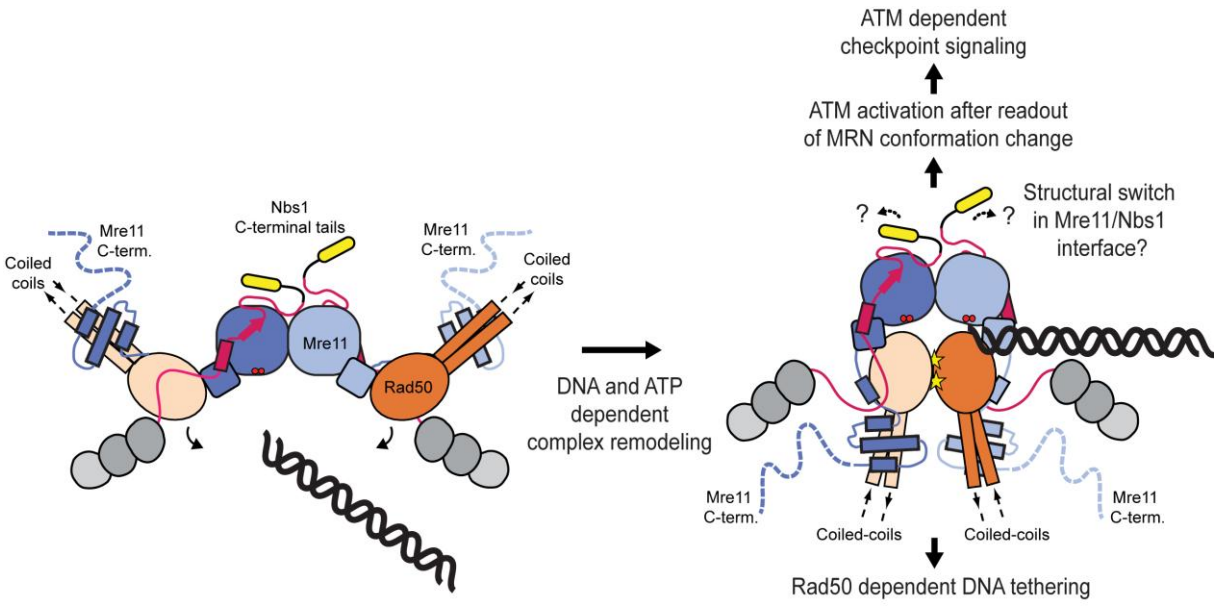

Figure 5.2: Speculative model for DNA double-strand break signaling by a DNA and Rad50 induced structural switch in the Mre11 dimer via Mre11 dimer sensing by Nbs1. Such a structural switch could alter Nbs1 binding geometry at the Mre11 dimer interface and hence reposition the adjacent ATM binding motifs (yellow). Subsequently, the binding motifs could interact with ATM HEAT repeats, resulting in recruitment and activation of ATM.

An altered Nbs1 interaction, however, could nicely explain DSB signaling, because the ATM binding motif of Nbs1 is adjacent to the KNFKxFxK motif at the Mre11 dimer interface. For example, Tel1/ATM has two HEAT repeat regions that interact with the C-terminus of Nbs1 (You et al. 2005), so it is plausible that a repositioning of both Nbs1 termini in the MRN complex by differential interaction with the Mre11 dimer could directly control recruitment and activation by binding to a single ATM protein at its two interaction sites. Furthermore, *in vitro* DNA binding studies with the Mre11 interaction region of Nbs1 showed a direct interaction of the KNFKxFxK motif to ssDNA and dsDNA substrates (4.9). Therefore, Nbs1 may also be involved in the recognition and signaling of DSBs by directly binding to DNA via the KNFKxFxK motif. This might induce the dissociation of this region from the Mre11 dimer and could thereby promote Mre11 dimer rotation and an MRN conformation which signals the damage to ATM.

In the future, further studies will be needed to understand how exactly the signal transduction of DNA DSBs is coupled to the conformational states of the MRN complex. This will likely

require a hybrid techniques approach to combine atomic resolution structures of the nucleotide and DNA bound Mre11-Rad50-Nbs1 complex and ATM/Tel1 with biochemical and cell biology methods.

6. REFERENCES

Ahnesorg, P., P. Smith and S. P. Jackson (2006). "XLF interacts with the XRCC4-DNA ligase IV complex to promote DNA nonhomologous end-joining." Cell **124**(2): 301-313.

Ajimura, M., S. H. Leem and H. Ogawa (1993). "Identification of new genes required for meiotic recombination in Saccharomyces cerevisiae." Genetics **133**(1): 51-66.

Al-Minawi, A. Z., Y. F. Lee, D. Hakansson, F. Johansson, C. Lundin, N. Saleh-Gohari, N. Schultz, D. Jenssen, H. E. Bryant, M. Meuth, J. M. Hinz and T. Helleday (2009). "The ERCC1/XPF endonuclease is required for completion of homologous recombination at DNA replication forks stalled by inter-strand cross-links." Nucleic Acids Res **37**(19): 6400-6413.

Alani, E., R. Padmore and N. Kleckner (1990). "Analysis of wild-type and rad50 mutants of yeast suggests an intimate relationship between meiotic chromosome synapsis and recombination." Cell **61**(3): 419-436.

Almeida, K. H. and R. W. Sobol (2007). "A unified view of base excision repair: lesion-dependent protein complexes regulated by post-translational modification." DNA Repair (Amst) **6**(6): 695-711.

Assenmacher, N. and K. P. Hopfner (2004). "MRE11/RAD50/NBS1: complex activities." Chromosoma **113**(4): 157-166.

Bartkova, J., J. Tommiska, L. Oplustilova, K. Aaltonen, A. Tamminen, T. Heikkinen, M. Mistrik, K. Aittomaki, C. Blomqvist, P. Heikkila, J. Lukas, H. Nevanlinna and J. Bartek (2008). "Aberrations of the MRE11-RAD50-NBS1 DNA damage sensor complex in human breast cancer: MRE11 as a candidate familial cancer-predisposing gene." Mol Oncol **2**(4): 296-316.

Berkovich, E., R. J. Monnat, Jr. and M. B. Kastan (2007). "Roles of ATM and NBS1 in chromatin structure modulation and DNA double-strand break repair." Nat Cell Biol **9**(6): 683-690.

Bonetti, D., M. Martina, M. Clerici, G. Lucchini and M. P. Longhese (2009). "Multiple pathways regulate 3' overhang generation at S. cerevisiae telomeres." Mol Cell **35**(1): 70-81.

Borde, V. (2007). "The multiple roles of the Mre11 complex for meiotic recombination." Chromosome Res **15**(5): 551-563.

Borde, V. and J. Cobb (2009). "Double functions for the Mre11 complex during DNA double-strand break repair and replication." Int J Biochem Cell Biol **41**(6): 1249-1253.

Bosco, E. E., C. N. Mayhew, R. F. Hennigan, J. Sage, T. Jacks and E. S. Knudsen (2004). "RB signaling prevents replication-dependent DNA double-strand breaks following genotoxic insult." Nucleic Acids Res **32**(1): 25-34.

Boulton, S. J. and S. P. Jackson (1998). "Components of the Ku-dependent non-homologous end-joining pathway are involved in telomeric length maintenance and telomeric silencing." EMBO J **17**(6): 1819-1828.

Bressan, D. A., H. A. Olivares, B. E. Nelms and J. H. Petrini (1998). "Alteration of N-terminal phosphoesterase signature motifs inactivates Saccharomyces cerevisiae Mre11." Genetics **150**(2): 591-600.

Bromberg, K. D., A. B. Burgin and N. Osheroff (2003). "A two-drug model for etoposide action against human topoisomerase IIalpha." J Biol Chem **278**(9): 7406-7412.

Bryson, K., L. J. McGuffin, R. L. Marsden, J. J. Ward, J. S. Sodhi and D. T. Jones (2005). "Protein structure prediction servers at University College London." Nucleic Acids Res **33**(Web Server issue): W36-38.

Buis, J., Y. Wu, Y. Deng, J. Leddon, G. Westfield, M. Eckersdorff, J. M. Sekiguchi, S. Chang and D. O. Ferguson (2008). "Mre11 nuclease activity has essential roles in DNA repair and genomic stability distinct from ATM activation." Cell **135**(1): 85-96.

Bzymek, M., N. H. Thayer, S. D. Oh, N. Kleckner and N. Hunter (2010). "Double Holliday junctions are intermediates of DNA break repair." Nature **464**(7290): 937-941.

Cadet, J., M. Berger, T. Douki and J. L. Ravanat (1997). "Oxidative damage to DNA: formation, measurement, and biological significance." Rev Physiol Biochem Pharmacol **131**: 1-87.

Carney, J. P., R. S. Maser, H. Olivares, E. M. Davis, M. Le Beau, J. R. Yates, 3rd, L. Hays, W. F. Morgan and J. H. Petrini (1998). "The hMre11/hRad50 protein complex and Nijmegen breakage syndrome: linkage of double-strand break repair to the cellular DNA damage response." Cell **93**(3): 477-486.

Chamankhah, M., T. Fontanie and W. Xiao (2000). "The Saccharomyces cerevisiae mre11(ts) allele confers a separation of DNA repair and telomere maintenance functions." Genetics **155**(2): 569-576.

Chamankhah, M. and W. Xiao (1999). "Formation of the yeast Mre11-Rad50-Xrs2 complex is correlated with DNA repair and telomere maintenance." Nucleic Acids Res **27**(10): 2072-2079.

Chapman, J. R. and S. P. Jackson (2008). "Phospho-dependent interactions between NBS1 and MDC1 mediate chromatin retention of the MRN complex at sites of DNA damage." EMBO Rep **9**(8): 795-801.

Chen, L., K. Trujillo, W. Ramos, P. Sung and A. E. Tomkinson (2001). "Promotion of Dnl4-catalyzed DNA end-joining by the Rad50/Mre11/Xrs2 and Hdf1/Hdf2 complexes." Mol Cell **8**(5): 1105-1115.

Ciccia, A. and S. J. Elledge (2010). "The DNA damage response: making it safe to play with knives." Mol Cell **40**(2): 179-204.

Clerici, M., D. Mantiero, I. Guerini, G. Lucchini and M. P. Longhese (2008). "The Yku70-Yku80 complex contributes to regulate double-strand break processing and checkpoint activation during the cell cycle." EMBO Rep **9**(8): 810-818.

Coic, E., G. F. Richard and J. E. Haber (2006). "Saccharomyces cerevisiae donor preference during mating-type switching is dependent on chromosome architecture and organization." Genetics **173**(3): 1197-1206.

Cole, C., J. D. Barber and G. J. Barton (2008). "The Jpred 3 secondary structure prediction server." Nucleic Acids Res **36**(Web Server issue): W197-201.

Connelly, J. C., E. S. de Leau and D. R. Leach (1999). "DNA cleavage and degradation by the SbcCD protein complex from Escherichia coli." Nucleic Acids Res **27**(4): 1039-1046.

Connelly, J. C., E. S. de Leau and D. R. Leach (2003). "Nucleolytic processing of a protein-bound DNA end by the E. coli SbcCD (MR) complex." DNA Repair (Amst) **2**(7): 795-807.

Costanzo, V., K. Robertson, M. Bibikova, E. Kim, D. Grieco, M. Gottesman, D. Carroll and J. Gautier (2001). "Mre11 protein complex prevents double-strand break accumulation during chromosomal DNA replication." Mol Cell **8**(1): 137-147.

Cowtan, K. (2006). "The Buccaneer software for automated model building. 1. Tracing protein chains." Acta Crystallogr D Biol Crystallogr **62**(Pt 9): 1002-1011.

Critchlow, S. E. and S. P. Jackson (1998). "DNA end-joining: from yeast to man." Trends Biochem Sci **23**(10): 394-398.

D'Amours, D. and S. P. Jackson (2001). "The yeast Xrs2 complex functions in S phase checkpoint regulation." Genes Dev **15**(17): 2238-2249.

de Jager, M., J. van Noort, D. C. van Gent, C. Dekker, R. Kanaar and C. Wyman (2001). "Human Rad50/Mre11 is a flexible complex that can tether DNA ends." Mol Cell **8**(5): 1129-1135.

Degrassi, F., M. Fiore and F. Palitti (2004). "Chromosomal aberrations and genomic instability induced by topoisomerase-targeted antitumour drugs." Curr Med Chem Anticancer Agents **4**(4): 317-325.

Deriano, L., T. H. Stracker, A. Baker, J. H. Petrini and D. B. Roth (2009). "Roles for NBS1 in alternative nonhomologous end-joining of V(D)J recombination intermediates." Mol Cell **34**(1): 13-25.

Deribe, Y. L., T. Pawson and I. Dikic (2010). "Post-translational modifications in signal integration." Nat Struct Mol Biol **17**(6): 666-672.

Desai-Mehta, A., K. M. Cerosaletti and P. Concannon (2001). "Distinct functional domains of nibrin mediate Mre11 binding, focus formation, and nuclear localization." Mol Cell Biol **21**(6): 2184-2191.

Di Virgilio, M., C. Y. Ying and J. Gautier (2009). "PIKK-dependent phosphorylation of Mre11 induces MRN complex inactivation by disassembly from chromatin." DNA Repair (Amst) **8**(11): 1311-1320.

Dianov, G. L. and J. L. Parsons (2007). "Co-ordination of DNA single strand break repair." DNA Repair (Amst) **6**(4): 454-460.

Dinkelmann, M., E. Spehalski, T. Stoneham, J. Buis, Y. Wu, J. M. Sekiguchi and D. O. Ferguson (2009). "Multiple functions of MRN in end-joining pathways during isotype class switching." Nat Struct Mol Biol **16**(8): 808-813.

Dudley, D. D., J. Chaudhuri, C. H. Bassing and F. W. Alt (2005). "Mechanism and control of V(D)J recombination versus class switch recombination: similarities and differences." Adv Immunol **86**: 43-112.

Dupre, A., L. Boyer-Chatenet and J. Gautier (2006). "Two-step activation of ATM by DNA and the Mre11-Rad50-Nbs1 complex." Nat Struct Mol Biol **13**(5): 451-457.

Emsley, P. and K. Cowtan (2004). "Coot: model-building tools for molecular graphics." Acta Crystallogr D Biol Crystallogr **60**(Pt 12 Pt 1): 2126-2132.

Errico, A. and V. Costanzo (2010). "Differences in the DNA replication of unicellular eukaryotes and metazoans: known unknowns." EMBO Rep **11**(4): 270-278.

Falck, J., J. Coates and S. P. Jackson (2005). "Conserved modes of recruitment of ATM, ATR and DNA-PKcs to sites of DNA damage." Nature **434**(7033): 605-611.

Falck, J., J. H. Petrini, B. R. Williams, J. Lukas and J. Bartek (2002). "The DNA damage-dependent intra-S phase checkpoint is regulated by parallel pathways." Nat Genet **30**(3): 290-294.

Fattah, F., E. H. Lee, N. Weisensel, Y. Wang, N. Lichter and E. A. Hendrickson (2010). "Ku regulates the non-homologous end joining pathway choice of DNA double-strand break repair in human somatic cells." PLoS Genet **6**(2): e1000855.

Faure, V., S. Coulon, J. Hardy and V. Geli (2010). "Cdc13 and telomerase bind through different mechanisms at the lagging- and leading-strand telomeres." Mol Cell **38**(6): 842-852.

Fernet, M., M. Gribaa, M. A. Salih, M. Z. Seidahmed, J. Hall and M. Koenig (2005). "Identification and functional consequences of a novel MRE11 mutation affecting 10 Saudi Arabian patients with the ataxia telangiectasia-like disorder." Hum Mol Genet **14**(2): 307-318.

Frappart, P. O. and P. J. McKinnon (2006). "Ataxia-telangiectasia and related diseases." Neuromolecular Med **8**(4): 495-511.

Furuse, M., Y. Nagase, H. Tsubouchi, K. Murakami-Murofushi, T. Shibata and K. Ohta (1998). "Distinct roles of two separable in vitro activities of yeast Mre11 in mitotic and meiotic recombination." EMBO J **17**(21): 6412-6425.

Game, J. C. and R. K. Mortimer (1974). "A genetic study of x-ray sensitive mutants in yeast." Mutat Res **24**(3): 281-292.

Goudsouzian, L. K., C. T. Tuzon and V. A. Zakian (2006). "S. cerevisiae Tel1p and Mre11p are required for normal levels of Est1p and Est2p telomere association." Mol Cell **24**(4): 603-610.

Haber, J. E. (1998). "The many interfaces of Mre11." Cell **95**(5): 583-586.

Haber, J. E. (1998). "Mating-type gene switching in Saccharomyces cerevisiae." Annu Rev Genet **32**: 561-599.

Haber, J. E. (2008). "Alternative endings." Proc Natl Acad Sci U S A **105**(2): 405-406.

Hari, F. J., C. Spycher, S. Jungmichel, L. Pavic and M. Stucki (2010). "A divalent FHA/BRCT-binding mechanism couples the MRE11-RAD50-NBS1 complex to damaged chromatin." EMBO Rep **11**(5): 387-392.

Harper, J. W. and S. J. Elledge (2007). "The DNA damage response: ten years after." Mol Cell **28**(5): 739-745.

Hector, R. E., R. L. Shtofman, A. Ray, B. R. Chen, T. Nyun, K. L. Berkner and K. W. Runge (2007). "Tel1p preferentially associates with short telomeres to stimulate their elongation." Mol Cell **27**(5): 851-858.

Helmink, B. A., A. L. Bredemeyer, B. S. Lee, C. Y. Huang, G. G. Sharma, L. M. Walker, J. J. Bednarski, W. L. Lee, T. K. Pandita, C. H. Bassing and B. P. Sleckman (2009). "MRN complex function in the repair of chromosomal Rag-mediated DNA double-strand breaks." J Exp Med **206**(3): 669-679.

Hendrickson, W. A., J. R. Horton and D. M. LeMaster (1990). "Selenomethionyl proteins produced for analysis by multiwavelength anomalous diffraction (MAD): a vehicle for direct determination of three-dimensional structure." EMBO J **9**(5): 1665-1672.

Henner, W. D., L. O. Rodriguez, S. M. Hecht and W. A. Haseltine (1983). "gamma Ray induced deoxyribonucleic acid strand breaks. 3' Glycolate termini." J Biol Chem **258**(2): 711-713.

Herdendorf, T. J., D. W. Albrecht, S. J. Benkovic and S. W. Nelson (2011). "Biochemical characterization of bacteriophage T4 Mre11-Rad50 complex." J Biol Chem **286**(4): 2382-2392.

Heyer, W. D. (2004). "Recombination: Holliday junction resolution and crossover formation." Curr Biol **14**(2): R56-58.

Hirano, Y., K. Fukunaga and K. Sugimoto (2009). "Rif1 and rif2 inhibit localization of tel1 to DNA ends." Mol Cell **33**(3): 312-322.

Hoeijmakers, J. H. (2001). "Genome maintenance mechanisms for preventing cancer." Nature **411**(6835): 366-374.

Hopfner, K. P., L. Craig, G. Moncalian, R. A. Zinkel, T. Usui, B. A. Owen, A. Karcher, B. Henderson, J. L. Bodmer, C. T. McMurray, J. P. Carney, J. H. Petrini and J. A. Tainer (2002). "The Rad50 zinc-hook is a structure joining Mre11 complexes in DNA recombination and repair." Nature **418**(6897): 562-566.

Hopfner, K. P., A. Karcher, L. Craig, T. T. Woo, J. P. Carney and J. A. Tainer (2001). "Structural biochemistry and interaction architecture of the DNA double-strand break repair Mre11 nuclease and Rad50-ATPase." Cell **105**(4): 473-485.

Hopfner, K. P., A. Karcher, D. Shin, C. Fairley, J. A. Tainer and J. P. Carney (2000). "Mre11 and Rad50 from Pyrococcus furiosus: cloning and biochemical characterization reveal an evolutionarily conserved multiprotein machine." J Bacteriol **182**(21): 6036-6041.

Huertas, P. (2010). "DNA resection in eukaryotes: deciding how to fix the break." Nat Struct Mol Biol **17**(1): 11-16.

Huertas, P., F. Cortes-Ledesma, A. A. Sartori, A. Aguilera and S. P. Jackson (2008). "CDK targets Sae2 to control DNA-end resection and homologous recombination." Nature **455**(7213): 689-692.

Huertas, P. and S. P. Jackson (2009). "Human CtIP mediates cell cycle control of DNA end resection and double strand break repair." J Biol Chem **284**(14): 9558-9565.

Hug, N. and J. Lingner (2006). "Telomere length homeostasis." Chromosoma **115**(6): 413-425.

Inagaki, A., S. Schoenmakers and W. M. Baarends (2010). "DNA double strand break repair, chromosome synapsis and transcriptional silencing in meiosis." Epigenetics **5**(4): 255-266.

Ivanov, E. L., V. G. Korolev and F. Fabre (1992). "XRS2, a DNA repair gene of Saccharomyces cerevisiae, is needed for meiotic recombination." Genetics **132**(3): 651-664.

Ivanov, E. L., N. Sugawara, J. Fishman-Lobell and J. E. Haber (1996). "Genetic requirements for the single-strand annealing pathway of double-strand break repair in Saccharomyces cerevisiae." Genetics **142**(3): 693-704.

Jacob, S., C. Miquel, A. Sarasin and F. Praz (2005). "Effects of camptothecin on double-strand break repair by non-homologous end-joining in DNA mismatch repair-deficient human colorectal cancer cell lines." Nucleic Acids Res **33**(1): 106-113.

Janke, R., K. Herzberg, M. Rolfsmeier, J. Mar, V. I. Bashkirov, E. Haghnazari, G. Cantin, J. R. Yates, 3rd and W. D. Heyer (2010). "A truncated DNA-damage-signaling response is activated after DSB formation in the G1 phase of Saccharomyces cerevisiae." Nucleic Acids Res **38**(7): 2302-2313.

Jones, D. T. (1999). "Protein secondary structure prediction based on position-specific scoring matrices." J Mol Biol **292**(2): 195-202.

Kabsch, W. (1993). "Automatic processing of rotation diffraction data from crystals of initially unknown symmetry and cell constants." Journal of Appl. Crystallogr. **26**(6): 795-800.

Keelagher, R. E., V. E. Cotton, A. S. Goldman and R. H. Borts (2011). "Separable roles for Exonuclease I in meiotic DNA double-strand break repair." DNA Repair (Amst) **10**(2): 126-137.

Keeney, S., C. N. Giroux and N. Kleckner (1997). "Meiosis-specific DNA double-strand breaks are catalyzed by Spo11, a member of a widely conserved protein family." Cell **88**(3): 375-384.

Keeney, S. and N. Kleckner (1995). "Covalent protein-DNA complexes at the 5' strand termini of meiosis-specific double-strand breaks in yeast." Proc Natl Acad Sci U S A **92**(24): 11274-11278.

Kim, S. T. (2005). "Protein kinase CK2 interacts with Chk2 and phosphorylates Mre11 on serine 649." Biochem Biophys Res Commun **331**(1): 247-252.

Konarev, P. V., M. V. Petoukhov, V. V. Volkov and D. I. Svergun (2006). "ATSAS 2.1, a program package for small-angle scattering data analysis." Journal of Applied Crystallography **39**(2): 277-286.

Kuzminov, A. (2001). "DNA replication meets genetic exchange: chromosomal damage and its repair by homologous recombination." Proc Natl Acad Sci U S A **98**(15): 8461-8468.

Laemmli, U. K. (1970). "Cleavage of structural proteins during the assembly of the head of bacteriophage T4." Nature **227**(5259): 680-685.

Lam, A. F., B. O. Krogh and L. S. Symington (2008). "Unique and overlapping functions of the Exo1, Mre11 and Pso2 nucleases in DNA repair." DNA Repair (Amst) **7**(4): 655-662.

Lammens, K., D. J. Bemeleit, C. Mockel, E. Clausing, A. Schele, S. Hartung, C. B. Schiller, M. Lucas, C. Angermuller, J. Soding, K. Strasser and K. P. Hopfner (2011). "The Mre11:Rad50 Structure Shows an ATP-Dependent Molecular Clamp in DNA Double-Strand Break Repair." Cell **145**(1): 54-66.

Langer, G., S. X. Cohen, V. S. Lamzin and A. Perrakis (2008). "Automated macromolecular model building for X-ray crystallography using ARP/wARP version 7." Nat Protoc **3**(7): 1171-1179.

Larkin, M. A., G. Blackshields, N. P. Brown, R. Chenna, P. A. McGettigan, H. McWilliam, F. Valentin, I. M. Wallace, A. Wilm, R. Lopez, J. D. Thompson, T. J. Gibson and D. G. Higgins (2007). "Clustal W and Clustal X version 2.0." Bioinformatics **23**(21): 2947-2948.

Lavin, M. F. (2008). "Ataxia-telangiectasia: from a rare disorder to a paradigm for cell signalling and cancer." Nat Rev Mol Cell Biol **9**(10): 759-769.

Lee, J. H., R. Ghirlando, V. Bhaskara, M. R. Hoffmeyer, J. Gu and T. T. Paull (2003). "Regulation of Mre11/Rad50 by Nbs1: effects on nucleotide-dependent DNA binding and association with ataxia-telangiectasia-like disorder mutant complexes." J Biol Chem **278**(46): 45171-45181.

Lee, J. H. and T. T. Paull (2005). "ATM activation by DNA double-strand breaks through the Mre11-Rad50-Nbs1 complex." Science **308**(5721): 551-554.

Lee, S. E., D. A. Bressan, J. H. Petrini and J. E. Haber (2002). "Complementation between N-terminal Saccharomyces cerevisiae mre11 alleles in DNA repair and telomere length maintenance." DNA Repair (Amst) **1**(1): 27-40.

Lengsfeld, B. M., A. J. Rattray, V. Bhaskara, R. Ghirlando and T. T. Paull (2007). "Sae2 is an endonuclease that processes hairpin DNA cooperatively with the Mre11/Rad50/Xrs2 complex." Mol Cell **28**(4): 638-651.

Lewis, L. K., F. Storici, S. Van Komen, S. Calero, P. Sung and M. A. Resnick (2004). "Role of the nuclease activity of Saccharomyces cerevisiae Mre11 in repair of DNA double-strand breaks in mitotic cells." Genetics **166**(4): 1701-1713.

Lieber, M. R. (2010). "The mechanism of double-strand DNA break repair by the nonhomologous DNA end-joining pathway." Annu Rev Biochem **79**: 181-211.

Lim, H. S., J. S. Kim, Y. B. Park, G. H. Gwon and Y. Cho (2011). "Crystal structure of the Mre11-Rad50-ATP{gamma}S complex: understanding the interplay between Mre11 and Rad50." Genes Dev.

Limbo, O., C. Chahwan, Y. Yamada, R. A. de Bruin, C. Wittenberg and P. Russell (2007). "Ctp1 is a cell-cycle-regulated protein that functions with Mre11 complex to control double-strand break repair by homologous recombination." Mol Cell **28**(1): 134-146.

Limoli, C. L., E. Giedzinski, W. M. Bonner and J. E. Cleaver (2002). "UV-induced replication arrest in the xeroderma pigmentosum variant leads to DNA double-strand breaks, gamma -H2AX formation, and Mre11 relocalization." Proc Natl Acad Sci U S A **99**(1): 233-238.

Lloyd, J., J. R. Chapman, J. A. Clapperton, L. F. Haire, E. Hartsuiker, J. Li, A. M. Carr, S. P. Jackson and S. J. Smerdon (2009). "A supramodular FHA/BRCT-repeat architecture mediates Nbs1 adaptor function in response to DNA damage." Cell **139**(1): 100-111.

Longhese, M. P., D. Bonetti, N. Manfrini and M. Clerici (2010). "Mechanisms and regulation of DNA end resection." EMBO J **29**(17): 2864-2874.

Mahaney, B. L., K. Meek and S. P. Lees-Miller (2009). "Repair of ionizing radiation-induced DNA double-strand breaks by non-homologous end-joining." Biochem J **417**(3): 639-650.

Mansour, W. Y., S. Schumacher, R. Rosskopf, T. Rhein, F. Schmidt-Petersen, F. Gatzemeier, F. Haag, K. Borgmann, H. Willers and J. Dahm-Daphi (2008). "Hierarchy of nonhomologous end-joining, single-strand annealing and gene conversion at site-directed DNA double-strand breaks." Nucleic Acids Res **36**(12): 4088-4098.

Matsumoto, Y., T. Miyamoto, H. Sakamoto, H. Izumi, Y. Nakazawa, T. Ogi, H. Tahara, S. Oku, A. Hiramoto, T. Shiiki, Y. Fujisawa, H. Ohashi, Y. Sakemi and S. Matsuura (2011). "Two unrelated patients with MRE11A mutations and Nijmegen breakage syndrome-like severe microcephaly." DNA Repair (Amst) **10**(3): 314-321.

McCoy, A. J. (2007). "Solving structures of protein complexes by molecular replacement with Phaser." Acta Crystallogr D Biol Crystallogr **63**(Pt 1): 32-41.

McKee, A. H. and N. Kleckner (1997). "A general method for identifying recessive diploid-specific mutations in Saccharomyces cerevisiae, its application to the isolation of mutants blocked at intermediate stages of meiotic prophase and characterization of a new gene SAE2." Genetics **146**(3): 797-816.

Meek, K., P. Douglas, X. Cui, Q. Ding and S. P. Lees-Miller (2007). "trans Autophosphorylation at DNA-dependent protein kinase's two major autophosphorylation site clusters facilitates end processing but not end joining." Mol Cell Biol **27**(10): 3881-3890.

Melander, F., S. Bekker-Jensen, J. Falck, J. Bartek, N. Mailand and J. Lukas (2008). "Phosphorylation of SDT repeats in the MDC1 N terminus triggers retention of NBS1 at the DNA damage-modified chromatin." J Cell Biol **181**(2): 213-226.

Mimitou, E. P. and L. S. Symington (2009). "DNA end resection: many nucleases make light work." DNA Repair (Amst) **8**(9): 983-995.

Mimitou, E. P. and L. S. Symington (2011). "DNA end resection--unraveling the tail." DNA Repair (Amst) **10**(3): 344-348.

Misteli, T. and E. Soutoglou (2009). "The emerging role of nuclear architecture in DNA repair and genome maintenance." Nat Rev Mol Cell Biol **10**(4): 243-254.

Moreau, S., J. R. Ferguson and L. S. Symington (1999). "The nuclease activity of Mre11 is required for meiosis but not for mating type switching, end joining, or telomere maintenance." Mol Cell Biol **19**(1): 556-566.

Moreno-Herrero, F., M. de Jager, N. H. Dekker, R. Kanaar, C. Wyman and C. Dekker (2005). "Mesoscale conformational changes in the DNA-repair complex Rad50/Mre11/Nbs1 upon binding DNA." Nature **437**(7057): 440-443.

Nairz, K. and F. Klein (1997). "mre11S--a yeast mutation that blocks double-strand-break processing and permits nonhomologous synapsis in meiosis." Genes Dev **11**(17): 2272-2290.

Nakada, D., K. Matsumoto and K. Sugimoto (2003). "ATM-related Tel1 associates with double-strand breaks through an Xrs2-dependent mechanism." Genes Dev **17**(16): 1957-1962.

New, J. H., T. Sugiyama, E. Zaitseva and S. C. Kowalczykowski (1998). "Rad52 protein stimulates DNA strand exchange by Rad51 and replication protein A." Nature **391**(6665): 407-410.

Palmbos, P. L., J. M. Daley and T. E. Wilson (2005). "Mutations of the Yku80 C terminus and Xrs2 FHA domain specifically block yeast nonhomologous end joining." Mol Cell Biol **25**(24): 10782-10790.

Pandita, T. K. and C. Richardson (2009). "Chromatin remodeling finds its place in the DNA double-strand break response." Nucleic Acids Res **37**(5): 1363-1377.

Paull, T. T. and M. Gellert (1998). "The 3' to 5' exonuclease activity of Mre 11 facilitates repair of DNA double-strand breaks." Mol Cell **1**(7): 969-979.

Paull, T. T. and M. Gellert (1999). "Nbs1 potentiates ATP-driven DNA unwinding and endonuclease cleavage by the Mre11/Rad50 complex." Genes Dev **13**(10): 1276-1288.

Porter-Goff, M. E. and N. Rhind (2009). "The Role of MRN in the S-Phase DNA Damage Checkpoint is Independent of its Ctp1-Dependent Roles in Double-Strand Break Repair and Checkpoint Signaling." Mol Biol Cell.

Prinz, S., A. Amon and F. Klein (1997). "Isolation of COM1, a new gene required to complete meiotic double-strand break-induced recombination in Saccharomyces cerevisiae." Genetics **146**(3): 781-795.

Raghavan, S. C., C. L. Hsieh and M. R. Lieber (2005). "Both V(D)J coding ends but neither signal end can recombine at the bcl-2 major breakpoint region, and the rejoining is ligase IV dependent." Mol Cell Biol **25**(15): 6475-6484.

Rahal, E. A., L. A. Henricksen, Y. Li, R. S. Williams, J. A. Tainer and K. Dixon (2010). "ATM regulates Mre11-dependent DNA end-degradation and microhomology-mediated end joining." Cell Cycle **9**(14): 2866-2877.

Rass, E., A. Grabarz, I. Plo, J. Gautier, P. Bertrand and B. S. Lopez (2009). "Role of Mre11 in chromosomal nonhomologous end joining in mammalian cells." Nat Struct Mol Biol **16**(8): 819-824.

Sambrook, J. and D. W. Russell (2001). Molecular Cloning: A Laboratory Manual. New York, Cold Spring Harbor Laboratory Press.

San Filippo, J., P. Sung and H. Klein (2008). "Mechanism of eukaryotic homologous recombination." Annu Rev Biochem **77**: 229-257.

Sartori, A. A., C. Lukas, J. Coates, M. Mistrik, S. Fu, J. Bartek, R. Baer, J. Lukas and S. P. Jackson (2007). "Human CtIP promotes DNA end resection." Nature **450**(7169): 509-514.

Sharples, G. J. and D. R. Leach (1995). "Structural and functional similarities between the SbcCD proteins of Escherichia coli and the RAD50 and MRE11 (RAD32) recombination and repair proteins of yeast." Mol Microbiol **17**(6): 1215-1217.

Shim, E. Y., W. H. Chung, M. L. Nicolette, Y. Zhang, M. Davis, Z. Zhu, T. T. Paull, G. Ira and S. E. Lee (2010). "Saccharomyces cerevisiae Mre11/Rad50/Xrs2 and Ku proteins regulate association of Exo1 and Dna2 with DNA breaks." EMBO J **29**(19): 3370-3380.

Shima, H., M. Suzuki and M. Shinohara (2005). "Isolation and characterization of novel xrs2 mutations in Saccharomyces cerevisiae." Genetics **170**(1): 71-85.

Shull, E. R., Y. Lee, H. Nakane, T. H. Stracker, J. Zhao, H. R. Russell, J. H. Petrini and P. J. McKinnon (2009). "Differential DNA damage signaling accounts for distinct neural apoptotic responses in ATLD and NBS." Genes Dev **23**(2): 171-180.

Soding, J., A. Biegert and A. N. Lupas (2005). "The HHpred interactive server for protein homology detection and structure prediction." Nucleic Acids Res **33**(Web Server issue): W244-248.

Soulas-Sprauel, P., P. Rivera-Munoz, L. Malivert, G. Le Guyader, V. Abramowski, P. Revy and J. P. de Villartay (2007). "V(D)J and immunoglobulin class switch recombinations: a paradigm to study the regulation of DNA end-joining." Oncogene **26**(56): 7780-7791.

Spycher, C., E. S. Miller, K. Townsend, L. Pavic, N. A. Morrice, P. Janscak, G. S. Stewart and M. Stucki (2008). "Constitutive phosphorylation of MDC1 physically links the MRE11-RAD50-NBS1 complex to damaged chromatin." J Cell Biol **181**(2): 227-240.

Stewart, G. S., R. S. Maser, T. Stankovic, D. A. Bressan, M. I. Kaplan, N. G. Jaspers, A. Raams, P. J. Byrd, J. H. Petrini and A. M. Taylor (1999). "The DNA double-strand

break repair gene hMRE11 is mutated in individuals with an ataxia-telangiectasia-like disorder." Cell **99**(6): 577-587.

Stracker, T. H. and J. H. Petrini (2011). "The MRE11 complex: starting from the ends." Nat Rev Mol Cell Biol **12**(2): 90-103.

Strahl-Bolsinger, S., A. Hecht, K. Luo and M. Grunstein (1997). "SIR2 and SIR4 interactions differ in core and extended telomeric heterochromatin in yeast." Genes Dev **11**(1): 83-93.

Sung, P. and H. Klein (2006). "Mechanism of homologous recombination: mediators and helicases take on regulatory functions." Nat Rev Mol Cell Biol **7**(10): 739-750.

Sutherland, B. M., P. V. Bennett, O. Sidorkina and J. Laval (2000). "Clustered DNA damages induced in isolated DNA and in human cells by low doses of ionizing radiation." Proc Natl Acad Sci U S A **97**(1): 103-108.

Symington, L. S. (2002). "Role of RAD52 epistasis group genes in homologous recombination and double-strand break repair." Microbiol Mol Biol Rev **66**(4): 630-670, table of contents.

Tonegawa, S. (1983). "Somatic generation of antibody diversity." Nature **302**(5909): 575-581.

Trujillo, K. M., D. H. Roh, L. Chen, S. Van Komen, A. Tomkinson and P. Sung (2003). "Yeast xrs2 binds DNA and helps target rad50 and mre11 to DNA ends." J Biol Chem **278**(49): 48957-48964.

Trujillo, K. M. and P. Sung (2001). "DNA structure-specific nuclease activities in the Saccharomyces cerevisiae Rad50*Mre11 complex." J Biol Chem **276**(38): 35458-35464.

Trujillo, K. M., S. S. Yuan, E. Y. Lee and P. Sung (1998). "Nuclease activities in a complex of human recombination and DNA repair factors Rad50, Mre11, and p95." J Biol Chem **273**(34): 21447-21450.

Tsukamoto, Y., C. Mitsuoka, M. Terasawa, H. Ogawa and T. Ogawa (2005). "Xrs2p regulates Mre11p translocation to the nucleus and plays a role in telomere elongation and meiotic recombination." Mol Biol Cell **16**(2): 597-608.

Uchisaka, N., N. Takahashi, M. Sato, A. Kikuchi, S. Mochizuki, K. Imai, S. Nonoyama, O. Ohara, F. Watanabe, S. Mizutani, R. Hanada and T. Morio (2009). "Two brothers with ataxia-telangiectasia-like disorder with lung adenocarcinoma." J Pediatr **155**(3): 435-438.

Ueno, M., T. Nakazaki, Y. Akamatsu, K. Watanabe, K. Tomita, H. D. Lindsay, H. Shinagawa and H. Iwasaki (2003). "Molecular characterization of the Schizosaccharomyces pombe nbs1+ gene involved in DNA repair and telomere maintenance." Mol Cell Biol **23**(18): 6553-6563.

Usui, T., T. Ohta, H. Oshiumi, J. Tomizawa, H. Ogawa and T. Ogawa (1998). "Complex formation and functional versatility of Mre11 of budding yeast in recombination." Cell **95**(5): 705-716.

Uziel, T., Y. Lerenthal, L. Moyal, Y. Andegeko, L. Mittelman and Y. Shiloh (2003). "Requirement of the MRN complex for ATM activation by DNA damage." EMBO J **22**(20): 5612-5621.

van der Linden, E., H. Sanchez, E. Kinoshita, R. Kanaar and C. Wyman (2009). "RAD50 and NBS1 form a stable complex functional in DNA binding and tethering." Nucleic Acids Res **37**(5): 1580-1588.

Varon, R., C. Vissinga, M. Platzer, K. M. Cerosaletti, K. H. Chrzanowska, K. Saar, G. Beckmann, E. Seemanova, P. R. Cooper, N. J. Nowak, M. Stumm, C. M. Weemaes, R. A. Gatti, R. K. Wilson, M. Digweed, A. Rosenthal, K. Sperling, P. Concannon and A. Reis (1998). "Nibrin, a novel DNA double-strand break repair protein, is mutated in Nijmegen breakage syndrome." Cell **93**(3): 467-476.

Waltes, R., R. Kalb, M. Gatei, A. W. Kijas, M. Stumm, A. Sobeck, B. Wieland, R. Varon, Y. Lerenthal, M. F. Lavin, D. Schindler and T. Dork (2009). "Human RAD50 deficiency in a Nijmegen breakage syndrome-like disorder." Am J Hum Genet **84**(5): 605-616.

Weemaes, C. M., T. W. Hustinx, J. M. Scheres, P. J. van Munster, J. A. Bakkeren and R. D. Taalman (1981). "A new chromosomal instability disorder: the Nijmegen breakage syndrome." Acta Paediatr Scand **70**(4): 557-564.

Weterings, E. and D. C. van Gent (2004). "The mechanism of non-homologous end-joining: a synopsis of synapsis." DNA Repair (Amst) **3**(11): 1425-1435.

Williams, G. J., S. P. Lees-Miller and J. A. Tainer (2010). "Mre11-Rad50-Nbs1 conformations and the control of sensing, signaling, and effector responses at DNA double-strand breaks." DNA Repair (Amst) **9**(12): 1299-1306.

Williams, G. J., R. S. Williams, J. S. Williams, G. Moncalian, A. S. Arvai, O. Limbo, G. Guenther, S. Sildas, M. Hammel, P. Russell and J. A. Tainer (2011). "ABC ATPase signature helices in Rad50 link nucleotide state to Mre11 interface for DNA repair." Nat Struct Mol Biol **18**(4): 423-431.

Williams, R. S., G. E. Dodson, O. Limbo, Y. Yamada, J. S. Williams, G. Guenther, S. Classen, J. N. Glover, H. Iwasaki, P. Russell and J. A. Tainer (2009). "Nbs1 flexibly tethers Ctp1 and Mre11-Rad50 to coordinate DNA double-strand break processing and repair." Cell **139**(1): 87-99.

Williams, R. S., G. Moncalian, J. S. Williams, Y. Yamada, O. Limbo, D. S. Shin, L. M. Groocock, D. Cahill, C. Hitomi, G. Guenther, D. Moiani, J. P. Carney, P. Russell and J. A. Tainer (2008). "Mre11 dimers coordinate DNA end bridging and nuclease processing in double-strand-break repair." Cell **135**(1): 97-109.

Xie, A., A. Kwok and R. Scully (2009). "Role of mammalian Mre11 in classical and alternative nonhomologous end joining." Nat Struct Mol Biol **16**(8): 814-818.

Xu, C., L. Wu, G. Cui, M. V. Botuyan, J. Chen and G. Mer (2008). "Structure of a second BRCT domain identified in the nijmegen breakage syndrome protein Nbs1 and its function in an MDC1-dependent localization of Nbs1 to DNA damage sites." J Mol Biol **381**(2): 361-372.

Yazdi, P. T., Y. Wang, S. Zhao, N. Patel, E. Y. Lee and J. Qin (2002). "SMC1 is a downstream effector in the ATM/NBS1 branch of the human S-phase checkpoint." Genes Dev **16**(5): 571-582.

Ye, Y. and A. Godzik (2004). "FATCAT: a web server for flexible structure comparison and structure similarity searching." Nucleic Acids Res **32**(Web Server issue): W582-585.

You, Z., C. Chahwan, J. Bailis, T. Hunter and P. Russell (2005). "ATM activation and its recruitment to damaged DNA require binding to the C terminus of Nbs1." Mol Cell Biol **25**(13): 5363-5379.

Zakharyevich, K., Y. Ma, S. Tang, P. Y. Hwang, S. Boiteux and N. Hunter (2010). "Temporally and biochemically distinct activities of Exo1 during meiosis: double-strand break resection and resolution of double Holliday junctions." Mol Cell **40**(6): 1001-1015.

Zha, S., C. Boboila and F. W. Alt (2009). "Mre11: roles in DNA repair beyond homologous recombination." Nat Struct Mol Biol **16**(8): 798-800.

Zha, S., C. Guo, C. Boboila, V. Oksenych, H. L. Cheng, Y. Zhang, D. R. Wesemann, G. Yuen, H. Patel, P. H. Goff, R. L. Dubois and F. W. Alt (2011). "ATM damage response and XLF repair factor are functionally redundant in joining DNA breaks." Nature **469**(7329): 250-254.

Zhuang, J., G. Jiang, H. Willers and F. Xia (2009). "Exonuclease function of human Mre11 promotes deletional nonhomologous end joining." J Biol Chem **284**(44): 30565-30573.

Zierhut, C. and J. F. Diffley (2008). "Break dosage, cell cycle stage and DNA replication influence DNA double strand break response." EMBO J **27**(13): 1875-1885.

Zwart, P. H., P. V. Afonine, R. W. Grosse-Kunstleve, L. W. Hung, T. R. Ioerger, A. J. McCoy, E. McKee, N. W. Moriarty, R. J. Read, J. C. Sacchettini, N. K. Sauter, L. C. Storoni, T. C. Terwilliger and P. D. Adams (2008). "Automated structure solution with the PHENIX suite." Methods Mol Biol **426**: 419-435.

7. ABBREVATIONS

6-FAM	6-carboxyfluorescein
Å	Angstrom
aa	amino acid (residue)
ABC	ATP binding cassette
AFM	Atomic force microscopy
APS	ammonium persulfate
A-TLD	Ataxia-telangiectasia like disorder
ATM	Ataxia telangiectasia mutated
ATP	adenosine triphosphate
bp	base pair
BRCT	breast cancer C-terminus
°C	degree celsius
CK2	casein kinase 2
DAPI	4‘,6-diamino-2-phenylindole
DNA	deoxyribonucleic acid
DNA-PK	DNA-dependent protein kinase
*Dr*Mre11	Mre11 from *Danio rerio*
DSB	DNA double-strand break
DSBR	DNA double-strand break repair
dsDNA	double-stranded DNA
E. coli	*Escherichia coli*
ECL	enhanced chemoluminiscence
EDTA	ethylenediaminetetraacetic acid
EMSA	electrophoretic mobility shift assay
FHA	forkhead associated
h	hours
HEAT	Huntingtin, elongation factor 3, the A subunit of protein
HR	homologous recombination
*Hs*Mre11	Mre11 from Homo sapiens
IPTG	Isopropyl-β-D-thiogalactopyranosid
kDa	kilo Dalton
L	litre
LB	Luria-Bertani
M	molar
min	minute
MMS	methyl methanesulfonate
Mn	manganese
Mre11	meiotic recombination 11

$Mre11^{cd}$	Mre11 catalytic domain
MRN	Mre11-Rad50-Nbs1
MRX	Mre11-Rad50-Xrs2 (*S. cerevisiae* complex)
n	nano
Nbs	Nijmegen breakage syndrome
$Nbs1^{mir}$	Mre11 interaction region of Nbs1
NHEJ	non-homologous end joining
NLS	nuclear localisation sequence
NMR	nuclear magnetic resonance spectroscopy
nt	nucleotide
OD_{600}	optical density at 600 nm
PAGE	polyacrylamide gelelectrophoresis
PBS	phosphate-buffered saline
PBS	phosphate buffered saline
PCR	polymerase chain reaction
PDB	protein data bank
PEG	polyethylene glycol
*Pf*Mre11	Mre11 from *Pyrococcus furiosus*
Pfu	*Pyrococcus furiosus*
pH	potential of hydrogen
PMSF	phenylmethanesulfonylfluoride
ROS	reactive oxygen species
rpm	rotation per minute
RT	room temperature
S. cerevisiae	*Saccharomyces cerevisiae*
S. pombe	*Schizosaccharomyces pombe*
SAD	single-wavelength anomalous dispersion
SAXS	small angle X-ray scattering
*Sc*Mre11	Mre11 from *Saccharomyces cerevisiae*
SDS	sodium dodecyl-sulphate
sec	second
*Sp*Mre11	Mre11 from *Schizosaccharomyces pombe*
TB	Tris/Borate
TBE	Tris/Borate/EDTA
TBS	tris-buffered saline
TBST	tris-buffered saline + Tween 20
TEMED	*N*,*N*,*N′*,*N′*-tetramethylethylenediamine
TEV	Tobacco Etch Virus

*Tm*Mre11	Mre11 from *Thermotoga maritima*
Tris	*tris*(hydroxymethyl)aminomethane
UV	ultraviolet
Wt	Wild type
XRCC1	X-ray repair cross-complementing protein 1
YPD	yeast extract, peptone, glucose containing medium
µ	micro

8. CURRICULUM VITAE

Personal Details

Name	Christian Bernd Schiller
Date of birth	November 28th, 1980
Place of birth	Kassel, Germany
Nationality	German

Education

1987 - 1991	Grundschule in Großalmerode, Germany
1991 - 1993	Orientierungsstufe in Großalmerode, Germany
1993 - 1997	Gymnasium in Großalmerode, Germany
1997 - 2000	Gymnasium in Hessisch Lichtenau, Großalmerode

Civilian service

2000 - 2001	Jugendwaldheim Meißner, Hessisch Lichtenau, Germany

Academic Training

2001 - 2006	Studies in biology, University of Göttingen, Germany
2005 - 2006	Diploma thesis in the group of Prof. Dr. Ralf Ficner at the Centre for Molecular Biosciences (GZMB), University of Göttingen Title: "Preparation and crystallisation of ribosomal proteins with the nuclear import factor Importin 7"
2006	Diploma in Biology
Since 12/2006	PhD thesis in the group of Prof. Dr. Karl-Peter Hopfner, Gene Center, Department of Biochemistry, University of Munich, Germany

9. ACKNOWLEDGEMENTS

First of all I want to thank my supervisor Prof. Dr. Karl-Peter Hopfner for giving me the chance to work on this fascinating project in the field of genome maintenance. I am especially grateful for him being always approachable to discuss scientific problems and for all his very helpful and creative ideas on the project.

I am also thankful to Prof. Dr. Dietmar Martin for being the second examiner of this thesis.

Many thanks go to all the members of the Hopfner group. I really enjoyed the friendly and inspiring working atmosphere and also the leisure time outside the lab. Thank you, for all your support with experiments and helpful scientific discussions. I want to acknowledge in particular also Alexandra Schele, Brigitte Keßler, Manuela Moldt and Olga Fettscher for the excellent organization of the laboratory.

My special thanks go to all the members of the "Fellowship of the Ring" who experienced with me to work on this very versatile complex, which still keeps some secrets to uncover: To Katja Lammens, Carolin Möckel, Alexandra Schele, Derk Bemeleit, Ania Rojowska, Maria Lucas and Matthew Bennett. I am really thankful for all your fruitful ideas, inspiring discussions and your important contributions to this project. It was a great experience to work with you.

I am especially grateful to Katja Lammens for her supervision on this project and her help and expertise in structural biology.

I would like to thank Ilaria Guerini and Prof. Steve Jackson for a very interesting and fruitful collaboration, which allowed us to combine the structural biology of this project with *in vivo* studies.

My special thanks go also to Britta Coordes for all her expertise and support with the budding yeast experiments.

I would further like to also thank my former bachelor students Florian Schlauderer, Anna-Kathrin Kopetzki and Irina Heckmann for their great enthusiasm and contributions to this project.

I deeply want to thank you Britta for your patience, love and support. You mean the world to me.

I am deeply grateful to my parents Gerhard and Siegrid for all their love and support, to my brother Armin, my sister Annette and their families.